IN-CYLINDER CONDITION ESTIMATION AND CONTROL APPLICATIONS ON DIESEL ENGINE COMBUSTION

IN-CYLINDER CONDITION ESTIMATION AND CONTROL APPLICATIONS ON DIESEL ENGINE COMBUSTION

By SONG CHEN, M.S.

A Thesis Submitted to the School of Graduate Studies in Partial Fulfilment of the Requirements for the Degree Doctor of Philosophy

McMaster University Doctor of Philosophy (2016) Hamilton, Ontario (Engineering)

TITLE: In-cylinder condition estimation and control applications on Diesel engine combustion

AUTHOR: Song Chen, M.S. (Beihang University), B.E. (Beihang University)

SUPERVISOR: Assistant Professor Fengjun Yan

NUMBER OF PAGES: xxi, 157

Lay abstract

To ultimately reduce the engine-out emissions and increase the thermal efficiency, advanced combustion modes provide promising solutions. However, several obstacles, including the narrow load range and difficulty of the combustion phasing control, prevent the advanced combustion from being widely applied in practice. To address these obstacles, detail estimation of in-cylinder gas conditions and robust control for air- and fuel-path are critical. This thesis focuses on the states estimation and control for Diesel engines aiming to address the obstacles laid by the advanced combustion modes.

Four journal papers with different objectives compose this thesis. Paper 1 and Paper 2 (Chapter II and III, respectively) propose methods of estimation of the in-cylinder temperature and oxygen concentration. Paper 3 (Chapter IV) introduces the method of coordinated control of the intake conditions and the combustion process. The unburned fuel is estimated in paper 4 (Chapter V).

The techniques introduced in the 4 papers are either validated through calibrated GT-Power simulations or experiments in a Diesel engine.

Abstract

Advanced combustion modes offer promising solutions for both emission reduction and efficiency improvement. The lower local equivalence ratio and lower peak temperature characterized by the advanced combustion mode significantly reduce the generation of the engine-out emissions (especially the soot and NOx). Although the advanced combustion mode enjoys extra-low emissions, some technical challenges prevent it from being widely applied in real practice. Combustion phasing control as auto-ignition and narrow load range are two main challenges to be addressed. The estimation and control techniques for Diesel engine targeting these two challenges are presented in four papers in this thesis.

Accessing to the in-cylinder conditions is essential for a more detailed combustion estimation and further combustion control. Paper 1 and Paper 2 (Chapter II and Chapter III) introduce methods of estimating two critical in-cylinder conditions, the in-cylinder temperature and oxygen concentration. The system dynamic models are derived and the Extended Kalman filter (EKF) and smooth variable structure filter (SVSF) are utilized for the in-cylinder temperature and in-cylinder oxygen concentration estimation, respectively.

The method of coordinated control for the intake conditions and the combustion process aiming at a fast and accurate combustion process response is proposed in paper 3 (Chapter IV). Disturbance rejection control in conjunction with sliding mode method is proposed to control the air- and fuel-path loop simultaneously.

As an indicator to show the combustion quality and to avoid significant incomplete combustion, the unburned fuel is estimated in paper 4 (Chapter V) based on

the oxygen concentration. Three filters are designed to estimate the trapped unburned fuel and their robustness against modeling errors are analyzed and compared theoretically.

Acknowledgement

Foremost, I would like to express my sincere gratitude to my advisor, Professor Fengjun Yan, for his patience, motivation, enthusiasm, criticism and financial support that he has provided throughout the course of my research and studies.

Besides my advisor, my sincere thanks also go to all other doctoral committee members, Professor Saeid Habibi, Professor Ali Emadi, for their efforts, time, and advice for my Ph.D. study.

I thank my fellow groupmates in Powertrain Control Lab, Liang Wang, Jinbiao Ning, Yi Huo, Chuan Hu, Yangliu Dou, Jiangtao He, Yicong Liu, Tongrui Li, for their friendship and assistance.

Last but not the least, I would like to thank my parents, Jianfeng Chen and Suxiang Liu, for giving birth to me at the first place and supporting me spiritually throughout my life.

Table of Content

List of tables

List of figures

Subscripts

int	intake manifold
exh	exhaust manifold
cyl	cylinder
$int-cyl$	the charge flows from intake manifold to cylinder
$cyl-exh$	the charge flows from cylinder to exhaust manifold
res	residual gas
bc	before combustion
ac	after combustion
egr	exhaust gas recirculation
air	fresh air
bd	blowdown gas
d	downstream
u	upstream
f	fuel
$comp$	compressor of VGT

turb	turbine of VGT
evo	crank angle degree of exhaust valve opening
evc	crank angle degree of exhaust valve closing
ivo	crank angle degree of intake valve opening
ivc	crank angle degree of intake valve closing

Variables

m	mass(kg)
T	temperature(K)
p	pressure(Pa)
γ_c	specific heat ratio before combustion
γ_e	specific heat ratio after combustion
V	volume(m^3)
Q_{LHV}	lower heating value of the fuel(kcal/g)
C_v	heat capacity at constant volume(J/kg/K)
R	ideal gas constant
θ	crank angle(degree)

θ_c	crank angle at the end of combustion(degree)
C_D	discharge coefficient
A_R	valve reference area(m^2)
N	engine speed(RPM)
V_d	swept volume of the cylinder(m^3)
τ	time-constant for thermocouple
V_g	gas velocity(m/s)
T_g	gas temperature(K)
T_w	wire temperature(K)
$\boldsymbol{Q}$	covariance matrix of system noise
$\boldsymbol{R}$	covariance matrix of measurement noise
$\boldsymbol{S}$	innovation covariance matrix
F	oxygen concentration (%)
PR	pressure ratio
$\dot{m}$	mass flow rate (kg/s)
N	turbocharger rotational speed (RPM)

λ_s	stoichiometric oxygen fuel ratio
λ_v	volumetric efficiency
η	combustion efficiency
$\boldsymbol{H}$	measurement matrix
$\boldsymbol{K}$	filter gain vector of SVSF
$\boldsymbol{W}$	filter gain vector of KF
$\boldsymbol{L}$	filter gain vector of linear parameter varying filter
J	moment of inertia of the rotating parts of VGT ($kg \cdot m^2$)
$P_{turbine}$	power of the turbine(w)
P_{comp}	power of the compressor(w)
ATDC	after top dead center
CA	crank angle
DOC	diesel oxidation catalyst
DPF	diesel particulate filter
SCR	selective catalytic reduction

Declaration of Academic Achievement

Journal Articles

J1. ***Song Chen*** and Fengjun Yan, "Trapped Unburned Fuel Estimation in a Turbocharged Diesel Engine with Negative Valve Overlap (NVO) Strategy," *ASME Transactions Journal of Dynamic Systems, Measurement, and Control*, 136(5), 137(6), 061004, 2014.

J2. ***Song Chen*** and Fengjun Yan, "Control of a Dual-Loop Exhaust Gas Recirculation System for a Turbocharged Diesel Engine," *International Journal of Automotive Technology*, 16(5), pp.733-738, 2015.

J3. ***Song Chen*** and Fengjun Yan, "Extended Kalman Filter Based In-Cylinder Temperature Estimation for Diesel Engines with Thermocouple Lag Compensation," *ASME Transactions Journal of Dynamic Systems, Measurement, and Control*, 136(5), 051010, 2014.

J4. Fengjun Yan, ***Song Chen***, Xiangrui Zeng, Junfeng Zhao, and Junmin Wang, "Modeling and Analysis of Fuel Injection Split for Diesel Engine Active Fueling Control," *ASME Transactions Journal of Dynamic Systems, Measurement, and Control*, 135(6), 061016, 2013.

J5. ***Song Chen***, Fuyuan Yang, Fengjun Yan and Changsheng Yao, "CA50 estimation based on Neural Network and smooth variable structure filter", *IEEE Transactions on Control Systems Technology*, 2016(submitted).

J6. ***Song Chen***, Fuyuan Yang, Fengjun Yan and Changsheng Yao, "In-cylinder oxygen concentration estimation with in-cylinder pressure information for turbocharged Diesel engines*", IEEE Transactions on Control Systems Technology*, 2016(submitted).

J7. ***Song Chen*** and Fengjun Yan, "Decoupled, Disturbance Rejection Control for a Turbocharged Engine with Dual-Loop EGR System," *Journal of Automobile Engineering*, 2016(submitted).

Peer-Reviewed Conference Papers

C1. ***Song Chen*** and Fengjun Yan, "Decoupled, disturbance rejection control for a turbocharged engine with dual-loop EGR system", 8th IFAC International Symposium on Advances in Automotive Control, (Accepted), 2016.

C2. ***Song Chen*** and Fengjun Yan, "Trapped Unburned Fuel Estimation for a Turbocharged Diesel Engine with Negative Valve Overlap (NVO) Strategy," 2014 Proceedings of the CSME International Congress, Toronto, 2014.

C3. ***Song Chen*** and Fengjun Yan, “Trapped Unburned Fuel Estimation for a Turbocharged Diesel Engine with Negative Valve Overlap (NVO) Strategy,” 2014 Proceedings of the CSME International Congress, Toronto, 2014.

C4. ***Song Chen*** and Fengjun Yan, "Input magnitude relaxation of output constrained control for a class of nonlinear system," 2014 Proceedings of the CSME International Congress, Toronto, 2014.

C5. ***Song Chen*** and Fengjun Yan, “Combustion Phasing and Work Output Modeling for HCCI Engines,” Proceedings of the American Control Conference, (Invited), 2014.

C6. ***Song Chen*** and Fengjun Yan, “Cycle-by-Cycle Based In-Cylinder Temperature Estimation for Diesel Engines,” Proceedings of the ASME Dynamic Systems and Control Conference, (Invited, 8 pages), 2013.

Chaper 1. Introduction

1.1. Background

Internal combustion (IC) engines are widely used as one of the key power sources in the automotive sector. There are plenty types of internal combustion engine classifications [1]. Most typically, internal combustion engines can be classified into two types: spark-ignition (SI) engines and compression-ignition (CI) engines. The conventional SI is named from the mechanism that the combustion is controlled by ignition timing of the spark discharge. Due to the fuel/air mixture is premixed and typically stoichiometric; the emissions of SI engines, especially the soot[2], are much lower than CI engines. However, higher pumping losses (especially at partial load) and lower compression ratio make the SI combustion suffer from lower efficiency. CI engines are typically presented by Diesel combustion. The high compression ratio of CI engines enables the combustion initiated by the fuel injection in a high temperature and pressure environment. As a consequence of the injection and piston compression, the auto-ignition process distinguishes the CI engines from SI engines (ignited by the spark plug). Although CI engines have higher efficiency, direct injection and high compression ratio lead fuel stratification and high peak temperature which cause the CI engines have higher soot and NOx (nitrogen oxide) emissions[3].

Pollutant emissions have serious environmental and health implications, and thus, the regulations on the engine-out emissions are becoming continually stringent in recent years. Fig. 1 is showing the emission regulations of NOx and PM (particulate matter) given by the US Environment Protect Agency for Diesel engines. Shown in Fig. 1, the PM standards have gone up from 1988 to 2007 by about 100 times.

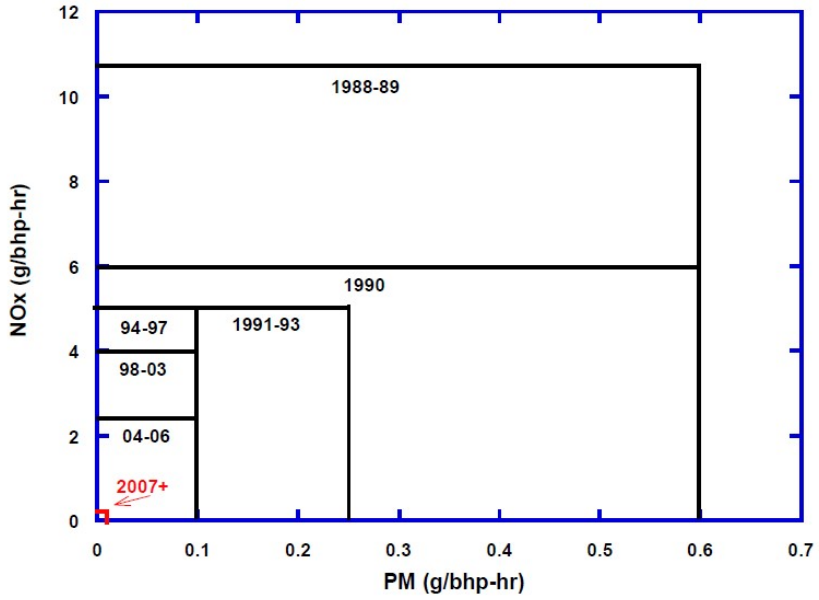

Fig. 1 Heavy duty diesel emissions standards since 1988 [4]

To improve the efficiency while reducing the engine-out emissions in Diesel engines, various technologies have been proposed, such as retarding the injection timing and increasing the injection pressure to avoid fuel rich equivalence ratios and reduce the soot emissions, increasing the EGR rate to lower the peak temperature and reduce the NOx formation. Fig. 2 shows different technologies developed since 1974, including higher compression ratio, modified fuel injection systems, intake air management, electronic engine control, exhaust gas recirculation (EGR) etc. to fulfill emission standards[5].

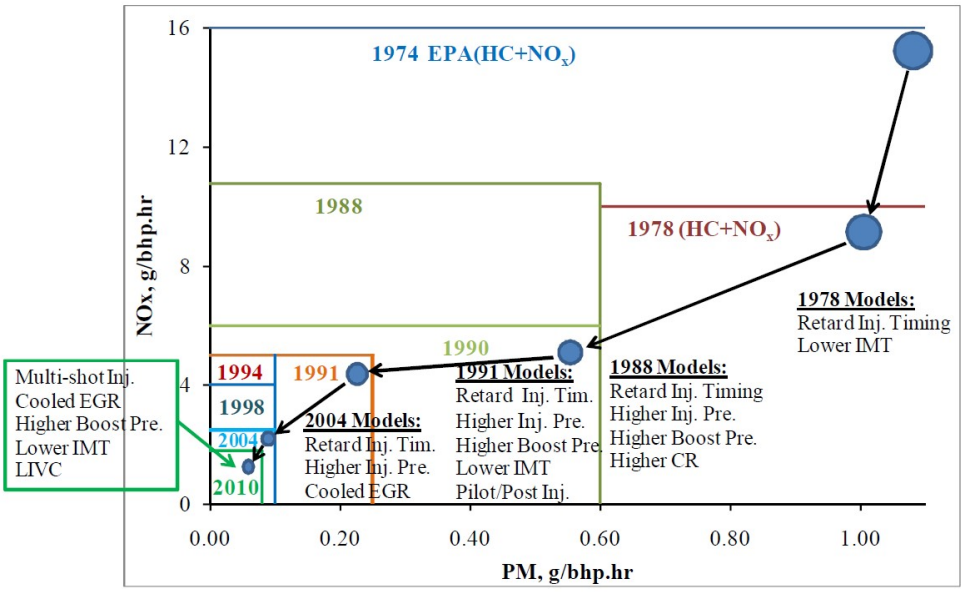

Fig. 2 Advancement in in-cylinder technologies to achieve low NOx and PM [5]

Advanced combustion modes such as homogeneous charge compression ignition (HCCI)[6][7][8][9], premixed charge compression ignition (PCCI)[10][11], and low temperature combustion (LTC) [12][5], etc. offer promising solutions for reduction of NOx and PM as well as increasing efficiency simultaneously. As told by Fig. 3 [12], the in-cylinder conditions spanned by the local equivalence ratio and local temperature for different combustion modes are comparing with the emissions (soot and NOx) islands. As one can see, the advanced combustion modes generally have lower local temperature and local equivalence ratio (around injector) such that the conditions can lead to ultra-low emissions.

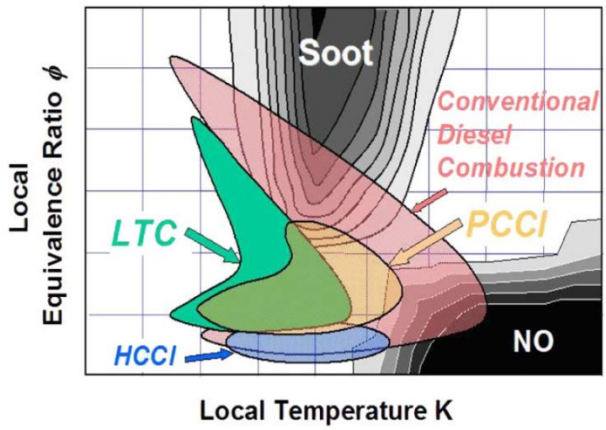

Fig. 3 Different combustion modes comparing with the emission islands [12]**.**

Among the advanced combustion modes, the HCCI enjoys the homogeneous mixture and the compression ignition, leading to the high efficiency and ultra-low emissions[13], which has been widely accepted as an ideal combustion mode. The LTC is a more practical combustion mode which focuses on reducing the NOx emissions by inducing a large amount of EGR. As a more feasible alternative of HCCI, PCCI lays in between the conventional combustion mode and HCCI. In Diesel engine PCCI, the air and fuel are premixed, usually by advancing the injection time, to reduce the PM and other emissions.

However, there are some challenges of advanced combustion modes that prevent them from real applications: 1) the combustion phasing control as auto-ignition. The auto-ignition of the advanced combustion mode largely depends on the thermodynamics of the mixture. It turns out that operating conditions, instead of the direct combustion triggers like injector or spark plug in conventional engines, are critical for the advanced combustion modes. In addition, different advanced combustion modes are achieved by different fueling and correspondingly different in-cylinder conditions. The complex and

indirect auto-ignition processes make the combustion phasing control difficult. 2) The advanced combustion modes have a limited speed-load region. Since advanced combustion modes typically work close to the boundary of stable combustion, misfire or sudden change of peak pressure may happen in relatively low or high load. Coordinated control of the air-path and fuel-path, and accessing in-cylinder condition information are required for more precise control and extending the load range of the advanced combustion mode.

The in-cylinder conditions, especially the in-cylinder temperature and in-cylinder oxygen concentration which are hardly accessible in commercial engines, have significant impacts on combustion auto-ignition process [14][15]. Therefore, to achieve smooth and stable advanced combustion, the in-cylinder conditions needs to be well estimated. The in-cylinder temperature is non-trivial in the estimation for residual gas for a Diesel engine in [16]. A nonlinear observer was designed in [17]based on a linear parameter-varying model for the estimation of the in-cylinder oxygen concentration at intake valve closing(IVC) on a cycle-by-cycle basis. By capturing the effects of the time-varying transport delay, a plug flow based oxygen concentration model was derived in [18], and the in-cylinder oxygen concentration can be predicted within an error of 0.2% of the true value in the RMS (root mean square)sense.

As for the ultra-low emissions offered by the advanced combustion mode[19], lower temperature and lower equivalence ratio offered by the low temperature combustion mode are the cause for the extremely low PM (particulate matter)and NOx: the conditions, i.e. higher temperature and higher equivalence ratio for generating the PM and NOx are avoided. However, a lower temperature is mostly achieved by introducing a

significantly amount of exhaust gas into the intake system, which deteriorates the combustion stability. Apart from the EGR, the pressure, temperature in air path loop and the injection conditions (injection timing, mass, pulses, etc.) in fuel loop, are all needed to be well regulated for a smooth combustion, slightly mismatch or calibration error could lead to misfire and even physical damage to the engine[20], especially when trying to extend the load range[21].

The fraction of exhaust gas inhaled to the intake system of the advanced combustion mode can be up to 50%. With such amount of residual gas in the cylinder, the trapped unburned fuel is not trivial. Furthermore, it has a significant impact on the combustion process[22]; on the other hand, the trapped unburned fuel introduces severe cyclic variability to the engines[23].

Therefore, the research in this thesis (the four papers) focuses on: 1) analyzing the characteristics of the target engine architecture, the Diesel engine with EGR loop and deriving system dynamic models; 2) proposing new methods to estimate the inaccessible in-cylinder conditions based on system dynamics and to control the air- and fuel-path coordinately. Since the auto-ignition process largely depends on the in-cylinder conditions, the in-cylinder temperature and oxygen concentration estimated in paper 1 (Chapter II) and paper 2 (Chapter III) give a more detailed combustion estimation and lay a foundation for the further combustion phasing control. Paper 1) and paper 2) estimate the two critical in-cylinder conditions (the in-cylinder temperature and in-cylinder oxygen concentration) by using extended Kalman filter (EKF) and smooth variable structure filter (SVSF) based on the system dynamics, respectively. Coordinated control of air-path and fuel-path introduced in paper 3 aims at a fast and accurate combustion

process response, which can also be potentially used to extend the operating range. The unburned fuel estimation in paper 4 shows the combustion cyclic variations, couplings, and abnormality, which tells if the EGR is too high to be accepted. The techniques given in the four papers constitute a whole picture for the Diesel engine combustion control.

1.2. The content of the four papers

To deal with the challenges of the advanced combustion, four papers in this thesis are introducing some techniques.

Paper 1) focuses on the in-cylinder temperature estimation. The in-cylinder temperature has significantly impact on the auto-ignition process. More accurate estimation of the in-cylinder temperature gives a deeper understanding of the ignition process and further better combustion phasing control. The in-cylinder temperature at intake valve closing (IVC) is a critical state of the mixture before combustion since after IVC there is almost no gas exchange between the cylinder and outside. Paper 1) derives the cycle-by-cycle dynamics of the temperatures at IVC, and the temperature of the intake and exhaust manifolds. Hence, the estimation of the inaccessible in-cylinder temperature turns to be the estimation of one state (the in-cylinder temperature) by using the other two measurable states (intake and exhaust manifolds temperature) based on the system dynamics. Extended Kalman filter is tailored for such a 3-state system. From the measurement point of view, the thermocouple is widely used as one of the temperature sensors. The measurement error brought by the slow response of the thermocouple is analyzed and attenuated by re-calculating the covariance matrices.

The estimation idea proposed in paper 1) was validated through GT-Power simulation. Since deriving the system dynamics and applying the estimation technique are the main contributions of this paper, the engine model in this paper is a normal Diesel engine with EGR (exhaust gas recirculation) loop. The characteristics of the in-cylinder temperature at IVC are well captured by the proposed method. Therefore, this method can be applied to other engine models.

Except the in-cylinder temperature, other in-cylinder conditions, including the in-cylinder pressure and especially the in-cylinder oxygen concentration (inaccessible in mass production), are the foundation for modeling and further controlling (model based control) the combustion phasing.

Paper 2) introduces the technique for a more accurate and robust estimation of in-cylinder oxygen concentration. The dynamics of the in-cylinder, intake, and exhaust oxygen concentrations are presented based on the mass conservation law. Considering the ignition delay (the duration of the injection time to the start of combustion) is well calculated by the in-cylinder pressure trace and it has a strong relationship with the oxygen concentration, the oxygen concentration is also modeled as a function of ignition delay. The in-cylinder oxygen concentration given by the two sources, the system dynamics (on the mass conservation basis) and the ignition delay (by the in-cylinder pressure) are estimated by utilizing the smooth variable structure filter (SVSF). The experimental results of a turbocharged Diesel engine with dual-loop EGR system validate that both accuracy and robustness are improved comparing to the cases by using each alone.

The information of the in-cylinder temperature and in-cylinder oxygen concentration lays a solid foundation for the further combustion phasing and work output control. The engine architecture applied in paper 2), turbocharged Diesel engine with dual-loop EGR system, gives great flexibility and potentiality for controlling the advanced combustion mode.

Paper 3) gives the strategy of coordinately control of the intake conditions and the combustion phasing. Ideally, the direct control for the in-cylinder conditions is preferable. However, the inaccessible and complex model of the in-cylinder temperature and oxygen concentration make the intake conditions control more applicable. As derived in paper 1) and paper 2), the in-cylinder conditions (in-cylinder temperature and oxygen concentration) are determined by the intake conditions (intake temperature, pressure, and oxygen concentration). Thus, in order to control the in-cylinder conditions, and further the combustion process, the dynamics of intake conditions are derived in paper 3). Taking the two EGR valves and the variable geometry turbocharger as three inputs, a controller based on the sliding mode idea is designed for a turbocharged Diesel engine with dual-loop EGR system. To compensate the coupling effect of the fuel-path loop on the air-path loop, the extended state observer based on the concept of super twisting is constructed. Thus, the coupling effect is estimated and compensated in real time.

As for the fuel path loop, control-oriented models for CA50 (crank angle when 50% of the fuel consumed) and IMEP (indicated mean effective pressure) are derived. The injection timing and injection mass are used to control the CA50 and IMEP, respectively. By taking the advantage of the time scaling of the two subsystems, the air-path (slow responses) and fuel-path (fast responses) are controlled in a decoupled fashion.

The controlling idea proposed in this paper is validated in a calibrated Diesel engine model by real experimental data.

Paper 4) deals with the combustion instability issue that caused by a large amount of exhaust gas within the cylinder. Introducing a large amount of exhaust gas, by the form of EGR or the form of residual gas, can significantly increase the heat capacity ratio of the fuel/gas mixture and thus reduce the combustion peak temperature. It turns out that with EGR strategy, NOx can be significantly reduced. However, with such amount of exhaust gas in the cylinder, the combustion quality tends to be deteriorated. The mass of unburned fuel is an indicator to show the cyclic variation, which tells the control quality and if the EGR level is too high to be acceptable. By utilizing the strong correlation of the in-cylinder oxygen concentration and the unburned fuel mass, the estimation for the unburned fuel is transferred to estimate the oxygen concentration. The system dynamics of in-cylinder oxygen fraction is derived and a linear parameter time-varying system is presented in this paper.

For such a 3-state linear system, three filters including Kalman filter (KF), smooth variable structure filter (SVSF) and linear parameter-varying (LPV) filter are designed. Their robustness against modeling errors is analyzed based on the theory of input to state stability. The estimation and robustness analysis were validated through a turbocharged Diesel engine with EGR model in GT-Power environment.

The whole picture of this thesis can be demonstrated in the following figure.

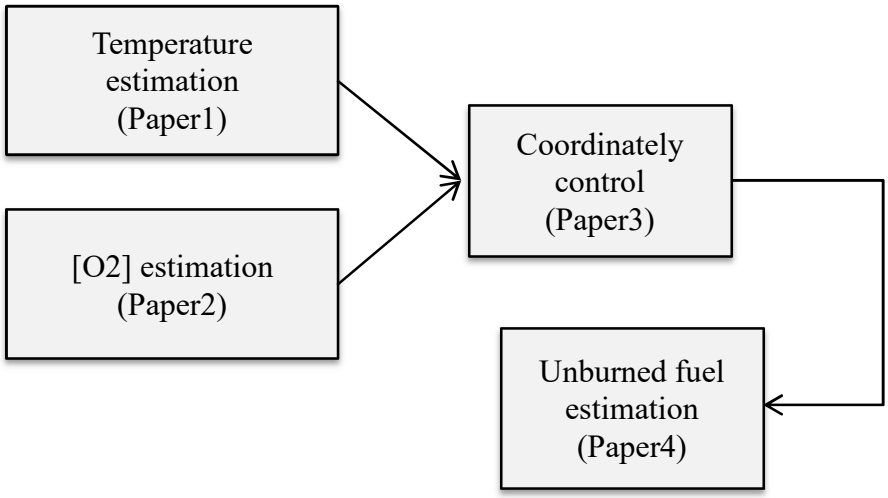

Fig. 4 The relation of the 4 four papers in this thesis

The in-cylinder temperature and oxygen concentration estimated in paper 1and paper 2 give more detailed combustion estimation and lay a foundation for the combustion phasing control. The air-path and fuel-path coordinately controlled in paper 3 can be potentially used other extend the operating range. As and good indicator to show the combustion cyclic variations, couplings, the unburned fuel is estimated in paper 4.

1.3. Contributions

The thesis contributions lie in the following aspects.

1. Based on the Extended Kalman filter the in-cylinder temperature estimation method is developed and the error caused by the thermocouple lag is attenuated by re-deriving the system process and measurement covariance matrices.

2. Based on the SVSF estimation method, the in-cylinder oxygen concentration extracted from two sources, the ignition delay model and the oxygen concentration dynamics are combined for a more accurate and robust estimation.

3. Control-oriented models for air- and fuel- path are proposed in a systematically way. The two loops are controlled in a decoupled fashion by taking the advantage of the different time scales of the two loops. By coordinately control the air- and fuel-path loops, the combustion process, i.e. the combustion phasing and work output can be regulated in a responsive and accurate fashion.

4. The information of oxygen fraction is first used to extract the unburned fuel in an iterative way. Three filters, namely KF, SVSF and LPV are designed and compared for estimating the unburned fuel. Their robustness is analyzed theoretically.

1.4. Outline

The materials in this thesis are organized as follows:

In Chapter 2, paper 1), extended Kalman Filter based in-cylinder temperature estimation for diesel engines with thermocouple lag compensation, and some remarks and comments are presented. Based on the in-cylinder temperature dynamics and the intake/exhaust manifolds temperature dynamics, the EKF is utilized to estimate the in-cylinder temperature in a predictor-corrector way. This method is validated through GT-Power simulation.

In Chapter 3, paper 2), In-cylinder oxygen concentration estimation with in-cylinder pressure information for turbocharged Diesel engines, and some remarks and comments are presented. For a more accurate and robust estimation for the in-cylinder oxygen concentration, the method based on SVSF to extract the oxygen information from two resources are proposed. This method is validated through experiments.

In Chapter 4, paper 3), air-path and fuel-path coordinated control for a turbo-charged engine with dual-loop EGR system, and some remarks and comments are presented. The controllers for air-path and fuel-path are designed separately. By taking the advantages of the ESO and the time scaling of the two loops, the air- and fuel-path are controlled in a decoupled fashion. This method is validated through calibrated engine model in GT-Power environment.

In Chapter 5, paper 4), trapped unburned fuel estimation and robustness analysis for a turbocharged Diesel engine with negative valve overlap strategy, and some remarks and comments are presented. The in-cylinder oxygen concentration is used to estimate the unburned fuel mass. Three different filters are applied to extract the unburned fuel from the in-cylinder oxygen concentration. Their robustness against modeling errors is analyzed and compared. This method is validated through GT-Power simulation.

In Chapter 6, this thesis is summarized and several further research directions are discussed.

1.5. Reference

[1] J. B. Heywood, *Internal Combustion Engine Fundamentals*, vol. 21. McGraw-Hill,Inc., 1988.

[2] L. M. Olesky, J. B. Martz, G. a. Lavoie, J. Vavra, D. N. Assanis, and A. Babajimopoulos, “The effects of spark timing, unburned gas temperature, and negative valve overlap on the rates of stoichiometric spark assisted compression ignition combustion,” *Appl. Energy*, vol. 105, pp. 407–417, May 2013.

[3] J. E. Dec, “Advanced compression-ignition engines—understanding the in-

cylinder processes," *Proc. Combust. Inst.*, vol. 32, no. 2, pp. 2727–2742, 2009.

[4] "Current US EPA Regulations, and Engineering Challenges in Automotive Industry | Energy, Technology, & Policy on WordPress.com." [Online]. Available: http://webberenergyblog.wordpress.com/2013/02/02/current-us-epa-regulations-and-engineering-challenges-in-automotive-industry/. [Accessed: 04-Sep-2014].

[5] and S. S. Brijesh, P., A. Chowdhury, "Effect of Ultra-cooled EGR and Retarded Injection Timing on Low Temperature Combustion in CI Engines," *SAE Tech. Pap.*, no. 2013–01–0321, 2013.

[6] C. Chiang and A. G. Stefanopoulou, "Stability Analysis in Homogeneous Charge Compression Ignition (HCCI) Engines With High Dilution Greek : Subscripts :," *IEEE Trans. Syst. Technol.*, vol. 15, no. 2, pp. 5–9, 2007.

[7] N. Ravi, L. Hsien-Hsin, F. Jungkunz, and J. Christian, "Modeling and Control of Exhaust Recompression HCCI," *IEEE Control Syst.*, no. August, pp. 26–42, 2012.

[8] A. Widd, P. Tunest, and R. Johansson, "Modeling for HCCI Control," *Lect. Notes Control Inf. Sci.*, vol. 418, pp. 283–302, 2012.

[9] X. Yang and G. G. Zhu, "A Two-Zone Control Oriented SI-HCCI Hybrid Combustion Model for the HIL Engine Simulation," in *American control conference*, 2011, pp. 973–978.

[10] S. M. Aceves, D. L. Flowers, and D. N. Assanis, "Analysis of Premixed Charge Compression Ignition Combustion with a Sequential Fluid Mechanics-Multizone Chemical Kinetics Model," *SAE Tech. Pap.*, no. No. 2005–01–0115, 2005.

[11] P. Borgqvist, "The Low Load Limit of Gasoline Partially Premixed Combustion

(PPC) Experiments in a Light Duty Diesel Engine," Lund University, 2013.

[12] J. Wang, "Hybrid Robust Air-Path Control for Diesel Engines Operating Conventional and Low Temperature Combustion Modes," *IEEE Trans. Control Syst. Technol.*, vol. 16, no. 6, pp. 1138–1151, Nov. 2008.

[13] N. Ravi, M. J. Roelle, H. Liao, A. F. Jungkunz, C. Chang, S. Park, and J. C. Gerdes, "Model-Based Control of HCCI Engines Using Exhaust Recompression," *IEEE Trans. Control Syst. Technol.*, vol. 18, no. 6, pp. 1289–1302, 2010.

[14] F. Karlsson, "Modelling the Intake Manifold Dynamics in a Diesel Engine," Linkoping, 2001.

[15] G. M. Shaver, M. Roelle, and J. C. Gerdes, "A two-input two-output control model of HCCI engines," *2006 Am. Control Conf.*, p. 6 pp., 2006.

[16] M. Sellnau, J. Sinnamon, L. Oberdier, and G. Technologies, "Development of a Practical Tool for Residual Gas Estimation in IC Engines Carroll Dase , Matthew Viele and Kris Quillen John Silvestri and Iakovos Papadimitriou," *SAE 2009-01-0695*, 2009.

[17] F. Yan and J. Wang, "Design and Robustness Analysis of Discrete Observers for Diesel Engine In-Cylinder Oxygen Mass Fraction Cycle-by-Cycle Estimation," *IEEE Trans. Control Syst. Technol.*, vol. 20, no. 1, pp. 72–83, 2012.

[18] J. Meyer, S. Midlam-mohler, and S. Yurkovich, "In-cylinder Oxygen Concentration Estimation for Diesel Engines Via Transport Delay Modeling," in *American control conference*, 2011, pp. 396–401.

[19] K. Akihama, Y. Takatori, K. Inagaki, a. M. Dean, and S. Sasaki, "Mechanism of the smokeless Rich Diesel combustion by reducing temperature," *SAE Tech. Pap.*,

vol. 2001, no. 2001–01–0655, pp. 2001–01–0655, 2001.

[20] F. Willems, E. Doosje, F. Engels, and X. Seykens, "Cylinder Pressure-Based Control in Heavy-Duty EGR Diesel Engines Using a Virtual Heat Release and Emission Sensor," 2010.

[21] T. Guohong, W. Zhi, W. Jianxin, H. Xu, and S. Shijin, "Effects of Key Factors on the Engine Combustion Mode Switching Between HCCI and SI," *J. Eng. Gas Turbines Power*, vol. 131, no. 1, p. 012803, 2009.

[22] E. Hellström, A. Stefanopoulou, J. Vavra, A. Babajimopoulos, D. Assanis, L.Jiang, and H.Yilmaz, "Understanding the dynamic evolution of cyclic variability at the operating limits of HCCI engines with negative valve overlap," *SAE Tech. Pap.*, no. No.2012–01–1106, 2012.

[23] S. Karagiorgis, N. Collings, K. Glover, N. Coghlan, and A.Petridis, "Residual Gas Fraction Measurement and Estimation on a Homogeneous Charge Compression Ignition Engine Utilizing the Negative Valve Overlap Strategy," *SAE Tech. Pap.*, no. No.2006–01–3276, 2006.

Chaper 2. Paper 1 Extended Kalman Filter Based In-Cylinder Temperature Estimation for Diesel Engines with Thermocouple Lag Compensation

2.1 Citation and Main Contributor

Chen, S., & Yan, F. Extended Kalman Filter Based In-Cylinder Temperature Estimation for Diesel Engines with Thermocouple Lag Compensation. *Journal of Dynamic Systems, Measurement, and Control*, 136(5), DOI: 10.1115/1.4027170, 2014.

The main contributor to this paper is the first author-Chen Song (contributes more than 70%).

2.2 Brief Introduction

The in-cylinder temperature information is critical for auto-ignition combustion control in Diesel engines, but difficult to be directly accessed at low cost in production engines. Through investigating the thermodynamics of T_{ivc} (the in-cylinder temperature at intake valve closure), cycle-by-cycle models are proposed in this paper for the estimation of in-cylinder temperature at the crank angle of intake valve closing (IVC), referred to as T_{ivc}. As another two states, the dynamics of the measurable intake (T_{int}) and exhaust (T_{exh}) manifolds temperature are also derived. Totally, a three states (T_{ivc}, T_{int} and T_{exh}) system is constructed and an Extended Kalman Filter (EKF) based method was devised by utilizing the measurable temperature information (T_{int} and T_{exh}) to estimate the T_{ivc}.

As for the measurement, the widely used temperature sensor, thermocouple, suffers from the slow responses due to its physical and chemical characteristics. The measurement error led by the thermocouples' lag is nontrivial, especially in fast transient

conditions. In this chapter, the thermocouples are modeled as first-order lags with varying time constants. It turns out that the measured temperature signals need to be reconstructed for a better accuracy. In the proposed EKF estimation method, this issue can be effectively addressed by analyzing the measurement errors and properly selecting the noises covariance matrices. The proposed estimation method was validated through a high-fidelity GT-power engine model.

The In-cylinder temperature will be used to model the combustion phasing, i.e. the CA50 (the crank angle when 50% of the fuel consumed) in further research. CA50 is a critical indicator to showing the combustion process. Comparing with other indicators, such as CA10 (the crank angle when 10% of the fuel consumed), CA50 is more robust and thus widely applied.

2.3 Main contributions

1) The in-cylinder temperature dynamics equation is derived.
2) The in-cylinder temperature dynamics combines with the intake and exhaust manifold temperature dynamics facilitating the estimation of the in-cylinder temperature in EKF.
3) The error caused by the thermocouple lag is attenuated by re-deriving the system process and measurement covariance matrices.

2.4 Full content of Paper 1

Extended Kalman Filter Based In-Cylinder Temperature Estimation for Diesel Engines with Thermocouple Lag Compensation

Song Chen and Fengjun Yan*
Department of Mechanical Engineering
McMaster University
Hamilton, ON, L8S 4L7 Canada

Abstract —The in-cylinder temperature information is critical for auto-ignition combustion control in Diesel engines, but difficult to be directly accessed at low cost in production engines. Through investigating the thermodynamics of T_{ivc}, cycle-by-cycle models are proposed in this paper for the estimation of in-cylinder temperature at the crank angle of intake valve closing (IVC), referred to as T_{ivc}. An Extended Kalman Filter (EKF) based method was devised by utilizing the measurable temperature information from the intake and exhaust manifolds. Due to the fact that measured temperature signals by typical thermocouples have slow responses which can be modeled as first order lags with varying time-constant, temperature signals need to be reconstructed in transient conditions. In the proposed EKF estimation method, this issue can be effectively addressed by analyzing the measurement errors and properly selecting the noises covariance matrices. The proposed estimation method was validated through a high-fidelity GT-Power engine model.

Keywords: In-cylinder temperature, Extended Kalman filter, Thermocouple, Time constant

---

Song Chen is with the Department of Mechanical Engineering at McMaster University, Hamilton, ON Canada, email: chens78@mcmaster.ca.
*Corresponding author. Fengjun Yan is with the Department of Mechanical Engineering at McMaster University, Hamilton, ON Canada, email: yanfeng@mcmaster.ca.
This research was supported by NSERC Discover Program Award RGPIN/436147-2013.

I. Introduction

In order to achieve high combustion efficiency and low pollutant emission, precisely control of in-cylinder conditions, such as the pressure, temperature and burned gas fraction (BGF) plays a vital role, especially in the field of engine advanced combustion modes including homogeneous charge compression ignition (HCCI), low temperature diffusion combustion (LTDC), and premixed charge compression ignition (PCCI) [1].

As one of the important conditions, the in-cylinder temperature, especially the temperature at the crank angle of intake valve closing, T_{ivc}, has significant impacts on combustion auto-ignition process and other gasses such as residual gas and burned gas[5] [6] . [7] introduced an air-path dynamics based strategy to accurately control the combustion phasing by using injection timing for conventional Diesel engines, in which the T_{ivc} is a critical term for the ignition modeling. The in-cylinder temperature is non-trivial in the estimation for residual gas for a Diesel engine in [8]. To control and estimate the in-cylinder burned gas rate, [9] proposed a control strategy by coordinating the low-level controllers acting separately on the EGR valve and on the variable valve actuator for a Diesel engine, where T_{ivc} has a significant impact on the final results.

As the in-cylinder temperature is difficult to be directly measured, some optical based approaches were introduced to estimate it[10]. Shearing interferometry is an estimating approach based on image processing [10]. Color-Ratio Pyrometry is another technique for estimating temperature and commonly used for characterizing combustion [11]. However, due to the high cost, complex equipment, and the high sensitivity to

vibrations, these optical methods can only be applied in experimental analysis and hardly be used in real production practice.

In some literature [6], T_{ivc} can be approximated by the weighted temperature of the mixing charge in the cylinder. In this method, T_{ivc} is determined by the weighting temperatures of the aspirated intake gas, the rebreathing gas, and the residual gas with different mass contributions. However, due to inadequate information on the mass and temperature of the residual gas, forcibly taking the exhaust temperature as the residual gas temperature and roughly estimating its mass making this method falls in low accuracy for in-cylinder auto-ignition applications in advanced combustion mode control.

The proposed method in this paper is to utilize the strong couplings between the intake/exhaust manifold conditions and T_{ivc} in a Diesel engine. Cycle-by-cycle dynamic models regarding T_{ivc} are proposed through engine breathing-in, breathing-out, mixing process, and thermodynamics. With the dynamics models, T_{ivc} can be estimated in a predictor-corrector fashion through an Extended Kalman Filter (EKF) approach.

From the temperature measurement point of view, thermocouples are widely used due to their low cost and robustness [14]. However, one of the main drawbacks of thermocouples is the slow response, which can be modeled as first-order lags with varying time constants. Such a first-order lag is not trivial in transient operating conditions and the temperature measurement signals required reconstructions/compensations with estimated time constants for the first order lag [16]. When the estimated time constants are inaccurate, temperature signals will go away from the real value in the transient operations. To address this issue, the measurement and

process errors caused by the improper thermocouple time constant estimation were considered in the noise covariance matrices derivation in EKF. The proposed in-cylinder temperature estimation method was further analyzed with the presence of thermocouple first order lag and validated in the situation with large thermocouple time-constant estimation error.

The proposed method was validated through a GT-Power (a widely used engine simulation software for industrial and academic fields) engine model.

The contributions of this paper are: 1) proposing cycle-by-cycle control-oriented dynamic models for T_{ivc} ; 2) developing EKF estimating method to estimate T_{ivc} in a predictor-corrector fashion; 3) analyzing and deriving the noise covariance matrices to compensate the estimation error for thermocouple first order lag time constants.

The arrangements of this paper are as follows: in the 2nd section, the dynamic models for the temperatures for T_{ivc} were constructed. The EKF-based state estimation method was devised in the 3rd section. The proposed method was validated in the 4th section. In the 5th section, the proposed method was improved and evaluated with delay responses of thermocouples. Conclusions are given in the last section.

II. SYSTEM MODELING

According to the mass conservation, the in-cylinder temperature at intake valve closing (T_{ivc}) is the weighted temperature of the mixed gas from the intake manifold and the residuals gas [5]:

$$T_{ivc}(k+1)=\frac{m_{int-cyl}(k)T_{int}(k)+m_{res}(k)T_{res}(k)}{m_{int-cyl}(k)+m_{res}(k)}, \quad (1)$$

where the subscript res stands for the residual gas, $int-cyl$ means the charge from intake manifold flows to the cylinder, m and T represent the mass and temperature respectively, and k means the k^{th} cycle.

As can be seen from Eq. (1), T_{ivc} is determined by the temperatures and the mass of the aspirated intake gas and residual gas. In the following two subsections, the dynamic models for intake/exhaust manifold temperature and residual gas are described.

A. Modeling for intake and exhaust manifold temperatures

The intake and exhaust manifold temperatures are strongly related to T_{ivc} as in Eq. (1). Their dynamic models are derived in this section.

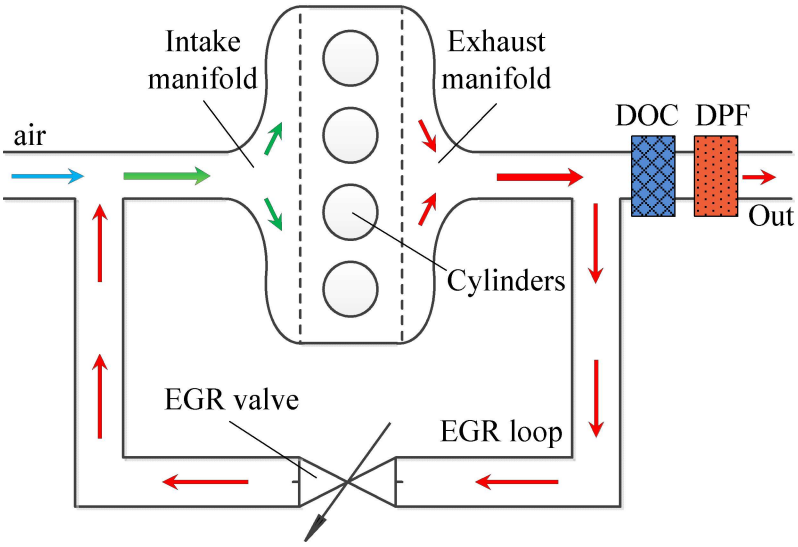

Fig.1 Diesel engine schematic diagram

The air-path loop with exhaust gas recirculation (EGR) is shown in Fig.1. Neglecting the heat transfer in the manifold wall and applying mass and energy conservation to the intake manifold gives [5]:

$$\dot{T}_{int} = \frac{RT_{int}}{P_{int}V_{int}}[\dot{m}_{egr}(\gamma_e T_{egr} - T_{int}) + \dot{m}_{air}(\gamma_c T_{air} - T_{int}) + \dot{m}_{int\text{-}cyl}(T_{int} - \gamma_c T_{cyl})], \tag{2}$$

where the subscript egr, air, int, cyl stand for exhaust gas recirculation, fresh air, the gas in the intake manifold, and the gas into the cylinder, respectively; $\dot{m}$ is the mass flow rate and γ is the heat specific ratio.

The mass flow rate through valves, including $\dot{m}_{egr}$ and $\dot{m}_{air}$, can be calculated by the orifice equations [17] as follows:

a) When the flow is not choked ($\frac{p_d}{p_u} > \left(\frac{2}{\gamma+1}\right)^{\gamma/(\gamma-1)}$),

$$\dot{m} = \frac{C_D A_R p_u}{\sqrt{RT_u}}\left(\frac{p_d}{p_u}\right)^{1/\gamma}\left\{\frac{2\gamma}{\gamma-1}\left[1-\left(\frac{p_d}{p_u}\right)^{(\gamma-1)/\gamma}\right]\right\}^{1/2}, \tag{3}$$

b) When the flow is choked ($\frac{p_d}{p_u} \le \left(\frac{2}{\gamma+1}\right)^{\gamma/(\gamma-1)}$),

$$\dot{m} = \frac{C_D A_R p_u}{\sqrt{RT_u}}\sqrt{\gamma}\left(\frac{2}{\gamma+1}\right)^{(\gamma+1)/2(\gamma-1)}, \tag{4}$$

where C_D is the discharge coefficient, subscript u and d stand for upstream and downstream respectively, A_R is the valve reference area, and γ is the specific heat ratio.

The air-mass to cylinders, $\dot{m}_{int\text{-}cyl}$, can be computed based on the speed density equation as follows:

$$\dot{m}_{int\text{-}cyl} = \frac{\lambda_v P_{int} V_d N}{2RT_{int}}, \tag{5}$$

where λ_v is the volumetric efficiency, N is the engine speed, and V_d is the swept volume.

Note that T_{cyl} in Eq. (2) cannot be directly measured but approximated by the intake manifold temperature. By ideal gas law and energy conservation, the dynamic of pressure can be expressed as[5]:

$$\dot{P}_{int} = \frac{R}{V_{int}}(\dot{m}_{egr}\gamma_e T_{egr} + \dot{m}_{air}\gamma_c T_{air} - \dot{m}_{int\text{-}cyl}\gamma_c T_{cyl}). \tag{6}$$

Combining Eq. (2) and Eq.(6) gives:

$$\dot{T}_{int} = \frac{T_{int}}{P_{int}}\dot{P}_{int} - \frac{RT_{int}^2}{P_{int}V_{int}}\left[\dot{m}_{egr} + \dot{m}_{air} - \dot{m}_{int\text{-}cyl}\right]. \tag{7}$$

Similarly, the dynamic model for exhaust manifold temperature can be expressed as:

$$\dot{T}_{exh} = \frac{RT_{exh}}{P_{exh}V_{exh}}[\dot{m}_{cyl-exh}(\gamma_e T_{res} - T_{exh}) + \dot{m}_{egr}(T_{exh} - \gamma_e T_{egr}) + \dot{m}_{out}(T_{exh} - \gamma_e T_{out})] \tag{8}$$

where the subscript $cyl-exh$ and out are the gas flows into the exhaust manifold and the ambiance respectively. $\dot{m}_{cyl-exh}$ is assumed equal to the air mass into cylinder, $\dot{m}_{int\text{-}cyl}$. $\dot{m}_{out}$ is calculated by $\dot{m}_{cyl-exh}$ subtracting $\dot{m}_{egr}$.

B. Modeling for residual gas

Motivated by [18], the residual gas model is derived as follows. For notation simplicity, the cycle index k is omitted in the following derivations.

It is assumed that the compression and expansion processes are. Based on the adiabatic assumption, the in-cylinder temperature right before the combustion can be calculated by the following equation:

$$T_{bc} = T_{ivc}\left(\frac{V_{cyl}(\theta_{ivc})}{V_c(\theta_c)}\right)^{(\gamma_c - 1)}, \tag{9}$$

where the subscript bc means before combustion, γ_c is the polytropic index of the gas before combustion, $V_{cyl}(\theta)$ is the volume of the engine at crank angle θ, θ_{ivc} and θ_c are the crank angles at IVC and the end of combustion respectively.

Assuming the heat of fuel released instantaneously during combustion, so the temperature right after combustion can be calculated as:

$$T_{ac} = T_{bc} + \Delta T, \tag{10}$$

where subscript ac means after combustion, ΔT is the increased temperature due to the heat from the combustion.

To be noted, this assumption is reasonable, since the combustion duration is quite small and it has little impact on the value of residual gas temperature from the chemical energy release point of view.

ΔT can be computed as:

$$\Delta T = e\frac{RT_{ivc}Q_{LHV}m_f}{C_v P_{ivc}V_{ivc}}, \tag{11}$$

where Q_{LHV} is the lower heating value of the fuel, m_f is the amount of fuel injected per cycle, e is a factor that captures the combustion efficiency and heat transfer through the cylinder totally. e can be pre-tabulated for varies combustion durations and AFRs(air-fuel ratios).

Based on the process from the end of combustion to the exhaust valve opening (EVO), the temperature at EVO , T_{evo}, can be derived as:

$$T_{evo} = T_{ac}\left(\frac{V_{cyl}(\theta_c)}{V_{cyl}(\theta_{evo})}\right)^{(\gamma_e - 1)}. \tag{12}$$

where γ_e is the polytropic index of the gas after combustion.

By the expansion process from EVO to the exhaust valve closing (EVC), the temperature of blowdown gas can be expressed as:

$$T_{bd} = T_{evo}\left(\frac{P_{exh}}{P_{evo}}\right)^{\frac{\gamma_e - 1}{\gamma_e}}, \tag{13}$$

where the subscript bd and exh stand for blowdown and exhaust manifold respectively, P is the pressure.

Assuming the temperature of residual gas equals to the blowdown gas, the residual gas temperature can be derived by combining Eq. (9) -(13):

$$T_{res} = T_{ivc}\left(\frac{P_{exh}}{P_{ivc}}\right)^{1-\frac{1}{\gamma_e}} \times \left\{\left(\frac{V_{cyl}(\theta_{ivc})}{V_{cyl}(\theta_c)}\right)^{\gamma_c-1}\left(\frac{V_{cyl}(\theta_c)}{V_{cyl}(\theta_{evo})}\right)^{\gamma_e-1} + \frac{eRQ_{LHV}m_f}{C_v V_{cyl}(\theta_{ivc})P_{ivc}}\left(\frac{V_{cyl}(\theta_c)}{V_{cyl}(\theta_{evo})}\right)^{\gamma_e-1}\right\}. \quad (14)$$

In Eq. (14), θ_c indicates the crank angle at the end of combustion and can be calculated based on the heat release equation[19]:

$$\frac{dQ_{HR}^{net}}{d\theta} = \frac{\gamma}{\gamma-1}p_{cyl}\frac{dV_{cyl}}{d\theta} + \frac{1}{\gamma-1}V_{cyl}\frac{dP_{cyl}}{d\theta}, \quad (15)$$

where Q_{HR}^{net} is the net released heat, V_{cyl} and p_{cyl} are the volume and pressure of the cylinder. Therefore, θ_c is a threshold at which crank angle the heat release rate goes below that threshold.

Applying the ideal gas law, the mass of the residual gas is:

$$m_{res} = \frac{P_{exh}V_{evc}}{RT_{res}}. \quad (16)$$

Discretizing Eq.(15), Eq. (16) and combining them with Eq. (1), Eq.(7) and Eq. (8) give the resultant models:

$$\begin{cases} T_{ivc}(k+1) = \dfrac{AT_{ivc}(k)[Rm_{int-cyl}(k)T_{int}(k) + P_{exh}(k)V_{evc}(k)]}{AT_{ivc}(k)m_{int-cyl}(k)R + P_{exh}(k)V_{evc}(k)} \\ T_{int}(k+1) = BT_{int}^2(k) + CT_{int}(k) \\ T_{exh}(k+1) = DT_{exh}^2(k) + ET_{exh}(k) + HT_{exh}(k)T_{ivc}(k) \end{cases}, \quad (17)$$

where

$$A = \left(\frac{P_{exh}(k)}{P_{ivc}(k)}\right)^{1-\frac{1}{\gamma_e}} \times \left\{\left(\frac{V_{cyl}(\theta_{ivc})}{V_{cyl}[\theta_c(k)]}\right)^{\gamma_c-1}\left(\frac{V_{cyl}[\theta_c(k)]}{V_{cyl}(\theta_{evo})}\right)^{\gamma_e-1} + \frac{eRQ_{LHV}m_f}{C_v V_{cyl}(\theta_{ivc})P_{ivc}(k)}\left(\frac{V_{cyl}[\theta_c(k)]}{V_{cyl}(\theta_{evo})}\right)^{\gamma_e-1}\right\}, \quad (18)$$

$$B = -\frac{R}{P_{int}(k)V_{int}}\left[\Delta m_{egr}(k) + \Delta m_{air}(k) - \Delta m_{int-cyl}(k)\right], \tag{19}$$

$$C = \frac{\Delta P_{int}(k)}{P_{int}(k)} + 1, \tag{20}$$

$$D = \frac{R}{P_{exh}(k)V_{exh}(k)}[\Delta m_{out}(k) + \Delta m_{exh}(k) - \Delta m_{cyl-exh}(k)], \tag{21}$$

$$E = \frac{R}{P_{exh}(k)V_{exh}(k)}[1 - \Delta m_{egr}(k)\gamma_e T_{egr}(k) - \Delta m_{out}(k)\gamma_e T_{out}(k)], \tag{22}$$

$$H = \frac{R}{P_{exh}(k)V_{exh}(k)}\Delta m_{cyl-exh}(k)\gamma_e. \tag{23}$$

In Eq. (19) -(23), Δ is the backward difference operator:

$$\Delta m(k) = m(k) - m(k-1). \tag{24}$$

III. Extended Kalman Filter Design

Rewriting Eq. (17) gets:

$$\begin{cases} T_{ivc}(k+1) = f(T_{ivc}(k), T_{int}(k)) \\ T_{int}(k+1) = g(T_{int}(k)) \\ T_{exh}(k+1) = h(T_{ivc}(k), T_{exh}(k)) \end{cases}. \tag{25}$$

As can be seen from Eq. (25), the in-cylinder temperature at IVC, i.e., T_{ivc} is one of the states in the dynamic models. The estimation can be addressed by utilizing the other two measurable states, i.e., T_{int} and T_{exh}. Considering the noise rejection and predictor-corrector properties, an Extended Kalman Filter (EKF)-based method was used in this paper.

The functions of Eq. (25) are denoted by:

$$\Phi = [f, g, h]^T. \tag{26}$$

Denote $\boldsymbol{Q}$ and $\boldsymbol{R}$ as the covariance matrices of model and measurement noises, respectively:

$$\begin{aligned} \boldsymbol{Q} &= diag[q_1, q_2, q_3]' \\ \boldsymbol{R} &= diag[r_1, r_2] \end{aligned} \tag{27}$$

where $q_i, i = 1,2,3$, refer to the process noise variance; r_j, $i = 1,2$, refer to the variance of the sensor noise.

There are two measurements in this system: T_{int} and T_{exh}. Denote the measurement matrix as $\boldsymbol{H}$:

$$\boldsymbol{H} = \begin{bmatrix} 0 & 1 & 0 \\ 0 & 0 & 1 \end{bmatrix}', \tag{28}$$

Denote $\boldsymbol{Z}$ as the measurement:

$$\boldsymbol{Z} = \boldsymbol{H} \begin{bmatrix} T_{ivc} \\ T_{int} \\ T_{exh} \end{bmatrix}. \tag{29}$$

The estimation procedure of EKF contains the following 6 steps [20].

1) State prediction:

$$\begin{bmatrix} \hat{T}_{ivc}(k+1,k) \\ \hat{T}_{int}(k+1,k) \\ \hat{T}_{exh}(k+1,k) \end{bmatrix} = \begin{bmatrix} f(T_{ivc}(k), T_{int}(k)) \\ g(T_{int}(k)) \\ h(T_{ivc}(k), T_{exh}(k)) \end{bmatrix}. \tag{30}$$

2) State prediction covariance:

$$\boldsymbol{P}(k+1,k)=\boldsymbol{F}(k)\boldsymbol{P}(k,k)\boldsymbol{F}(k)^{T}+\boldsymbol{Q}, \tag{31}$$

where $\boldsymbol{F}(k)$ is the Jacobian matrix of Φ at the cycle of k:

$$\boldsymbol{F}(k)=\begin{bmatrix} \left.\frac{\partial f}{\partial T_{ivc}}\right|_{\hat{T}_{ivc}(k,k),\hat{T}_{int}(k,k)} & \left.\frac{\partial f}{\partial T_{int}}\right|_{\hat{T}_{ivc}(k,k),\hat{T}_{int}(k,k)} & 0 \\ 0 & \left.\frac{\partial g}{\partial T_{int}}\right|_{\hat{T}_{int}(k,k)} & 0 \\ \left.\frac{\partial h}{\partial T_{ivc}}\right|_{\hat{T}_{ivc}(k,k),\hat{T}_{exh}(k,k)} & 0 & \left.\frac{\partial h}{\partial T_{exh}}\right|_{\hat{T}_{ivc}(k,k),\hat{T}_{exh}(k,k)} \end{bmatrix}. \tag{32}$$

3) Innovation covariance:

$$\boldsymbol{S}(k+1)=\boldsymbol{R}+\boldsymbol{H}\boldsymbol{P}(k+1,k)\boldsymbol{H}^{T}. \tag{33}$$

4) Filter gain:

$$\boldsymbol{W}(k+1)=\boldsymbol{P}(k+1,k)\boldsymbol{H}^{T}\boldsymbol{S}(k+1)^{-1}. \tag{34}$$

5) Updated state estimate:

$$\begin{bmatrix} \hat{T}_{ivc}(k+1,k+1) \\ \hat{T}_{int}(k+1,k+1) \\ \hat{T}_{exh}(k+1,k+1) \end{bmatrix}=\begin{bmatrix} \hat{T}_{ivc}(k+1,k) \\ \hat{T}_{int}(k+1,k) \\ \hat{T}_{exh}(k+1,k) \end{bmatrix}+\boldsymbol{W}(k+1)\left\{\boldsymbol{Z}(k+1)-\boldsymbol{H}\begin{bmatrix} \hat{T}_{ivc}(k+1,k) \\ \hat{T}_{int}(k+1,k) \\ \hat{T}_{exh}(k+1,k) \end{bmatrix}\right\}. \tag{35}$$

6) Updated state covariance:

$$\boldsymbol{P}(k+1,k+1)=\boldsymbol{F}(k)\boldsymbol{P}(k,k)\boldsymbol{F}(k)^{T}+\boldsymbol{Q} \tag{36}$$

The EKF was, therefore, developed by repeating the above procedures for each cycle.

IV. SIMULATION EVALUATION RESULTS

In this section, the proposed in-cylinder temperature (at IVC) estimation method was validated through a high-fidelity GT-Power engine model.

In the GT-Power model, a Diesel engine equipped with EGR system was constructed, as illustrated in Fig.1. The air-path and fuel-path actuators, including the EGR valve opening and the mass of injected fuel, are tuned to achieve desired in-cylinder conditions and combustion. The simulated engine operating condition is from middle-load goes to low-load conditions, by actively changing the injected fuel mass amounts, as shown in Fig.2, and the EGR valve opening, as shown in FIG.3.

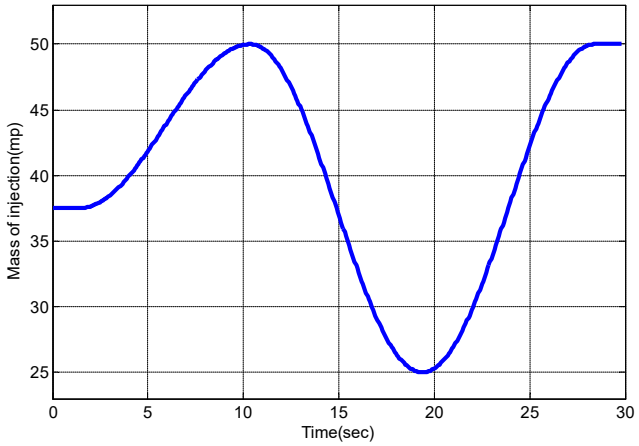

Fig.2 Mass of injected fuel

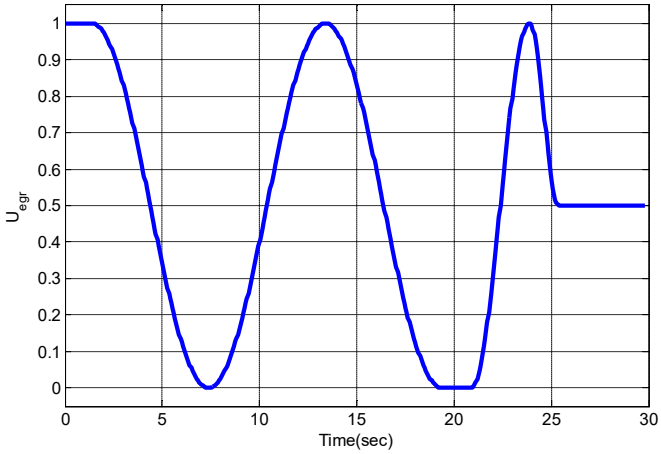

Fig.3 Normalized EGR valve opening (0 - fully close; 1 - fully open)

To mimic real situations, white noise with the magnitude of 5 was added on the simulated temperatures of intake and exhaust manifold as shown in Fig.4 and Fig.5.

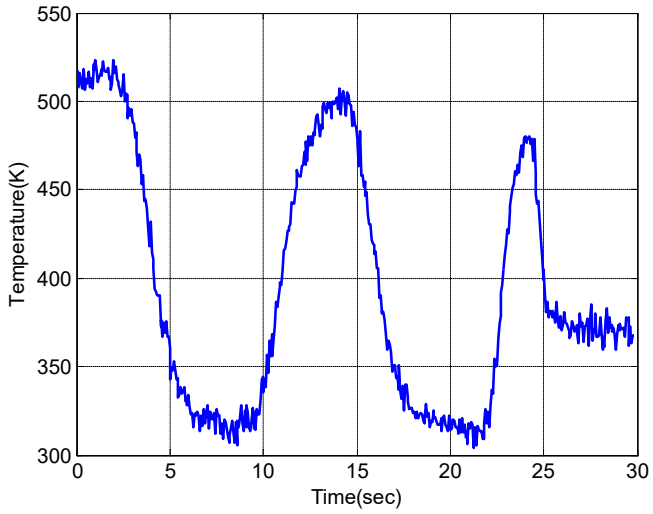

Fig.4 Simulated intake manifold temperature

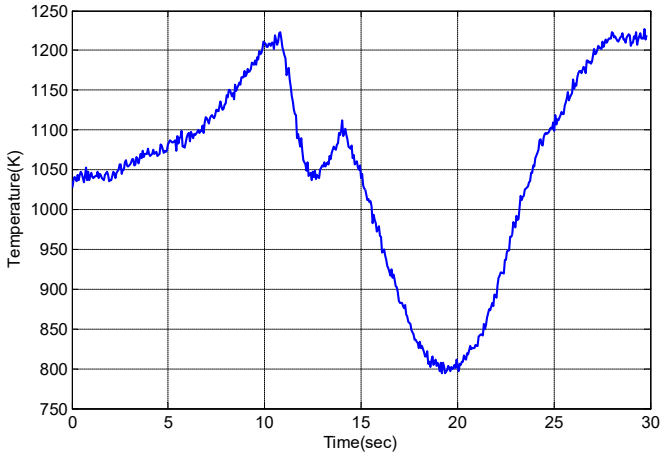

Fig.5 Simulated exhaust manifold temperature

Based on the added noises of intake and exhaust manifold temperatures as shown in Fig.4 and Fig.5, the noise covariance matrix of measurement $\boldsymbol{R}$ was set as:

$$\boldsymbol{R} = \begin{bmatrix} 5^2 & 0 \\ 0 & 5^2 \end{bmatrix} \tag{37}$$

Since the T_{ivc} is mostly composed of the inhaled gas from the intake manifold, i.e. T_{int} weights more than T_{exh} on T_{ivc}, the process noise covariance matrix $\boldsymbol{Q}$ was tuned as:

$$\boldsymbol{Q} = \begin{bmatrix} 8^2 & 0 & 0 \\ 0 & 5^2 & 0 \\ 0 & 0 & 5^2 \end{bmatrix} \tag{38}$$

Following the estimation procedure of *EKF* introduced above, the comparison between the estimated T_{ivc} and the GT-Power calculated $T_{ivc}(actual)$, which can be seen as the actual value, is shown in Fig.6.

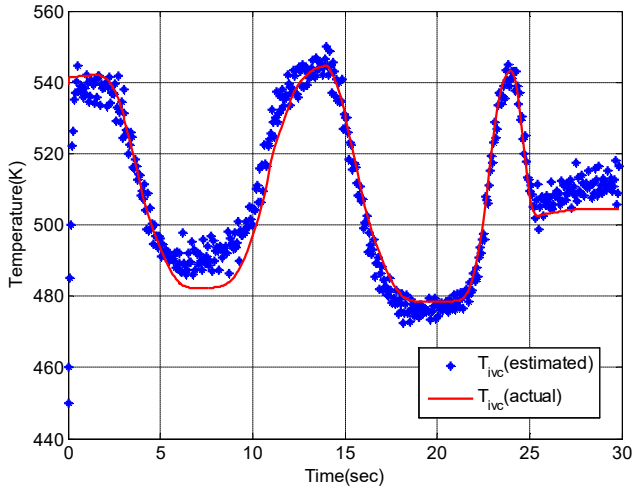

Fig.6 Comparison between the estimated and actual in-cylinder temperatures at *IVC*

The errors of the estimated T_{ivc} are shown in the following figure.

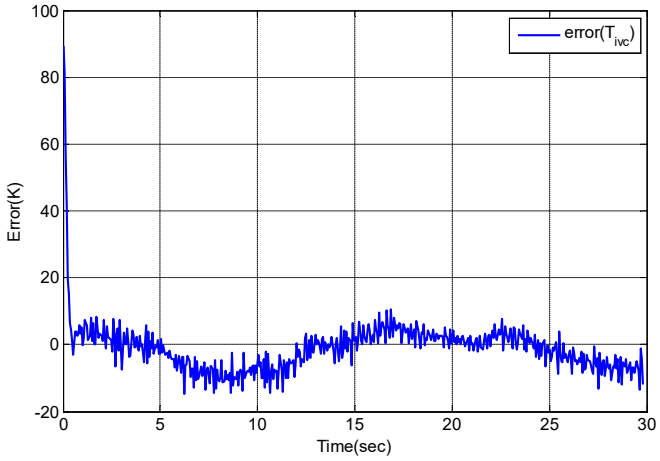

Fig.7 Error of the estimated in-cylinder temperature at *IVC*

From Fig.6 and Fig., the T_{ivc} can be well estimated by the proposed method. Generally, the maximum value of the error is around 10K (Kelvin), which is around 10% of overall temperature variation.

V. IN-CYLINDER TEMPERATURE ESTIMATION WITH DELAY OF THERMOCOUPLE RESPONSES

The thermocouple is widely used in many industrial applications such as in the manifolds of Diesel engines. However, it does not quickly respond to temperature fluctuations, and their cut-off frequencies are usually less than 10 Hertz [16]. In this section, a real engineering scenario is mimicked: the thermocouples suffer from the first order lag response and the measured temperature signals are reconstructed with inaccurate time-constant. The proposed estimation method was then modified for the in-cylinder temperature estimation with the presence of delayed thermocouple responses for the typical transient operating conditions as Fig.2 and Fig.3.

A. Analyzing and deriving the covariance matrices with delay of thermocouple responses

The measurement and process errors caused by the delayed responses of thermocouples will be derived in this subsection. Typically, the temperature signal obtained from a thermocouple has a first order lag and can typically be modeled as a first-order dynamic system [15]:

$$\tau \frac{dT_w}{dt} + T_w = T_g, \tag{39}$$

where T_w is the wire temperature, i.e. the measured temperature, and T_g is the gas temperature which can be seen as the actual temperature.

τ is the time-constant determined by the sensor's materials and operating conditions:

$$\tau = jD^{2-n}v_g^{-n}, \tag{40}$$

where j is almost constant; D is the diameter of the thermocouple wire; and v_g is the velocity of the gas which can be calculated based on the mass flow rate, gas density, and pipe diameter; n is an exponent arises from thermodynamics conditions, which is generally in the following range:

$$0.3 \le n \le 0.7 \cdot \tag{41}$$

To be noted, Eq. (40) is an empirical model only roughly describes the major factors of the thermocouple time constant and is not exactly known for real applications. A default value of the time constant can be found in the sensor datasheet. Also, there are many approaches to estimating the time constants, such as introducing another thermocouple with different time-constant [14] [21]or by utilizing the strong couplings between temperature and pressure [17].

With the errors on the estimated time-constant or the time constants from the sensor data sheet, there are temperature measurement errors during the transient operating conditions where the time constants vary over time. In this section, the EKF will be developed to address such a temperature measurement inaccuracy.

Assume that the gas temperature can be reconstructed from a measured temperature as:

$$T_g'(k+1) = \tau_e T_w(k+1) + (1-\tau_e)T_w(k) \cdot \tag{42}$$

where τ_e is the estimated time-constant (here we assume it is a default value in the sensor datasheet), T_g' is the reconstructed gas temperature based on the τ_e. Assuming the error on the estimated time constant is $\Delta\tau$, then the actual gas temperature should be:

$$T_g(k+1) = (\tau_e + \Delta\tau)T_w(k+1) + (1 - \tau_e - \Delta\tau)T_w(k). \tag{43}$$

Thus, the error of the reconstructed temperature is:

$$\Delta T_g(k+1) = T_g(k+1) - T_g'(k+1) = \Delta\tau[T_w(k+1) - T_w(k)] = \Delta\tau R_T. \tag{44}$$

As can be seen from Eq.(44), the measured temperature error is proportional to $\Delta\tau$ and the changing rate of the measured temperature - R_T.

Based on the definition, the measurement noise covariance in EKF can be expressed as:

$$\boldsymbol{R} = E\left\{\begin{bmatrix} \Delta T_{int}' + \Delta T_{int} \\ \Delta T_{exh}' + \Delta T_{exh} \end{bmatrix}\begin{bmatrix} \Delta T_{int}' + \Delta T_{int} & \Delta T_{exh}' + \Delta T_{exh} \end{bmatrix}\right\} \tag{45}$$

where $\Delta T'$ is the sensor noise and ΔT is the introduced error by $\Delta\tau$. Assuming $\Delta T'$ and ΔT are independent, then, $\boldsymbol{R}$ can be simplified as:

$$\boldsymbol{R} = \begin{bmatrix} u_{int} + v_{int} & 0 \\ 0 & u_{exh} + v_{exh} \end{bmatrix}, \tag{46}$$

where u is the variance of sensor noise, v is the variance of the introduced error by $\Delta\tau$ which can be calculated by Eq. (44).

According to Eq.(46), $\boldsymbol{R}$ is the combination of the variance of the sensor noise (as show Eq.(37)) and the error caused by the imperfect estimation of the time constant for the thermocouple first-order lag.

Taking the measurement error calculated from Eq.(44) back to the system dynamics Eq.(17) and neglecting the high order terms, the process uncertainties can be expressed as:

$$\begin{cases} \Delta T_{ivc}(k+1) = \dfrac{AT_{ivc}(k)Rm_{int-cyl}(k)\Delta T_{int}}{AT_{ivc}(k)Rm_{int-cyl}(k) + P_{exh}(k)V_{evc}(k)} \\ \Delta T_{int}(k+1) = 2BT'_{int}(k)\Delta T_{int} + C\Delta T_{int} \\ \Delta T_{exh}(k+1) = 2DT'_{exh}(k)\Delta T_{exh} + E\Delta T_{exh} \end{cases}, \tag{47}$$

where, T'_{int} and T'_{exh} are the reconstructed temperature for intake and exhaust manifolds respectively; ΔT is the reconstructed temperature error.

Similarly as deriving $\boldsymbol{R}$, the process noise covariance matrix $\boldsymbol{Q}$ can be calculated by:

$$\boldsymbol{Q} = \begin{bmatrix} \alpha_{ivc} + \beta_{ivc} & 0 & 0 \\ 0 & \alpha_{int} + \beta_{int} & 0 \\ 0 & 0 & \alpha_{exh} + \beta_{exh} \end{bmatrix}, \tag{48}$$

where the α is the process noise variance which has to be tuned Eq.(38), β is the introduced process uncertainty which can be calculated based on Eq.(47) .

B. Simulation validation

Assuming the diameter of the wire is 0.3mm, the exponent is 0.5 and typically choosing the j as 2×10^6, then the actual time-constant for thermocouples in the intake and exhaust manifolds are simulated by Eq.(40) in the following two figures:

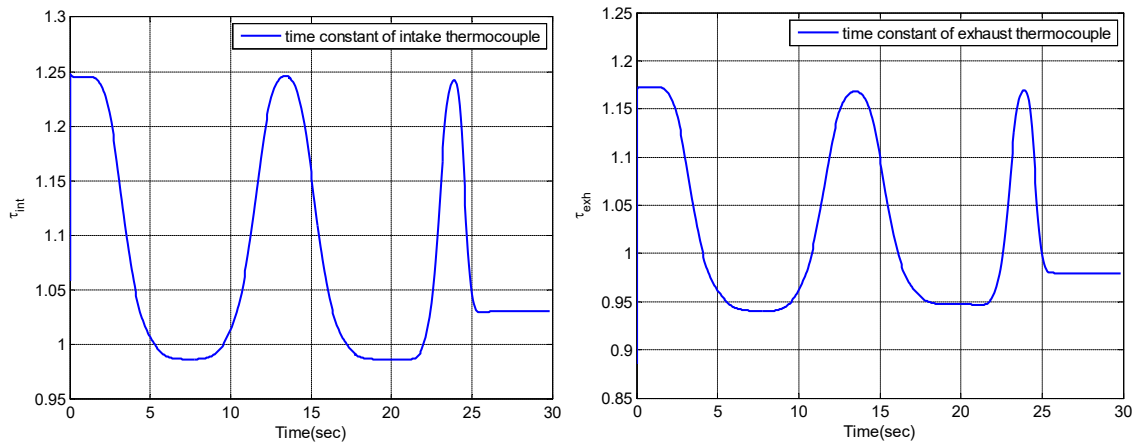

a) The time-constant of the thermocouple in the intake manifold

b) The time- constant of the thermocouple in the exhaust manifold

Fig.8 the simulated time-constant for the thermocouples in intake and exhaust manifolds

Assume that the default time-constants for the thermocouples in the intake and exhaust manifold are constant (these values can be found in the sensor datasheet.):

$$\begin{aligned} \tau_{int} &= 1.0s \\ \tau_{exh} &= 1.0s \end{aligned} \quad (49)$$

Comparing with the actual values as shown in Fig.8, the default time constants (Eq. (49)) have errors which are up to 0.25s.

From Fig.4 and Fig.5, the maximum changing rate is around 150K/s. Combining with the introduced noise caused by the differentiation, the changing rate, R_T was set as 200K/s. Since the time-constant errors are up to 0.25s, the temperature measurement errors are around 50K.

In the EKF design, the temperature inaccuracy due to the thermocouple property can be viewed as the measurement disturbances. Therefore, the matrix $\boldsymbol{R}$ was redefined as:

$$\boldsymbol{R} = \begin{bmatrix} 55^2 & 0 \\ 0 & 55^2 \end{bmatrix}. \tag{50}$$

Based on Eq.(38) and Eq.(50) -(48), the process covariance matrix $\boldsymbol{Q}$ was set as:

$$\boldsymbol{Q} = \begin{bmatrix} 58^2 & 0 & 0 \\ 0 & 55^2 & 0 \\ 0 & 0 & 55^2 \end{bmatrix}. \tag{51}$$

The estimated in-cylinder temperature at IVC and the estimation error without consideration of the sensor delay are showing in Fig.9 and the performance of the proposed method is showing in Fig.10.

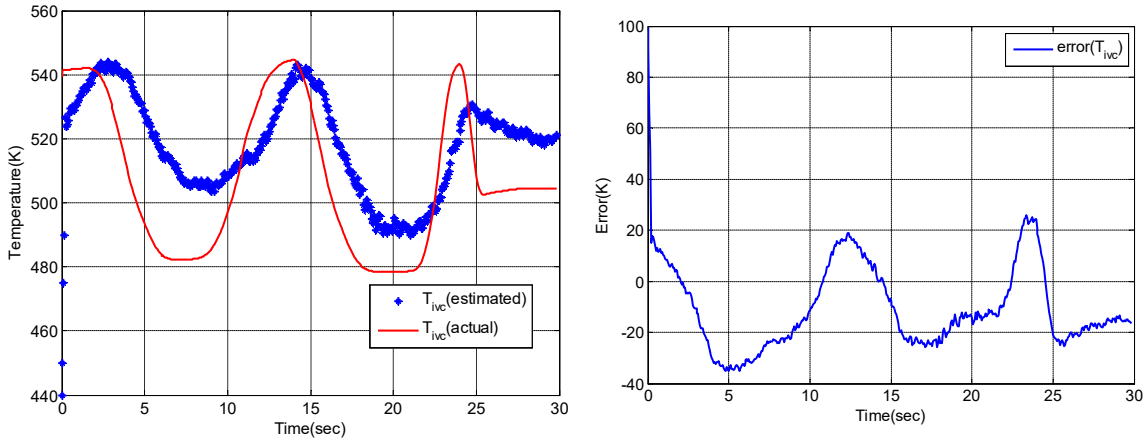

a) Estimated T_{ivc} b) Error of estimation

Fig.9 Estimated T_{ivc} without consideration of the thermocouple delay

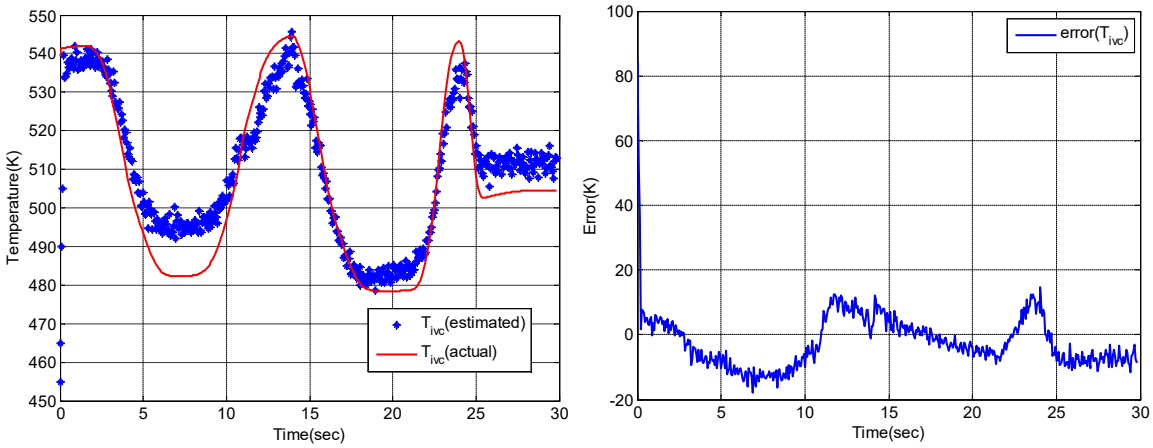

a) Estimated T_{ivc} b) Error of estimation

Fig.10 Estimated T_{ivc} by the proposed method

As can be seen from Fig.9, if the thermocouple delay was not considered, the largest estimation error can up to 30K. However, from Fig.10 the largest estimation error by the proposed method with imperfect compensation for the time-constant is around 15K. Therefore, by properly selecting $\boldsymbol{R}$ and $\boldsymbol{Q}$, the T_{ivc} can be relativity well estimated by the proposed method even with large time-constant estimation error.

VI. Conclusions

In this paper, dynamic models of in-cylinder temperature at IVC, temperatures in the intake and exhaust manifolds were derived. Based on the proposed models, the T_{ivc} was estimated by cycle-by-cycle based, EKF method. A GT-Power engine model was utilized to validate the effectiveness of the in-cylinder temperature estimation approach. Through the simulation results, the effectiveness of the proposed method was validated.

In order to evaluate the proposed method further, signals of thermocouples with delay responses were simulated for the measurement of the manifold temperatures.

Through analyzing the introduced measurement error and process uncertainties by the delay responses, the measurement and process noises covariance matrices were recalculated. Based on the recalculated covariance matrices, the proposed method was further validated in the case when there exists big (25%) time-constant estimation error for the thermocouple.

REFERENCES

[1] Bengtsson, J., Johansson, R., and Strandh, P., 2004, "Closed-loop combustion control of homogeneous charge compression ignition (HCCI) engine dynamics," International Journal of Adaptive Control and Signal Proceeding, pp.167-179.

[2] Chiang, C., Jankovic, M., and Stefanopoulou, A.G., 2007, "Nonlinear Observer-Based Control of Load Transitions in Homogeneous Charge Compression Ignition Engines," Transactions on Control Systems Technology, **15**(3), pp. 438–448.

[3] Aceves, S.M., Killingsworth, N. J., Flowers, D.L., and Miroslav, K., 2006, "A Simple HCCI Engine Model for Control," *Proc. 2006 IEEE International Conference on Control Applications*, IEEE, Munich, pp. 2424–2429.

[4] Shaver,G. M., Roelle, M., and Gerdes, J. C., 2005, "Decoupled Control of Combustion Timing and Work Output in Residual-Affected HCCI Engines," *2005 American Control Conference*, IEEE, Portland, pp. 3871–3876.

[5] Karlsson, F., 2001, "Modelling the Intake Manifold Dynamics in a Diesel engine," Swedish National Road and Transport Research Institute, Sweden.

[6] Shaver, G. M., Roelle, M., and Gerdes, J. C., 2006, "A Two-Input Two-Output Control Model of HCCI Engines," *Proc. 2006 American Control Conference*, IEEE, Minneapolis, pp. 472–477.

[7] Hillion, M., Buhlbuck , H., Chauvin, and J., 2009, "Combustion Control of Diesel Engines Using Injection Timing," SAE Paper No. 09PFL-0507.

[8] Sellnau, M., Sinamon, J., Oberdier, L., Dase, C., Viele, M., Quillen, K., and Papadimitriou, I., 2009, "Development of a Practical Tool for Residual Gas Estimation in IC Engines," SAE Paper No. 2009-01-0695.

[9] Leroy, T., Bitauld, M., Chauvinist, J., and Petit, N., 2009, "In-cylinder Burned Gas Rate Estimation and Control on VVA Diesel Engines," SAE Paper No. 2009-01-0366.

[10] Liu, D., Feng, H., 2006, "In-cylinder temperature field measurement with laser shearing interferometry for spark ignition engines," Optics and Lasers in Engineering, Elsevier Ltd., **44** (12) , pp.1258–1269.

[11] Ma, H., Stevens, R., and Stone, R., 2005, "In-Cylinder Temperature Estimation from an Optical Spray- Guided DISI Engine with Color-Ratio Pyrometry (CRP),"SAE Paper No. 06P-551.

[12] Dec, J. E., 2009, "Advanced compression-ignition engines—understanding the in-cylinder processes," Proceedings of the Combustion Institute, Elsevier Ltd., **32** (2), pp. 2727–2742.

[13] Yan, F. J., and Wang, J. M., 2012, "Engine Cycle-by-Cycle Cylinder Wall Temperature Observer-Based Estimation through Cylinder Pressure Signals," Journal of Dynamic Systems Measurement and Control, ASME, **134**(6), 061014.

[14] O'Reilly, P., Kee, R., Fleck, R., and McEntee, P., 2001, "Two-wire thermocouples: A nonlinear state estimation approach to temperature reconstruction," Review of Scientific Instruments, American Institute of Physics, **72**(8), pp. 3449-3457.

[15] Tagawa, M., Kato, K., and Ohta, Y., 2003, "Response compensation of temperature sensors: Frequency-domain estimation of thermal time constants," Review of Scientific Instruments, American Institute of Physics, **74**(6), pp.3171-3174.

[16] Hung, P. C., Irwin, G., Kee, R., and McLoone, S., 2005, "Difference equation approach to two-thermocouple sensor characterization in constant velocity flow environments," Review of Scientific Instruments, American Institute of Physics, **76**(2), 024902 .

[17] Yan, F. J., and Wang, J. M., 2012, "Pressure-based transient intake manifold temperature reconstruction in Diesel engines," Control Engineering Practice, Elsevier Ltd., **20** (5), pp. 531–538.

[18] Rausen, D. J., and Stefanopoulou, A. G., 2005, "A Mean-Value Model for Control of Homogeneous Charge Compression Ignition (HCCI)Engines," Journal of Dynamic Systems Measurement and Control, ASME , **127**(3), pp. 355-362.

[19] Grimm, B. M., and Jhonson, R. T., 1990, "Review of Simple Heat Release Computations," SAE Paper No. 90045.

[20] La Scala, B. F., Bitmead, R. R., and James, M. R., 1995, "Conditions for stability of the extended Kalman filter and their application to the frequency tracking problem," Mathematics of Control, Signals, and Systems, Springer-Verlag London Limited, **8**(1), pp.1-26.

[21] McLoone, S., Hung, P., Irwin, G., and Kee, R., 2006, "Exploiting A Priori Time Constant Ratio Information in Difference Equation Two-Thermocouple Sensor Characterization," Sensors Journal, IEEE, **6**(6), pp.1627-1637.

2.5 Remarks and Comments

1) GT-Suite is an engine simulation software, widely used in both industrial and academic fields. Numerous papers that benefited from GT-Suite can be found from journal articles and conference papers such as International Journal of Hydrogen Energy, Control Engineering Practice, IEEE transactions on Control Systems Technology and Journal of Dynamic Systems, Measurement and Control. Searching "GT-Suite" in Google Scholar gives more than 1000 results. Thus, GT-Suite is extensively used in this thesis to validate the proposed techniques.

2) The T_{ivc} model derived in this paper considers the effects of residual gas, intake gas, as well as the combustion process, thus, it can be directly applied to engines with other architectures, such as the engines with dual-loop EGR (exhaust gas recirculation) system.

3) In this paper, the heat transfer through the manifold wall is neglected. This assumption is necessary for the model based in-cylinder temperature estimation. Its effect on the results can be roughly evaluated as follows. Applying the energy conservation law to the intake manifold gives:

$$\frac{d(m_{\text{int}} c_v T_{\text{int}})}{dt} = \dot{m}_{air} c_p T_{air} + \dot{m}_{EGR} c_p T_{EGR} - \dot{m}_{\text{int}-cyl} c_p T_{\text{int}} - \dot{q}_{\text{int}} . \quad (1)$$

Therefore, the effect of heat transfer is captured by the last term: $\dot{q}_{\text{int}}$. Rearranging the equation 2 and equation 6 in the above paper gets:

$$\dot{T}_{int} = \frac{RT_{int}}{P_{int}V_{int}}[\dot{m}_{egr}(\gamma_e T_{egr} - T_{int}) + \dot{m}_{air}(\gamma_c T_{air} - T_{int}) + \dot{m}_{int\text{-}cyl}(T_{int} - \gamma_c T_{cyl}) - \frac{\dot{q}_{\text{int}}}{c_v}]. \quad (2)$$

$$\dot{P}_{int} = \frac{R}{V_{int}}(\dot{m}_{egr}\gamma_e T_{egr} + \dot{m}_{air}\gamma_c T_{air} - \dot{m}_{\text{int}-cyl}\gamma_c T_{cyl} - \frac{\dot{q}_{\text{int}}}{c_v}). \quad (3)$$

The expression for $\dot{q}_{\text{int}}$ is:

$$\dot{q}_{\text{int}} = h_{HT}A(T_{\text{int}} - T_{wall}). \quad (4)$$

where ,A is the intake manifold surface area, T_{wall} is the intake manifold wall temperature. h_{HT} is the heat transfer coefficient which determined by the intake pressure, temperature and gas velocity.

[1] Mentions that the heat transfer coefficient for the cylinder can be around 300 w/m^2/k. It should be much smaller for the intake manifold since the average pressure, temperature and gas velocity are much lower than them in the cylinder. Then the following assumptions can be safely made: h_{HT} is 100 w/m^{2}k , T_{wall} is 440k, T_{int} is in the range of [350k,500k] and A has the order of 10^{-2}m^2. Thus, $\frac{\dot{q}_{\text{int}}}{c_v}$ will be in the bound of: $\left|\frac{\dot{q}_{\text{int}}}{c_v}\right| \le 0.1$. It is less than 5% of other terms in the above equations.

Chaper 3. Paper 2 In-cylinder oxygen concentration estimation with in-cylinder pressure information for turbocharged Diesel engines

3.1 Citation and Main Contributor

Chen, S., Yan, F., Yao, C., and Yang, F. In-cylinder Oxygen Concentration Estimation with In-cylinder Pressure Information for Turbocharged Diesel Engines. *IEEE Transactions on Control Systems Technology* (under review).

The main contributor to this paper is the first author-Chen Song (contributes more than 70%).

3.2 Brief Introduction

The advanced combustion mode, also known as the low-temperature combustion can only be achieved in a very narrow range of operating conditions and close to the combustion stability boundaries. Therefore, in-cylinder conditions, such as the in-cylinder oxygen concentration, temperature and pressure are of critical importance in controlling advanced combustion modes.

In paper 1(Chapter II), the in-cylinder temperature is estimated by utilizing EKF, this paper deals with in-cylinder oxygen concentration estimation.

The in-cylinder oxygen concentration is hard to be accessed in commercial measurements. Conventionally, it is predicted by using the information from intake and exhaust manifolds (oxygen dynamics) even though that too many sources of uncertainties in this approach contaminate the accuracy of the final results. In this paper, the in-cylinder pressure information is also utilized to improve the robustness and performance of the in-cylinder oxygen concentration estimation. In the proposed method, the in-

cylinder oxygen information is modeled as a function of ignition delay which can be calculated by the in-cylinder pressure trace. Once the ignition delay obtained, the in-cylinder oxygen information can be obtained accordingly. By combining this information from ignition delay with oxygen dynamics, the in-cylinder oxygen concentration is estimated in a predictor-corrector fashion. The Smooth variable structure filter (SVSF) was utilized to associate the information of in-cylinder oxygen fraction from the two different sources (oxygen dynamics and ignition delay). The proposed method in this paper was validated through experimental research.

3.3 Main contributions

1) The ignition delay is utilized to extract the in-cylinder oxygen concentration for better estimation accuracy.
2) To combine the in-cylinder oxygen concentration from system dynamics and ignition delay, the relative new algorithm SVSF is applied in the engine research area.

3.4 Full content of Paper 2

In-cylinder oxygen concentration estimation with in-cylinder pressure information for turbocharged Diesel engines

Song Chen[1], Fengjun Yan[1,*], Changsheng Yao[2], Fuyuan Yang[2]
1. Department of Mechanical Engineering
McMaster University
Hamilton, ON, L8S 4L7 Canada
2. Department of Automotive Engineering, State Key Laboratory of Automotive Safety and Energy,
Tsinghua University
Beijing 100084, PR China

Abstract —The information of in-cylinder oxygen concentration is critical for advanced combustion control for Diesel engines running in a high-efficiency and low-emission mode, especially when the exhaust gas recirculation is extensively used. Since it is difficult to be accessed in commercial measurements, the in-cylinder oxygen concentration is conventionally predicted by using the information from intake and exhaust manifolds (oxygen dynamics), even though many sources of uncertainties in this approach will contaminate the estimation accuracy. In this paper, we applied a combined strategy by using both the oxygen dynamic models and the in-cylinder pressure signal to improve the accuracy and robustness of the in-cylinder oxygen concentration estimation. In the proposed method, the in-cylinder oxygen information is modeled as a function of ignition delay which can be calculated by the in-cylinder pressure trace. Thus, the in-cylinder oxygen concentration can be estimated in a predictor-corrector fashion, through combining the information from ignition delay and oxygen dynamics in the manifolds. A Smooth variable structure filter (SVSF) was utilized to associate the information of in-cylinder oxygen fraction from the two different sources (oxygen dynamics and in-cylinder pressure signal). The proposed method in this paper was validated through experimental research.

*Corresponding author. Fengjun Yan is with the Department of Mechanical Engineering at McMaster University, Hamilton, ON Canada, email: yanfeng@mcmaster.ca.

Keywords: In-cylinder oxygen concentration, Smooth variable structure filter

I. INTRODUCTION

Advanced combustion modes, including homogeneous charge compression ignition (HCCI)[1][2][3], low temperature diffusion combustion (LTDC)[4][5] and premixed charge compression ignition (PCCI) [6][7],etc. offer a promising solution for reducing the engine-out emissions and increasing engine efficiency for commercial vehicles. However, they can only be achieved in a very narrow range of operating conditions and close to the combustion stability boundaries[8][9]. It turns out that the in-cylinder conditions, such as the in-cylinder oxygen concentration, temperature and pressure are of critical importance in controlling advanced combustion modes[3]. Misfire and knock may occur due to slightly mismatched in-cylinder conditions[10][11].

It has been demonstrated that the in-cylinder conditions can be controlled by air-path system[12][4]. A typical air-path system of engines is shown in Fig. 1[13]. With the help of variable geometry turbocharger (VGT), EGR valve and variable valve time (VVT) system, the in-cylinder conditions can be controlled in a flexible fashion. However, given the high sensitivity of the advanced combustion modes on in-cylinder conditions, successfulness of the control strategy implementation requires highly accurate information of the in-cylinder conditions.

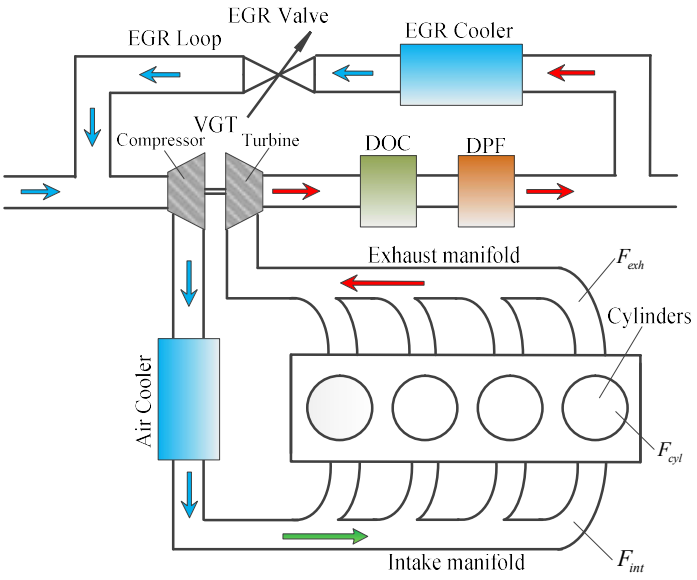

Fig. 1Engine architecture with variable geometry turbocharger

As one of the key in-cylinder conditions, the in-cylinder oxygen concentration can hardly be directly measured in commercial applications. The model-based observer is thus developed to estimate it. A nonlinear observer was designed in [14] based on a linear parameter-varying model for the estimation of the in-cylinder oxygen concentration at intake valve closing(IVC) on a cycle-by-cycle basis. The robustness of three observers for in-cylinder oxygen fraction was analyzed in [15] based on input to state stability(ISS) theory. By capturing the effects of the time-varying transport delay, a plug flow based oxygen concentration model was derived in [16], and the in-cylinder oxygen concentration can be predicted within an error of 0.2% of the true value in the RMS sense. However, the existing dynamic models are mostly derived based on mass/energy conservation and vulnerable to uncertainties, such as the inaccuracy of volumetric efficiency and the imperfectly calibrated orifice equation, etc.

In this paper, besides the oxygen dynamics, the in-cylinder pressure information was used for in-cylinder concentration estimation. For the in-cylinder oxygen concentration estimation, the in-cylinder oxygen concentration before combustion was modeled as a function of ignition delay, which can be captured by the in-cylinder pressure trace. A smooth variable structure filter (SVSF) was utilized to associate the information from the two different sources, i.e. the cylinder pressure signal and the oxygen dynamics through manifolds. Therefore, the in-cylinder oxygen concentration estimation was enabled in a predictor-corrector fashion. The proposed method in this paper was validated through experimental research and the results show that the estimation accuracy and robustness can be improved.

The arrangement of the rest of this paper is as follows: In section II, the conventional oxygen dynamic models are proposed. The in-cylinder oxygen concentration is modeled as a function of ignition delay in section III. Data association algorithm is designed in section IV. Experimental validation is presented in section V. Conclusive remarks are given in section VI.

II. DYNAMICS MODELING

The in-cylinder oxygen concentration can be captured by the dynamic relations between the air mass within cylinders and manifolds. In this section, the models for the residual gas mass, the oxygen fractions in the cylinder, and in the intake and exhaust manifolds, as well as for the fuel mass are introduced.

A. Variable geometry turbocharger (VGT)

The VGT consists of a compressor connected to a turbine via a shaft. The turbine is driven by the exhaust gas, and thus part of the energy kept in the exhaust system is

transferred to the compressor through the shaft. The turbocharger rotational speed (*N*) is derived from the power balance between the turbine and compressor[17].

$$JN\frac{dN}{dt} = P_{turbine} - P_{comp}, \tag{1}$$

where, $P_{turbine}, P_{comp}$ are the power of the turbine and the compressor, they can be expressed as follow[4][12]:

$$\begin{cases} P_{turbine} = \dot{m}_{turbine} C_p \eta_{turbine} T_{exh} \left[1 - \left(\frac{1}{PR_{turbine}} \right)^{\frac{\gamma-1}{\gamma}} \right], \\ P_{comp} = \dot{m}_{comp} C_p \frac{1}{\eta_{comp}} T_{uc} \left(PR_{comp}^{\frac{\gamma-1}{\gamma}} - 1 \right) \end{cases} \tag{2}$$

where, subscripts *comp*, *turbine*, *exh* are compressor, turbine and exhaust manifold; *PR* is pressure ratio, C_p is the heat specific ratio at constant pressure, η is the efficiency of the VGT, *T* is temperature.

The compressor efficiency and pressure ratio are given by maps, which depend on compressor speed and mass flow.

B. Cylinder, intake and exhaust manifolds oxygen fraction

Here, we take the instant of intake valve closing (IVC) as the boundary point for adjacent cycles. The in-cylinder gas in the next cycle is composed of the residual gas plus the injection and the aspirated gas from the intake manifold in the present cycle and then minus the exhaled gas:

$$m_{cyl}(k+1) = m_r(k) + m_i(k) + m_{int\text{-}c}(k) - m_{c-e}(k), \tag{3}$$

where, subscript, i is injection, $int-c$ is the charge flows from intake manifold to cylinder, $c-e$ is the charge flows from cylinder to exhaust manifold, r is the residual gas, cyl refers to cylinder; variable m is the air mass.

Applying ideal gas law, the residual mass, $m_r(k)$, can be estimated as:

$$m_r(k) = \frac{P_{ivc}(k)V_{ivc}(k)}{R\overline{T}_{int}(k)} - [m_{int\text{-}c}(k) + m_f(k)], \tag{4}$$

where, subscript int is the intake manifold, ivc is the crank angle at intake valve closing, f is the fuel; variable V is the cylinder volume.

To be noted, since the in-cylinder temperature is hard to be measured directly, it is replaced by $\overline{T}_{int}$ in equation (4). The introduced error by this approximation is acceptable. Assuming the $\overline{T}_{int}$ is 50 Kelvin less than the in-cylinder temperature, the residual fraction is 30%, and the combustion efficiency is 90%, then the estimation error for trapped unburned fuel mass is within 3%.

The aspirated gas from intake manifold to the cylinder, $m_{int\text{-}c}$, can be obtained by integrating the speed-density model:

$$\dot{m}_{int\text{-}c} = \frac{\lambda_v P_{int} V_d N_e}{120 R T_{int}}, \tag{5}$$

where λ_v is the volumetric efficiency which needs to be calibrated, λ_s is the stoichiometric oxygen fuel ratio, V_d is the swept volume, N_e is engine speed, R is the ideal gas constant.

Applying the oxygen conservation, the next in-cylinder oxygen is composed of present in-cylinder oxygen plus aspirated minus the consumed and the exhaled and then divided by the present cylinder mass:

$$F_{cyl}(k+1)=\frac{F_{cyl}(k)m_{cyl}(k)-m_f(k)\lambda_s-m_{c-e}(k)F_{c-e}(k)+F_{int}(k)m_{int\text{-}c}(k)}{m_{cyl}(k+1)}, \tag{6}$$

where, subscript $c-e$ is the charge flows from cylinder to exhaust manifold, variable F is the oxygen concentration.

The oxygen mass fraction of the gas exhales from cylinder to the exhaust manifold, or the oxygen concentration after combustion, F_{c-e}, is computed by the in-cylinder oxygen before combustion minus the consumed oxygen and then divided by the total gas mass:

$$F_{c-e}(k)=\frac{F_{cyl}(k)m_{cyl}(k)-m_f(k)\lambda_s}{m_{cyl}(k)+m_i(k)}. \tag{7}$$

The in-cylinder gas minus the residual gas is the gas exhales from cylinder to the exhaust manifold:

$$m_{c-e}(k)=m_{cyl}(k)-m_r(k). \tag{8}$$

The oxygen fraction dynamic equations for intake manifold can be computed as follows. The next intake manifold oxygen can be computed as the present oxygen in the manifold minus the aspirated gas, plus the turbocharged EGR gas and the fresh air:

$$F_{int}(k+1)=\frac{F_{int}(k)[m_{int}(k)-m_{int\text{-}c}(k)]+m_{egr}(k)F_{exh}(k)+F_{air}[m_{comp}(k)-m_{egr}(k)]}{m_{int}(k)+m_{comp}(k)-m_{int\text{-}c}(k)}. \tag{9}$$

Similarly, the current exhaust manifold oxygen can be computed as the previous oxygen in the manifold minus the turbocharged gas, plus the gas exhaled from cylinder:

$$F_{exh}(k+1)=\frac{F_{exh}(k)[m_{exh}(k)-m_{turbine}(k)]+F_{c-e}(k)m_{c-e}(k)}{m_{exh}(k)+m_{c-e}(k)-m_{turbine}(k)}. \tag{10}$$

where, the gas mass of the EGR valve, m_{egr} is calculated by the following orifice equation:

a) When the flow is not choked ($\frac{p_{ds}}{p_{up}}>\left(\frac{2}{\gamma+1}\right)^{\gamma/(\gamma-1)}$),

$$\dot{m}=\frac{C_D A_R p_{up}}{\sqrt{RT_{up}}}\left(\frac{p_{ds}}{p_{up}}\right)^{1/\gamma}\left\{\frac{2\gamma}{\gamma-1}\left[1-\left(\frac{p_{ds}}{p_{up}}\right)^{(\gamma-1)/\gamma}\right]\right\}^{1/2}, \tag{11}$$

b) When the flow is choked ($\frac{p_{ds}}{p_{up}}\le\left(\frac{2}{\gamma+1}\right)^{\gamma/(\gamma-1)}$),

$$\dot{m}=\frac{C_D A_R p_{up}}{\sqrt{RT_{up}}}\sqrt{\gamma}\left(\frac{2}{\gamma+1}\right)^{(\gamma+1)/2(\gamma-1)}, \tag{12}$$

where, γ is specific heat ratio.

The gas mass in the intake (exhaust) manifold, $m_{int(exh)}(k)$, can be computed by the ideal gas law:

$$m_{int(exh)}(k)=\frac{\overline{P}_{int(exh)}(k)V_{int(exh)}}{R\overline{T}_{int(exh)}}, \tag{13}$$

where, $\overline{P}_{int(exh)}$ and $\overline{T}_{int(exh)}$ are the mean pressure and temperature of the intake (exhaust).

C. System dynamic equations in state-space form

Taking the oxygen fractions of intake and exhaust manifolds and in-cylinder as three states, rearranging the above equation into state-space form:

$$\begin{bmatrix} F_{int}(k+1) \\ F_{exh}(k+1) \\ F_{cyl}(k+1) \end{bmatrix} = \begin{bmatrix} A_{1,1} & A_{1,2} & 0 \\ 0 & A_{2,2} & A_{2,3} \\ A_{3,1} & 0 & A_{3,3} \end{bmatrix} \begin{bmatrix} F_{int}(k) \\ F_{exh}(k) \\ F_{cyl}(k) \end{bmatrix} + \begin{bmatrix} B_{1,1} \\ B_{2,1} \\ B_{3,1} \end{bmatrix}, \tag{14}$$

where

$$A_{1,1} = \frac{m_{int}(k) - m_{int\text{-}c}(k)}{m_{int}(k) + m_{comp}(k) - m_{int\text{-}c}(k)}, A_{1,2} = \frac{m_{egr}(k)}{m_{int}(k) + m_{comp}(k) - m_{int\text{-}c}(k)},$$

$$A_{2,2} = \frac{m_{exh}(k) - m_{turbine}(k)}{m_{exh}(k) + m_{c-e}(k) - m_{turbine}(k)}, A_{2,3} = \frac{m_{cyl}(k) m_{c-e}(k)}{[m_{cyl}(k) + m_f(k)][m_{exh}(k) + m_{c-e}(k) - m_{turbine}(k)]},$$

$$A_{3,1} = \frac{m_{int\text{-}c}(k)}{m_r(k) + m_i(k) + m_{int\text{-}c}(k) - m_{c-e}(k)},$$

$$A_{3,3} = \frac{m_{cyl}(k)[m_{cyl}(k) + m_f(k)] - m_{cyl}(k) m_{c-e}(k)}{[m_{cyl}(k) + m_f(k)][m_r(k) + m_i(k) + m_{int\text{-}c}(k) - m_{c-e}(k)]},$$

$$B_{1,1} = \frac{F_{air}[m_{comp}(k) - m_{egr}(k)]}{m_{int}(k) + m_{comp}(k) - m_{int\text{-}c}(k)}, B_{2,1} = \frac{-m_f(k)\lambda_s m_{c-e}(k)}{[m_{cyl}(k) + m_f(k)][m_{exh}(k) + m_{c-e}(k) - m_{turbine}(k)]},$$

$$B_{3,1} = \frac{m_{c-e}(k) m_f(k)\lambda_s - m_f(k)\lambda_s [m_{cyl}(k) + m_f(k)]}{[m_{cyl}(k) + m_f(k)][m_r(k) + m_i(k) + m_{int\text{-}c}(k) - m_{c-e}(k)]}.$$

Generally, the intake and exhaust manifolds oxygen concentrations can be measured by sensors. Taking these two states as measurement, then we have the measurement equation:

$$\boldsymbol{Z}(k) = \underbrace{\begin{bmatrix} 1 & 0 & 0 \\ 0 & 1 & 0 \end{bmatrix}}_{\boldsymbol{H}} \begin{bmatrix} F_{int}(k) \\ F_{exh}(k) \\ F_{cyl}(k) \end{bmatrix}, \tag{15}$$

where, $\boldsymbol{H}$ is the measurement matrix.

One can see from equation (14), this is a linear, parameter time-varying system and smooth variable structure filter (SVSF) will be used to estimate the in-cylinder oxygen concentration, F_{cyl}, on account of its robustness and easy to implement.

Since the in-cylinder oxygen concentration is predicted by the dynamic equations rather than directly obtained, and to distinguish it from the ignition delay function derived in the following section, here we call equation (14), (15) as “dynamic model”.

To be noted, too many variables of gas masses are involved in this system and they can only be obtained either by integrating the mass flow rate, as speed-density equation (5) and orifice equation (11) and (12), or by looking up maps, as λ_v, or by other means, as m_{comp} and $m_{turbine}$. Almost none of them are directly measured by physical sensors in real engines, which brings the accuracy of the final estimation result of the in-cylinder oxygen concentration is rather vulnerable.

As aforementioned in the introduction section, to improve the accuracy and robustness of this system, a combined strategy was applied as detailed in the following sections.

III. MODELING THROUGH CYLINDER PRESSURE SIGNAL

To improve the accuracy and robustness of the in-cylinder oxygen concentration estimation, more available information should be utilized. As demonstrated in [18][19], apart from the temperature, pressure and injection mass, the in-cylinder oxygen concentration also has an effect on the ignition delay for Diesel engines. Moreover, ignition delay can be tracked by checking the in-cylinder pressure trace, which becomes measurable for some of the commercial engines. Therefore, the oxygen information calculated from ignition delay will be utilized to refine the result from the dynamic model in section II.

Here, assuming the rail pressure and the fuel type are fixed and then, to a large extent, the ignition delay can be captured by the intake temperature, pressure, in-cylinder oxygen concentration, injection mass as well as injection time:

$$\tau_{id} = A p_{int}^{-a} e^{\frac{b}{T_{int}}} F_{cyl}^{-c} m_f^{-d} \tau_{inj}^{e}, \tag{16}$$

where, τ_{id} represents the ignition delay, τ_{inj} is the injection time and *A*, *a*, *b*, *c, d* and *e* are constant need to be determined.

A. Ignition delay

Detecting the ignition delay is actually detecting the combustion starting point, since the injection timing is given by ECU or the injection current. Once the combustion starting time is calculated, the ignition delay is accordingly obtained as the crank angle degree starting from injection timing until the combustion begins. Conventionally, it is defined as:

$$\tau_{id} = CA_{10} - \tau_{inj}, \tag{17}$$

where CA_{10} is the crank angle when 10% of the fuel is consumed.

Usually, CA_{10} is given by taking the integral of the following heat release rate model:

$$dQ_h = pdV + \frac{\gamma}{\gamma - 1} pdV + \frac{1}{\gamma - 1} Vdp + dQ_w, \tag{18}$$

where, the first term on the right side, $_{pdV}$ accounts for the piston movement work, $\frac{\gamma}{\gamma-1}pdV+\frac{1}{\gamma-1}Vdp$ accounts for the change in sensible energy and the last term, dQ_w is the work caused by heat transfer between the charge and cylinder wall, which is ignored here.

The integral of the heat release rate, or the accumulated heat release, is plotted in Fig.2 for a typical cycle. The start of combustion, represented as CA_{10}, and the ignition delay both are easily calculated, and indicated in the figure.

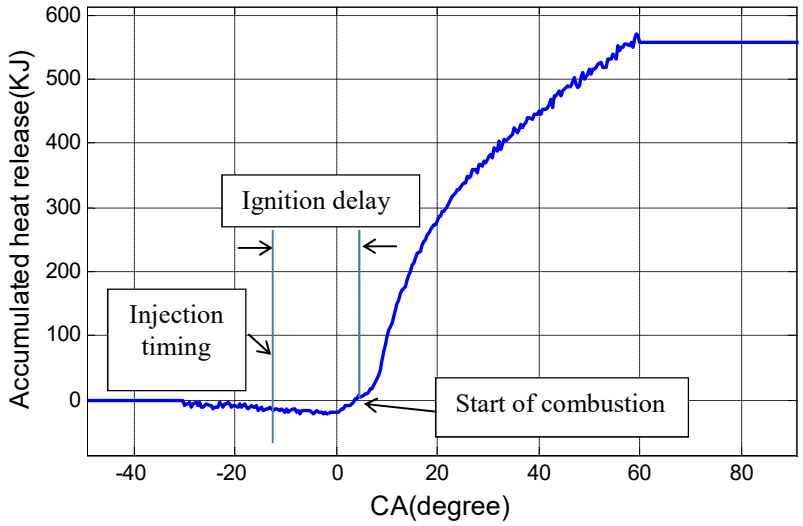

Fig.2 Ignition delay demonstrated by accumulated heat release

B. Calibration and validation

This model (equation (16)) was calibrated on a four-cylinder Diesel engine with displacement as 1.9L running in medium-duty. The specifications of the engine are detailed in Table I.

TABLE I. ENGINE SPECIFICATIONS

Items	Description
Compression ratio	17.5
Displacement (L)	1.9
Stroke (mm)	92.4
Bore (mm)	81
Rated power (kW))	93
Max. torque (Nm)	271
Fuel injection system	Common rail

As shown in Fig.3, the engine test bench equips Horiba HT250 dynamometer, Turbocharger, intercooler and DPF (diesel particulate filter) in the EGR loop.

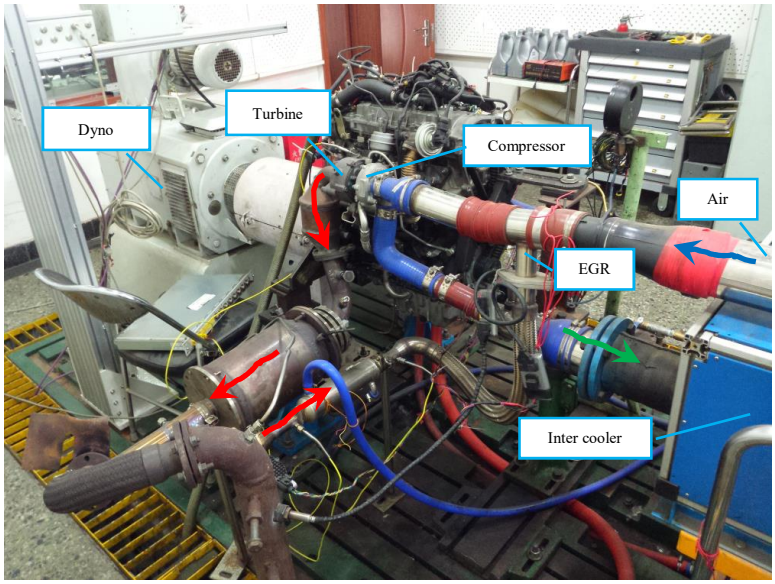

Fig.3 Engine test bench

Except for ignition delay, another term which is indirectly obtained in equation (16) is the in-cylinder oxygen concentration, F_{cyl}. For each operating condition, 100 contiguous cycles of in-cylinder pressure were recorded when the engine reaches steady state. Then the following assumptions are made to calculate F_{cyl} in steady state as the reference for validation: 1) the mass flow rates of the intake gas go into- and out of the

cylinder is equal; 2) the temperatures of the residual gas and the exhaust manifold is equal. Then the F_{cyl} can be calculated as:

$$F_{cyl\_real}(k) = \frac{m_{egr}(k)F_{exh}(k) + F_{air}[m_{comp}(k) - m_{egr}(k)]}{\bar{m}_r(k) + m_{comp}(k)}. \tag{19}$$

where, $\bar{m}_r(k)$ is the residual gas mass in steady state, which is calculated by:

$$\bar{m}_r(k) = \frac{P_{evc}(k)V_{evc}}{RT_{exh}(k)}, \tag{20}$$

where, the subscript evc is the crank angle degree at exhaust valve closing.

To be noted, in steady state, the aforementioned 2 assumptions are reasonable and hence the in-cylinder oxygen concentration derived in equation (19) can be used as reference value to calibrate the ignition model and validate the proposed oxygen concentration estimation technique in the following section.

To cover a wide range of operating conditions and make the calibration representative while the combustion is still stable, we changed the injection timing, EGR rate and injection mass as tabulated in the following table. Fixing the engine speed on 1800RPM and with 2 different injection timings, 5 EGR rates, and 6 injection masses, 60 operating condition combinations were carried out. For each operating conditions, 100 contiguous cycles of in-cylinder pressure were recorded. To reduce the noise and cyclic variabilities, the pressure was averaged for every 10 cycles, therefore, there are 600 cycles in-cylinder pressure data altogether for the calibration and validation. Among them, the operating condition combinations with injection mass as 15, 17,19 and 21 were used

to calibrate the ignition delay model, while the rest combinations were applied to validate the model and the proposed estimation method.

TABLE II. OPERATING CONDITIONS

Injection timing (ADTC)	EGR(%)	Injection mass(mg)
-10	10	15
		17
	15	
	20	19
-15		21
	25	
		23
	30	
		25

The ignition delay model (16) is calibrated as expressed in equation (21) and the comparisons between the modeled and the experimental (calculated by the pressure trace, as demonstrated in Fig.2) are shown in Fig.4. The combinations with injection mass rate as 15mg, 17mg, 19 mg and 21 mg were used to calibrate the ignition delay model, as plotted in Fig.4 (a), while the rest for validating are plotted in Fig.4 (b).

$$\tau_{id} = e^{5.22} p_{int}^{-1.87} e^{\frac{890.45}{T_{int}}} F_{cyl}^{-1.97} m_f^{-1.05} \tau_{inj}^{0.04}, \tag{21}$$

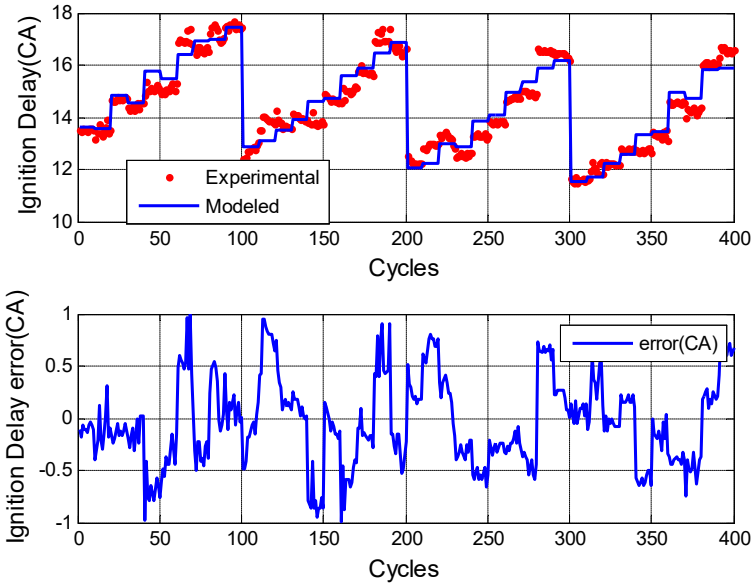

(a) calibration

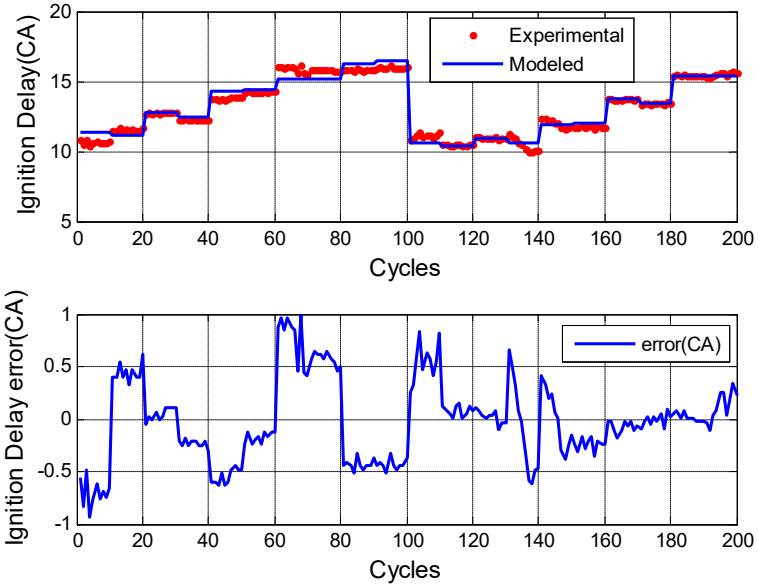

(b) validation

Fig.4 The modeled vs. experimental ignition delay

As one can see, the calibrated model has ignition delay errors within 1 crank angle degree. As long as the ignition delay is calculated by using the pressure trace and the intake pressure, temperature, injection mass and the injection timing are measured,

the in-cylinder oxygen concentration can be calculated by taking the inverse of the equation (21).

The in-cylinder oxygen was calculated in Fig.5, where the oxygen concentration given by equation (19) is treated as "experimental" and the modeled is given by the inverse of equation (21) accordingly.

$$F_{cyl} = exp\left(\frac{5.22 - 1.87ln(p_{int}) + \frac{890.45}{T_{int}} - 1.05ln(m_f) + 0.04ln(\tau_{inj}) - ln(\tau_{id})}{1.97}\right). \quad (22)$$

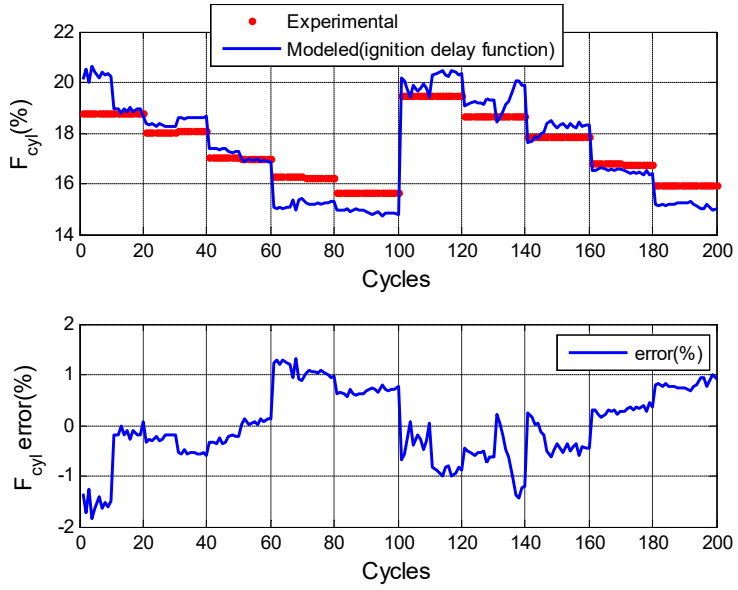

Fig.5 The accordingly oxygen concentration vs. experimental

Fig.5 tells the oxygen concentration error is less than 2%, which meets well with the error analysis. This information of error level will be used for the smooth variable structure filter (SVSF) design.

C. Error and sensitivity analysis

Sensitivity analysis

According to equation (22), the sensitivity of the in-cylinder oxygen concentration with respect to p_{int} can be calculated as follows.

$$S_{\tau_{id}} = \frac{\tau_{id}}{F_{cyl}}\left(\frac{\partial F_{cyl}}{\partial \tau_{id}}\right)100\% \cdot \tag{23}$$

Since the sensitivity largely depends on the operating conditions, to quantify the analysis the same operating conditions as the validation are applied. The sensitivity of the in-cylinder oxygen concentration with respect to other factors are similarly calculated and tabulated as follow.

TABLE III. THE SENSITIVITY OF THE IN-CYLINDER OXYGEN CONCENTRATION WITH RESPECT TO $\tau_{id}, p_{int}, T_{int}, m_f$ AND τ_{inj}

$S_{\tau_{id}}$	S_{Pint}	S_{Tint}	S_{mf}	$S_{\tau_{inj}}$
-20.35% to -22.89%	-38.06% to 42.81%	-54.13% to 41.98%	-10.17% to -11.44	0.81% to 0.92%

As can be seen, the ignition delay, pressure and temperature are dominant factors than the others in determining the in-cylinder oxygen concentration. This is reasonable in that the sensitivity equation in (23) is based on the ignition delay model. p_{int}, T_{int} can be well measured and given the high sensitivity of ignition delay to the oxygen concentration, by inverting the ignition delay to calibrate the in-cylinder oxygen concentration is feasible.

Error analysis

Assuming the ignition delay modeling error is the only error source of F_{cyl}, then taking the first order Taylor expansion for equation (21) tells that 1 crank angle degree error of ignition delay brings roughly 2% of oxygen concentration error, such a modeling error level is acceptable. It is worth noting that except the model error, the pressure measurement noise, offset, etc., can also damage the accuracy of the calculated F_{cyl}. Therefore, the proposed oxygen concentration estimation method which combines the information of oxygen dynamics (equation (14)) and the ignition delay model (equation (21)) is more feasible in real applications.

IV. DATA ASSOCIATION ALGORITHM

Combining in-cylinder pressure information with the system dynamics in section II facilitates the estimation be conducted in a predictor-corrector fashion. Considering its robustness, smooth variable structure filter (SVSF) was utilized to associate the oxygen concentration information from the two different sources.

Then, the measurement equation of equation (15) turns to be:

$$\boldsymbol{Z}(k)=\underbrace{\begin{bmatrix}1 & 0 & 0\\ 0 & 1 & 0\\ 0 & 0 & 1\end{bmatrix}}_{\bar{\boldsymbol{H}}}\begin{bmatrix}F_{int}(k)\\ F_{exh}(k)\\ \bar{F}_{cyl}(k)\end{bmatrix}, \tag{24}$$

where, $\bar{H}$ is the measurement matrix, and $\bar{F}_{cyl}$ is the value calculated by inverting equation (21).

3.5 SVSF design

As a relatively new filter, the SVSF was first introduced in [20] in 2007. It derived based on the idea of variable structure filter, but in a predictor-corrector form.

Thereafter, theoretical research on SVSF, including the information form in [21], the combination of particle filter and SVSF in [22], the optimal time-varying smoothing boundary layer derivation in [23], etc. have been carried out, and been applied in various situations, such as the estimation for the unburned gas in a Diesel engine in [24], and fault diagnosis for an electro-hydrostatic actuation (EHA) system in [25]. In this paper, the classic form of SVSF will be applied. The estimation procedure for SVSF contains the following 4 steps[20].

1) Prior state and measurement:

$$\begin{bmatrix} \hat{F}_{int}(k+1,k) \\ \hat{F}_{exh}(k+1,k) \\ \hat{F}_{cyl}(k+1,k) \end{bmatrix} = \boldsymbol{A}(k) \begin{bmatrix} \hat{F}_{int}(k,k) \\ \hat{F}_{exh}(k,k) \\ \hat{F}_{cyl}(k,k) \end{bmatrix} + \boldsymbol{B}(k), \tag{25}$$

$$\hat{\boldsymbol{Z}}(k+1,k) = \boldsymbol{H} \begin{bmatrix} \hat{F}_{int}(k+1,k) \\ \hat{F}_{exh}(k+1,k) \\ \hat{F}_{cyl}(k+1,k) \end{bmatrix}, \tag{26}$$

2) The prior and posterior output error:

$$\boldsymbol{e}_{z(k+1,k)} = \boldsymbol{Z}(k+1) - \hat{\boldsymbol{Z}}(k+1,k), \tag{27}$$

$$\boldsymbol{e}_{z(k,k)} = \boldsymbol{Z}(k) - \hat{\boldsymbol{Z}}(k,k), \tag{28}$$

3) Filter gain:

$$\boldsymbol{K}(k+1) = \left(\left| \boldsymbol{e}_{z(k+1,k)} \right| + \gamma \left| \boldsymbol{e}_{z(k,k)} \right| \right) \circ sat(\boldsymbol{e}_{z(k+1,k)}, \boldsymbol{\Psi}), \tag{29}$$

4) Posterior state and measurement:

$$\begin{bmatrix} \hat{F}_{int}(k+1,k+1) \\ \hat{F}_{exh}(k+1,k+1) \\ \hat{F}_{cyl}(k+1,k+1) \end{bmatrix} = \begin{bmatrix} \hat{F}_{int}(k+1,k) \\ \hat{F}_{exh}(k+1,k) \\ \hat{F}_{cyl}(k+1,k) \end{bmatrix} + \boldsymbol{K}(k+1), \tag{30}$$

$$\hat{\boldsymbol{Z}}(k+1,k+1)=\boldsymbol{H}\begin{bmatrix}\hat{F}_{int}(k+1,k+1)\\ \hat{F}_{exh}(k+1,k+1)\\ \hat{F}_{cyl}(k+1,k+1)\end{bmatrix}, \tag{31}$$

where, γ in equation (29) is the convergence rate, $\boldsymbol{Z}$ in equation (27) and (28) is the measurement matrix with the value from the in-cylinder pressure signal included, and to reduce the chattering effect, the saturation function in equation (29) can be defined as:

$$sat(\boldsymbol{a},\boldsymbol{b})=\begin{cases}a_i/b_i & for\left|a_i/b_i\right|\le 1\\ sign(a_i/b_i)\ for\left|a_i/b_i\right|>1\end{cases}, \tag{32}$$

the smoothing boundary layer width, $\boldsymbol{\Psi}$ can be selected based on the dynamic model error boundary.

The SVSF was, therefore, developed by repeating the above procedures for each cycle.

V. EXPERIMENTAL VALIDATION

As mentioned in section II, several gas-mass uncertainties can contaminate the performance of the dynamic model, including the volumetric efficiency which is pressure- and temperature-varying and hard to be calculated accurately, and the VGT equation which is a function of hardly measured factors such as upstream/downstream pressure ratio and mass flow efficiency, etc. The oxygen concentration given by the system dynamics and by the experiments is compared in Fig.6. The experimental oxygen concentration, represented by the red dotted line in Fig.6, was identical with the red dotted line in Fig.5. In other words, the operating conditions for validation the ignition

delay model were also applied to test the performance of the oxygen dynamics as well as the proposed method as stated in the following part.

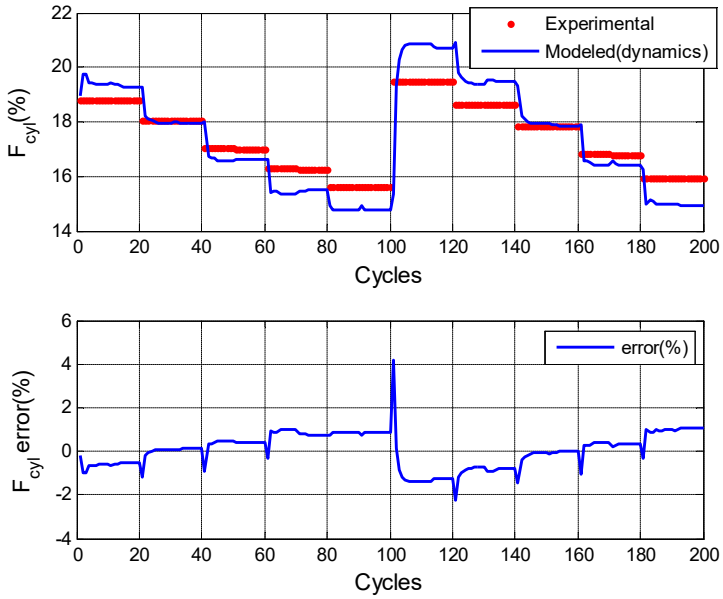

Fig.6 The oxygen concentration given by the dynamics

From Fig.6, the oxygen concentration given by the system dynamics (equation(14)) has an error more than 4%. This is the contribution of all the modeling uncertainties.

To be noted, the stair effect in Fig.6 is caused by the reason as follows. The 20 0 cycles contain 20 operating condition combinations (2 injection timings, 5 EGR levels, and 2 injection masses as 23 and 25mg). For each combination, 100 contiguous cycles of in-cylinder pressure were recorded after the steady state reached and then averaged for every 10 cycles. Therefore, every stair in Fig.6 corresponds with one operating condition combination. This stair-shape oxygen concentration given by equation (19), indicated as "experimental" in the top figure of Fig.6, suggests that the operating condition suddenly changed at every stair edge. This explains the ridges of oxygen concentration error in the

bottom figure in Fig.6 in that the slow response of the air path dynamics brings large error when the operating condition suddenly switched, especially at cycle number 100.

The proposed method for estimating the in-cylinder oxygen concentration is for the purpose of overcoming the delay of the air path dynamics and the inevitably imperfect pressure measurement of the ignition delay model. By applying the SVSF to combine the two information sources (i.e. the oxygen concentration comes from ignition delay model and oxygen dynamics), the final oxygen estimation can be more accurate.

The smoothing boundary layer width, $\boldsymbol{\Psi}$, in equation (29) indicating the estimation trade-off between system model (25) error and measurement error. For the final estimation results, larger $\boldsymbol{\Psi}$ suggests more weighting on the system model, while smaller (but still larger than the system smooth boundary to reduce the chattering) $\boldsymbol{\Psi}$ plays more emphasis on the measurement. Based on the in-cylinder oxygen concentration error from the cylinder pressure signal (Fig.5) and the error from the dynamic model (Fig.6), $\boldsymbol{\Psi}$ was tuned as:

$$\boldsymbol{\Psi} = \begin{bmatrix} 2 \\ 2 \\ 5 \end{bmatrix}. \tag{33}$$

The estimation results given by the proposed method is demonstrated in the following figure.

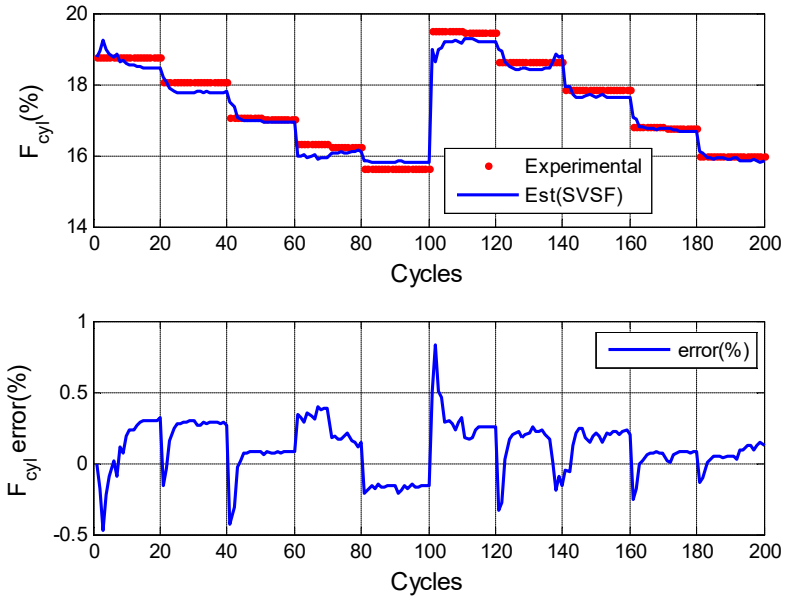

Fig.7 The oxygen concentration given by the proposed method

Fig.7 tells that the estimation error of the proposed method is within 1%. Comparing to the results given by applying the ignition delay (equation (21)) or the system dynamics (equation (14)) only, significantly improvement is received by using the ignition delay function and the oxygen dynamic model through SVSF.

VI. CONCLUSIONS

In this paper, a novel strategy for estimating the in-cylinder oxygen concentration for Diesel engines is proposed. The commonly happened uncertainties of gas masses and slow response can easily contaminate the accuracy of the in-cylinder oxygen concentration estimated by air path dynamics. To overcome it, a special measurement modeled as a function of ignition delay is used. By combining the oxygen concentration obtained from ignition delay (through in-cylinder pressure trace), and the air-path dynamic model, the smooth variable structure filter (SVSF) in a predictor-corrector fashion can be applied. Analysis and experiments confirmed that, by introducing the

combined estimation strategy, the proposed method shows significant improvement on accuracy.

ACKNOWLEDGEMENT

This research was supported by NSERC Discover Program Award RGPIN/436147-2013.

REFERENCES

[1] X.-C. Lü, W. Chen, and Z. Huang, "A fundamental study on the control of the HCCI combustion and emissions by fuel design concept combined with controllable EGR. Part 2. Effect of operating conditions and EGR on HCCI combustion," *Fuel*, vol. 84, no. 9, pp. 1084–1092, Jun. 2005.

[2] N. J. Killingsworth, S. M. Aceves, D. L. Flowers, F. Espinosa-Loza, and M. Krstic, "HCCI Engine Combustion-Timing Control: Optimizing Gains and Fuel Consumption Via Extremum Seeking," *IEEE Trans. Control Syst. Technol.*, vol. 17, no. 6, pp. 1350–1361, Nov. 2009.

[3] N. Ravi, M. J. Roelle, H. Liao, A. F. Jungkunz, C. Chang, S. Park, and J. C. Gerdes, "Model-Based Control of HCCI Engines Using Exhaust Recompression," *IEEE Trans. Control Syst. Technol.*, vol. 18, no. 6, pp. 1289–1302, 2010.

[4] J. Wang, "Hybrid Robust Air-Path Control for Diesel Engines Operating Conventional and Low Temperature Combustion Modes," *IEEE Trans. Control Syst. Technol.*, vol. 16, no. 6, pp. 1138–1151, Nov. 2008.

[5] and S. S. Brijesh, P., A. Chowdhury, "Effect of Ultra-cooled EGR and Retarded Injection Timing on Low Temperature Combustion in CI Engines," *SAE Tech.*

Pap., no. 2013–01–0321, 2013.

[6] S. M. Aceves, D. L. Flowers, and D. N. Assanis, "Analysis of Premixed Charge Compression Ignition Combustion with a Sequential Fluid Mechanics-Multizone Chemical Kinetics Model," *SAE Tech. Pap.*, no. No. 2005–01–0115, 2005.

[7] C. M. Hall, D. Van Alstine, L. Kocher, G. M. Shaver, and D. Lee, "COMBUSTION TIMING MODELING AND CONTROL FRAMEWORK FOR BIODIESEL / DIESEL BLENDS DURING PRE-MIXED COMBUSTION," pp. 1–10, 2012.

[8] C. J. Chiang and A. G. Stefanopoulou, "Sensitivity analysis of combustion timing and duration of homogeneous charge compression ignition (HCCI) engines," *2006 Am. Control Conf.*, pp. pp.1857–1862, 2006.

[9] E. Hellström, A. Stefanopoulou, J. Vavra, A. Babajimopoulos, D. Assanis, L.Jiang, and H.Yilmaz, "Understanding the dynamic evolution of cyclic variability at the operating limits of HCCI engines with negative valve overlap," *SAE Tech. Pap.*, no. No.2012–01–1106, 2012.

[10] X. Yang and G. G. Zhu, "A Two-Zone Control Oriented SI-HCCI Hybrid Combustion Model for the HIL Engine Simulation," in *American control conference*, 2011, pp. 973–978.

[11] G. Haraldsson, P. Tunestål, B. Johansson, and J. Hyvönen, "HCCI Combustion Phasing in a Multi Cylinder Engine Using Variable Compression Ratio," *SAE Tech. Pap.*, no. No.2002–01–2858, Oct. 2002.

[12] O. Grondin, P. Moulin, and J. Chauvin, "Control of a Turbocharged Diesel Engine

Fitted with High Pressure and Low Pressure Exhaust Gas Recirculation Systems," *IEEE Conf. Decis. Control Eur. Control Conf.*, pp. 6582–6589, 2009.

[13] A.G.Stefnanopoulou, I.Kolmanovsky, and J. S. Freudenberg, "Control of Variable Geometry Turbocharged Diesel Engines for Reduced Emissions," *IEEE Trans. Control Syst. Technol.*, vol. 8, no. 4, pp. 733–745, 2000.

[14] A. D. Model, "In-Cylinder Oxygen Mass Fraction Cycle-by-Cycle Estimation via a Lyapunov-based Observer Design," in *American control conference*, 2010, pp. 652–657.

[15] F. Yan and J. Wang, "Design and Robustness Analysis of Discrete Observers for Diesel Engine In-Cylinder Oxygen Mass Fraction Cycle-by-Cycle Estimation," *IEEE Trans. Control Syst. Technol.*, vol. 20, no. 1, pp. 72–83, 2012.

[16] J. Meyer, S. Midlam-mohler, and S. Yurkovich, "In-cylinder Oxygen Concentration Estimation for Diesel Engines Via Transport Delay Modeling," in *American control conference*, 2011, pp. 396–401.

[17] M. P. Kolmanovsky I and V. N. M, "issues in modeling and control of intake flow in variable geometry turbocharged engines.pdf." Chapman and Hall CRC research notes in mathematics, pp. 436–445, 1999.

[18] Y. Zhang, Z. Huang, L. Wei, and S. Niu, "Experimental and kinetic study on ignition delay times of methane/hydrogen/oxygen/nitrogen mixtures by shock tube," *Chinese Sci. Bull.*, vol. 56, no. 26, pp. 2853–2861, Aug. 2011.

[19] J. B. Heywood, *Internal Combustion Engine Fundamentals*, vol. 21. McGraw-Hill,Inc., 1988.

[20] B. S. Habibi, "The Smooth Variable Structure Filter," *Proc. ieee*, vol. 95, no. 5, pp. 1026–1059, 2007.

[21] S. A. Gadsden and S. R. Habibi, "A new form of the smooth variable structure filter with a covariance derivation," *Proc. IEEE Conf. Decis. Control*, pp. 7389–7394, 2010.

[22] M. Engineering, C. Engineering, C. E-mail, R. March, and A. June, "The smooth particle variable structure filter 1," vol. 36, no. 2, pp. 177–193, 2012.

[23] S. a. Gadsden and S. R. Habibi, "A New Robust Filtering Strategy for Linear Systems," *J. Dyn. Syst. Meas. Control*, vol. 135, no. 1, p. 014503, 2012.

[24] S. Chen and F. Yan, "Trapped Unburned Fuel Estimation and Robustness Analysis for a Turbocharged Diesel Engine With Negative Valve Overlap Strategy," *J. Dyn. Syst. Meas. Control*, vol. 137, no. 6, p. 061004, 2015.

[25] S. A. Gadsden, Y. Song, and S. R. Habibi, "Novel Model-Based Estimators for the Purposes of Fault Detection and Diagnosis," *IEEE/ASME Trans. Mechatronics*, vol. 18, no. 4, pp. 1237–1249, 2013.

3.6 Remarks

The ignition delay model in equation (16) in the paper is for a normal Diesel engine in which there is almost no EGR. In order to cover a wide range of operating condition, the EGR of the engine test bench was set up to 30%. The model performs well; the estimation method for the in-cylinder oxygen concentration proposed in this paper is experimentally validated.

The in-cylinder conditions, namely the in-cylinder temperature, oxygen concentration and pressure are critical for the advanced combustion mode in which the auto-ignition is entirely initialized by them. The in-cylinder temperature estimated in the paper 1 and the method of in-cylinder oxygen estimation in this paper are laying a solid foundation for the further advanced combustion mode control. The next paper introduces a technique to control the air- and fuel-path loops coordinately.

Chaper 4. Paper 3 Air-path and Fuel-path Coordinated Control for a Turbo-Charged Engine with Dual-loop EGR System

4.1 Citation and Main Contributor

Chen, S., & Yan, F. Air-path and fuel-path coordinated control for a turbo-charged engine with dual-loop EGR system. *IEEE Transactions on Control Systems Technology*(under review).

The main contributor to this paper is the first author-Chen Song (contributes more than 70%).

4.2 Brief Introduction

The previous two papers introduce the estimation method for the in-cylinder conditions, which are critically important for the combustion phasing control. This paper gives the combustion phasing and work output control through air- and fuel-path coordinated regulation.

Air path control for the intake conditions, including the intake temperature, pressure, and oxygen concentration are critical for switching to and maintaining stable and smooth advanced combustion mode. The thermal dynamics boundary of advanced combustion mode, including homogeneous charge compression ignition (HCCI), premixed charge compression ignition (PCCI) as well as low-temperature combustion (LTC) is significantly narrow, comparing with conventional combustions. Hence, desired intake conditions are the basis for smooth and stable low-temperature combustion, although the effect of intake conditions on the combustion process is indirect and slow.

To achieve pre-designed combustion phasing and work output, in terms of CA50 (crank angle degree at 50% fuel consumed) and IMEP (indicated mean effective pressure), especially in transient situations, the combining of air-path and fuel-path control is introduced in the following paper. An extended state observer based on the super twisting idea is designed to estimate the coupling effect of fuel path on the air path. The control law for air path compensates the coupling effect in real time. Since the air path has indirect and slow impacts on the combustion process, the fuel path control law is designed in a decoupled fashion. To test the effectiveness of the proposed strategy, a four cylinder Diesel engine was constructed in GT-Power and the combustion model was calibrated by experimental data on a real engine with the same architecture. A series of coupling simulations between Simulink and GT-Power tell that the proposed idea works well and the intake conditions and the combustion process can be controlled simultaneously.

Control oriented models for the fuel-path are presented. Normally, the combustion phasing, CA50, can be modeled as a function of in-cylinder temperature, oxygen concentration, etc. In this paper, a simplified model is applied. The CA50 is modeled as a difference function of injection timing, injection mass and intake temperature. The work output is modeled as a function of injection mass and CA50.

4.3 Main Contributions

1) The conventional extended state observer (ESO) is enhanced by the concept of the super twisting idea.

2) The sliding mode controller is designed for the air-path loop and compensating the disturbance.

3) The analysis tells that the air-path loop has a slow impact on the combustion while fuel-path path is a relatively fast response. Thus, the two loops are controlled in a decoupled fashion by taking the advantage of the different time scales of the two loops.

4.4 Full content of Paper 3

Air-path and fuel-path coordinated control for a turbo-charged engine with dual-loop EGR system

Song Chen, Fengjun Yan*,
Department of Mechanical Engineering
McMaster University
Hamilton, ON, L8S 4L7 Canada

Abstract —Air path control for the intake conditions, including the intake temperature, pressure, and oxygen concentration are critical to achieving advanced combustion mode. However, the effect of intake conditions on the combustion process is indirect and slow. To achieve pre-designed combustion phasing and work output, in terms of CA50 (crank angle degree at 50% fuel consumed) and IMEP (indicated mean effective pressure), especially in transient situations, the combining of air-path and fuel-path control is necessary. There are two difficulties that need to overcome: 1) the coupling effect between that air- and fuel path; 2) the different time scale for the two loops. In this paper, an extended state observer based on the super twisting idea is designed to estimate the effect of fuel path on the air path, and the control law for air path compensates the effect in real time. Since the air path has indirect and slow impacts on the combustion process, the fuel path control law is designed in a decoupled fashion. To test the effectiveness of the proposed strategy, a four cylinder Diesel engine was constructed in GT-Power and the combustion model was calibrated by experimental data on a real engine with the same architecture. A series of coupling simulations between Simulink and GT-Power tell that the proposed idea works well and the intake conditions and the combustion process can be controlled simultaneously.

*Corresponding author. Fengjun Yan is with the Department of Mechanical Engineering at McMaster University, Hamilton, ON Canada, email: yanfeng@mcmaster.ca.

Keywords: CA50, IMEP, super twisting, disturbance rejection control, intake conditions

I. INTRODUCTION

The advanced combustion mode, usually including homogeneous charge compression ignition (HCCI) [1], premixed charge compression ignition (PCCI) [2] as well as low temperature diffusion combustion (LTDC) [3], shows great potentiality to reduce the strictly regulated engine out emissions and increase the thermal efficiency. As demonstrated in [4], lower temperature and lower equivalence ratio offered by the low temperature combustion mode are the cause for the extremely low PM (particulate matter)and NOx: the conditions, i.e. higher temperature and higher equivalence ratio for generating the PM and NOx are no longer available. However, a lower temperature is mostly achieved by introducing a significantly amount of exhaust gas into the intake system, either in the form of EGR [5] (exhaust gas recirculation, also called external EGR) or residual gas (or internal EGR) [6][7], which deteriorates the combustion stability. Apart from the EGR, the pressure, temperature in air path loop and the injection conditions (injection timing, mass, pulses, etc.) in fuel loop, are all need to be well regulated for a smooth combustion, slightly mismatch or calibration error could lead to misfire and even physical damage to the engine[8], especially when trying to extend the load range[9].

For air-path control, several techniques have been introduced by researchers. An LQR based, with two feedforward loops control law is given in [10] for an engine with dual-loop EGR system. To deal with the different time scales between the high-pressure EGR loop (faster) and low-pressure EGR loop (slower), a singular perturbation method is introduced [11]. The experimental results tell this method can appropriately coordinate

the dual-loop EGR air-path actuators. In [12], adjustable intake conditions priorities is achieved by the reference governor control.

The air path control is critical to achieving smooth and stable advanced combustion mode. However, the coordinated control of air- and fuel path is more desirable for fast combustion response, especially for combustion mode switching or load range extending process. To improve the transient operations on advanced combustion transition, [13] introduces an idea that combines the reference governor method for air-path and injection technique for fuel-path.

In this paper, a novel control strategy based on disturbance rejection with the super twisting concept is designed. The widely used, control oriented air-path model suffers from several errors, such as the neglect of the heat transfer between the mixture and the manifold wall, the hardly accurately calibrated volumetric efficiency, etc. The active disturbance rejection control (ADRC) [14] is enhanced by utilizing the super twisting sliding mode control. The controlling idea is summarized as: 1) by employing the enhanced ADRC, the air- and fuel- path is controlled in a decoupled fashion; 2) the extended state observer is designed for each loop of the air-path to estimate the modeling error and the coupling effect brought from fuel-path; 3) the control law for the air-path is designed to regulate the intake conditions approaching desired trajectories and compensate the coupling effect of fuel-path as well; 4) the control law for the fuel-path is designed for a fast combustion phasing-CA50 (the crank angle when 50% combust) and IMEP(indicated mean effective pressure) response.

A four cylinder Diesel engine was constructed in GT-Power and the combustion model was calibration by experimental data on a real engine with the same architecture. The proposed control strategy is validated through a series of simulations on the high-fidelity engine model.

The arrangements of this paper are as follows: in Section II, the CA50 and IMEP calculation based on pressure trace is introduced and the measurement error effects are demonstrated. In section III, Neural Network for CA50 is presented. Data association algorithm, the smooth variable structure filter is designed in section IV. Experimental results are stated in section V. Conclusions and remarks are summarized in the section VI.

II. SYSTEM DYNAMICS

With variable geometry turbocharger (VGT) (as shown in Fig.1), the dual-loop exhaust gas recirculation (EGR) system has been extensively focused on in recent years[15][10]. It provides a flexible and also complex control architecture which has been commonly utilized in modern engines to achieve desired intake manifold conditions and further the in-cylinder conditions. With three actuators in such an engine setup, including high pressure loop (HPL) EGR valve, low pressure loop (LPL) EGR valve, and the rack position of the turbine, as indicated in Fig.1, the intake manifold conditions, including the temperature, pressure, and burned gas fraction can be well controlled. The flexible control authorities of the intake manifold conditions provide effective tools to for further in-cylinder condition control.

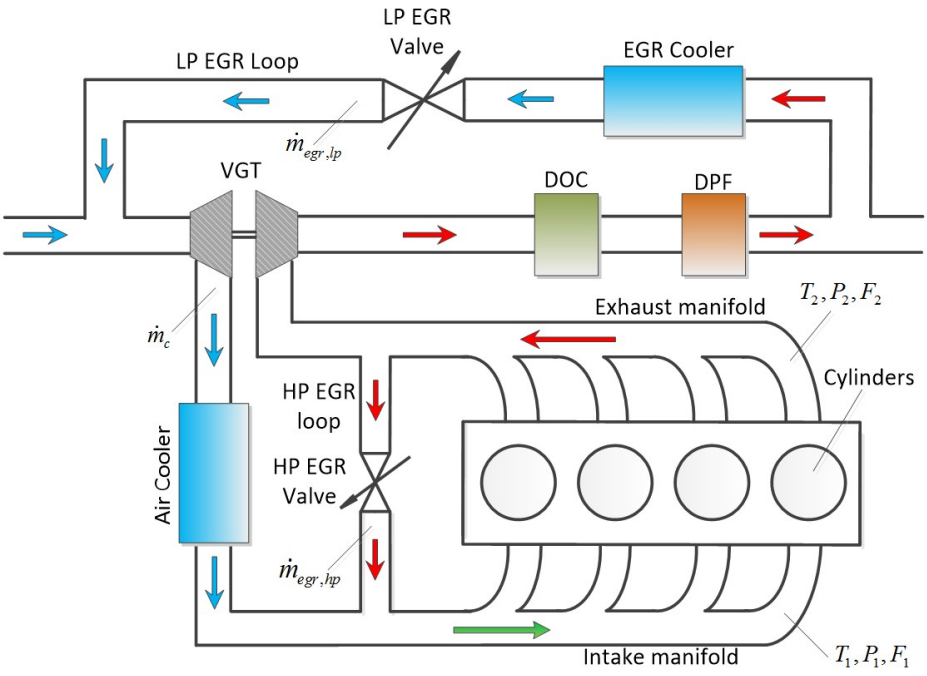

Fig.1 Engine architecture with a variable geometry turbocharger and dual-loop EGR system

The control target system is a modern four-cylinder engine as shown in Fig.1. A VGT, high-pressure loop (HPL) EGR and low-pressure loop (LPL) EGR, LPL cooler, air cooler and the after-treatment system are equipped with this engine. The dynamic models of each part of the engine air-path loop are presented in the following subsections.

Air path

C. Intake manifold Conditions

Neglecting the heat transfer between the mixture and pipe walls, and applying the energy and mass conservation law [10][15], the intake manifold conditions dynamics is derived as:

$$\begin{cases} \dot{T}_1 = \dfrac{RT_1^2}{P_1V_1}\dot{m}_{cyl}(1-\gamma) + \dfrac{RT_1}{P_1V_1}(\gamma T_{ac} - T_1)\dot{m}_c + \\ \qquad \dfrac{RT_1}{P_1V_1}(\gamma T_2 - T_1)\dot{m}_{egr,hp} \\ \dot{P}_1 = -\dfrac{R\gamma}{V_1}\dot{m}_{cyl}T_1 + \dfrac{R\gamma}{V_1}T_{ac}\dot{m}_c + \dfrac{R\gamma}{V_1}T_2\dot{m}_{egr,hp} \\ \dot{F}_1 = \dfrac{RT_1}{P_1V_1}(F_{air} - F_1)\dot{m}_{maf} + \dfrac{RT_1}{P_1V_1}(F_2 - F_1)\dot{m}_{egr,hp} + \\ \qquad \dfrac{RT_1}{P_1V_1}[\breve{F}_2 - F_1]\dot{m}_{egr,lp} \end{cases}, \tag{1}$$

where T_{ac} is the temperature in the area behind the compressor:

$$T_{ac} = \frac{m_{maf}T_{air} + m_{egr,lp}[\eta_{ic}T_{coolant} + (1-\eta_{ic})T_2]}{m_{maf} + m_{egr,lp}}, \tag{2}$$

and T, P and F represent temperature, pressure and oxygen concentration fraction, respectively; $\dot{m}_c$, $\dot{m}_{egr,hp}$, and $\dot{m}_{egr,lp}$ are the mass flow rate of the gas flow through compressor, the valve in the high-pressure loop and the valve in the low-pressure loop respectively ; m_{maf} is the mass of air flow; T_{cyl} and is the temperature in the cylinder; R and γ are the ideal gas constant and specific heat ratio; subscript 1, 2 stand for the intake and exhaust manifolds respectively; $\breve{F}_2$ is the delayed oxygen concentration due to long distance, and can be simplified as a constant delay to F_2:

$$\breve{F}_2(t) = F_2(t-\tau). \tag{3}$$

where τ is the delay time.

In equation (1), $\dot{m}_{cyl}$ is the engine intake gas flow rate, which can be calculated by speed-density models as:

$$\dot{m}_{cyl} = \frac{\lambda_v P_1 V_d N}{120 R T_1}, \tag{4}$$

where λ_v is the volumetric efficiency which needs to be calibrated, N is the engine speed and V_d is the swept volume.

The mass flow rate through valves, including $\dot{m}_{egr,hp}$ and $\dot{m}_{egr,lp}$, can be calculated by the orifice equations[16] as follows:

a) When the flow is not choked ($\frac{p_d}{p_u} > \left(\frac{2}{\gamma+1}\right)^{\gamma/(\gamma-1)}$),

$$\dot{m} = \frac{C_D A_R p_u}{\sqrt{RT_u}} \left(\frac{p_d}{p_u}\right)^{1/\gamma} \left\{\frac{2\gamma}{\gamma-1}\left[1-\left(\frac{p_d}{p_u}\right)^{(\gamma-1)/\gamma}\right]\right\}^{1/2}, \tag{5}$$

b) When the flow is choked ($\frac{p_d}{p_u} \le \left(\frac{2}{\gamma+1}\right)^{\gamma/(\gamma-1)}$),

$$\dot{m} = \frac{C_D A_R p_u}{\sqrt{RT_u}} \sqrt{\gamma}\left(\frac{2}{\gamma+1}\right)^{(\gamma+1)/2(\gamma-1)}, \tag{6}$$

where C_D is the discharge coefficient, which is experimentally determined, subscript u and d stand for upstream and downstream respectively, A_R is the valve reference area.

D. EGR cooler and intercooler

The model of EGR cooler in the low-pressure EGR loop and the intercooler can be approximately expressed by a linear model[3]:

$$T_{down} = T_{up} - \eta_{cooler}(T_{up} - T_{coolant}), \tag{7}$$

where T_{down} and T_{up} are the gas temperature downstream and upstream, $T_{coolant}$ is the temperature of the coolant and η_{cooler} is the cooler efficiency.

E. Variable Geometry Turbocharger

The VGT consists of a compressor connected to a turbine via a shaft. The turbine is driven by the exhaust gas, and thus part of the energy kept in the exhaust system is transferred to the compressor through the shaft. The turbocharger rotational speed (N) is derived from the power balance between the turbine and compressor [17]:

$$JN\frac{dN}{dt} = P_t - P_c, \tag{8}$$

where J is the moment of inertia of the rotating parts; P_t, P_c are the power of the turbine and the compressor they can be expressed as follow [11]:

$$\begin{cases} P_t = \dot{m}_t C_p \eta_t T_2 \left[1 - \left(\frac{1}{PR_t} \right)^{\frac{\gamma-1}{\gamma}} \right], \\ P_c = \dot{m}_c C_p \frac{1}{\eta_c} T_{wc} \left(PR_c^{\frac{\gamma-1}{\gamma}} - 1 \right) \end{cases} \tag{9}$$

where, $\dot{m}_c$ is the mass flow rate of the compressor, η_t and η_c are the efficiency of the turbine and compressor, PR_t and PR_c stand for the pressure ratio of turbine and compressor, C_p is the heat specific ratio at constant pressure. The compressor efficiency and pressure ratio are given by maps, which depend on compressor speed and mass flow.

Fuel path

A. CA50

Theoretically, the CA50 is determined by integrating the chemical kinetics of Arrhenius rate equation and the combustion duration[18]. However, the unavailability of analytical solution and complexity of the equation make it hard to be applied to real applications. Here, the control-oriented model in a polynomial form in applied for CA50:

$$CA50(k+1) = c_1' CA50(k) + c_2' \tau_{inj}(k) + c_3' mg(k) + c_4' T_1(k) + c_5', \quad (10)$$

where, τ_{inj} is the injection timing and mg is the injection mass, $c_1' ... c_5'$ are the constant coefficients.

To be noted, since the residual gas kept in the cylinder brings coupling effects to adjacent engine cycles, so the model as in equation (10) is a difference equation: the CA50 in time-step *k* will have an impact on time-step *k+1*.

B. IMEP

Normally, the injection mass is the dominant factor for the work output-IMEP [19]. In this paper, since the intake conditions and the combustion phasing swipe a wide range, other factors, especially CA50, is also involved in the model:

$$IMEP = c_6' CA50 + c_7' mg + c_8', \quad (11)$$

where, $c_6' ... c_8'$ are the constant coefficients.

III. CONTROLLER DESIGN

For notation simplicity, taking intake temperature as x_1, the intake pressure as x_3 ,and the oxygen concentration as x_5, the air-path dynamics in equation (1) are expressed as:

$$\begin{cases} \dot{x}_1 = f_1 + b_1 \dot{m}_c + b_1' \dot{m}_{egr,hp} \\ \dot{x}_3 = f_2 + b_2 \dot{m}_c + b_2' \dot{m}_{egr,hp} \\ \dot{x}_5 = f_3 + b_3 \dot{m}_{egr,hp} + b_3' \dot{m}_{egr,lp} \end{cases}, \quad (12)$$

where, $f_1 = \frac{RT_1^2}{P_1 V_1} \dot{m}_{cyl}(1-\gamma), b_1 = \frac{RT_1}{P_1 V_1}(\gamma T_{ac} - T_1), b_1' = \frac{RT_1}{P_1 V_1}(\gamma T_2 - T_1),\ f_2 = -\frac{R\gamma}{V_1} \dot{m}_{cyl} T_1,$

$b_2 = \frac{R\gamma}{V_1} T_{ac}, b_2' = \frac{R\gamma}{V_1} T_2, f_3 = \frac{RT_1}{P_1 V_1}(F_{air} - F_1),\ b_3 = \frac{RT_1}{P_1 V_1}(F_2 - F_1), b_3' = \frac{RT_1}{P_1 V_1}[F_2(t-\tau) - F_1].$

A. ESO

Lump the modeling error and coupling effects given by the fuel path for each loop as one external state, then applying the concepts of extended state observer (ESO) and the super twisting, the system in (12) turns into:

$$\begin{cases} \dot{\hat{x}}_1 = f_1 + b_1\dot{m}_c + b_1'\dot{m}_{egr,hp} + \hat{x}_2 + k_1\left|e_1\right|^{\frac{1}{2}} sign(e_1) \\ \dot{\hat{x}}_2 = k_2 sign(e_1) \\ \dot{\hat{x}}_3 = f_2 + b_2\dot{m}_c + b_2'\dot{m}_{egr,hp} + \hat{x}_4 + k_3\left|e_3\right|^{\frac{1}{2}} sign(e_3) \\ \dot{\hat{x}}_4 = k_4 sign(e_3) \\ \dot{\hat{x}}_5 = f_3 + b_3\dot{m}_{egr,hp} + b_3'\dot{m}_{egr,lp} + \hat{x}_6 + k_5\left|e_5\right|^{\frac{1}{2}} sign(e_5) \\ \dot{\hat{x}}_6 = k_6 sign(e_5) \end{cases}, \tag{13}$$

where, $\hat{x}_2, \hat{x}_4, \hat{x}_6$ are the extended states for each loop, $k_1 \ldots k_6$ are filter gains and need to be tuned, $e_i, i = 1,3,5$ is the estimation error and defined as: $e_1 = T_1 - \hat{x}_1, e_3 = P_1 - \hat{x}_3, e_3 = F_1 - \hat{x}_5$.

Theorem : For a system like equation (13) with bounded disturbance terms $\hat{x}_2, \hat{x}_4, \hat{x}_6$, there exist filter gains $k_1 \ldots k_6$, such that the system state $\hat{x}_1 \ldots \hat{x}_6$ will converge to their real value $x_1 \ldots x_6$, in finite-time.

Proof: As we can see that, the loops in equation (13) are identical in terms of system structure. Without loss of generality, takes the temperature loop as an example. Let the estimation error as: $e_1 = x_1 - \hat{x}_1, e_2 = x_2 - \hat{x}_2$, then combines with equation (12)(13), the error dynamics for the temperature loop turns to be:

$$\begin{cases} \dot{e}_1 = e_2 - \dfrac{1}{2}k_1\left|e_1\right|^{\frac{1}{2}} sign(e_1) \\ \dot{e}_2 = -k_2 sign(e_1) \end{cases}, \tag{14}$$

Let $z_1 = |e_1|^{\frac{1}{2}} sign(e_1)$ and $z_2 = e_2$, then one can see that z_1 is differentiable and its derivative is: $\dot{z}_1 = \frac{1}{2}|e_1|^{-\frac{1}{2}}\dot{e}_1$. The error dynamics is transferred to:

$$\begin{bmatrix} \dot{z}_1 \\ \dot{z}_2 \end{bmatrix} = |e_1|^{-\frac{1}{2}} \begin{bmatrix} -\frac{1}{2}k_1 & \frac{1}{2} \\ -k_2 & 0 \end{bmatrix} \begin{bmatrix} z_1 \\ z_2 \end{bmatrix}. \tag{15}$$

Therefore, the system becomes into a standard super twisting observer. Applying theorem 2 in [20], the convergence of equation (13) can be guaranteed.

Especially, for this particular system, to make the filter gains tuning convenient, the following process can be applied.

Let $A = \begin{bmatrix} -\frac{1}{2}k_1 & \frac{1}{2} \\ -k_2 & 0 \end{bmatrix}$, and select the Lyapunov function candidate as:

$$V = \begin{bmatrix} z_1 & z_2 \end{bmatrix} P \begin{bmatrix} z_1 \\ z_2 \end{bmatrix}, \tag{16}$$

where, $\boldsymbol{P}$ is a positive definite symmetric matrix. Then, the derivative of V is given by:

$$\dot{V} = |e_1|^{-\frac{1}{2}} \begin{bmatrix} z_1 & z_2 \end{bmatrix} \left(A^T P + PA \right) \begin{bmatrix} z_1 \\ z_2 \end{bmatrix}, \tag{17}$$

Thus, the proof for the stability of equation (17) turns into finding a positive definite matrix $\boldsymbol{Q}$ to satisfy the following expression:

$$A^T P + PA = -Q. \tag{18}$$

Actually, equation (18) is equivalent to all the eigenvalues of A have a real negative part. The eigenvalue of A is calculated by the following equation:

$$\lambda^2 + \frac{1}{2}k_1\lambda + \frac{1}{2}k_2 = 0. \tag{19}$$

The roots of equation (19) are:

$$\lambda_1 = \frac{-\frac{1}{2}k_1 + \sqrt{\frac{1}{4}k_1^2 - 2k_2}}{2}, \lambda_2 = \frac{-\frac{1}{2}k_1 - \sqrt{\frac{1}{4}k_1^2 - 2k_2}}{2}. \tag{20}$$

Therefore, according to the Vieta's formulas, any $k_1 > 0$ and $k_2 > 0$ can make the real part of both λ_1 and λ_2 negative. Theorem is proved. By applying this theorem, the effort for tuning the observer gain is significantly related.

To be noted, here the ESO is designed by applying the super twisting idea. Hence, the robustness of the ESO is supposed to be superior to the commonly used linear ESO [14], especially for this MIMO, highly non-linear system.

B. Control law of the air-path

Once the disturbance term, $\hat{x}_2, \hat{x}_4, \hat{x}_6$ are estimated by equation (13), by canceling their impact on the final result, the control law is designed as follows.

Since $\hat{x}_1, \hat{x}_3, \hat{x}_5$ will converge to T_1, P, F_1, respectively as proved above, then the system can be expressed as:

$$\underbrace{\begin{pmatrix}\dot{x}_1\\ \dot{x}_3\\ \dot{x}_5\end{pmatrix}}_{\dot{x}}=\underbrace{\begin{pmatrix}f_1+\hat{x}_2\\ f_2+\hat{x}_4\\ f_3+\hat{x}_6\end{pmatrix}}_{A(x)}+\underbrace{\begin{pmatrix}b_1' & b_1 & 0\\ b_2' & b_2 & 0\\ b_3 & 0 & b_3'\end{pmatrix}}_{B(x)}\underbrace{\begin{pmatrix}u_1\\ u_2\\ u_3\end{pmatrix}}_{u}=A(x)+B(x)u \quad . \tag{21}$$

Based on the sliding mode control idea, the hypersurface is set as:

$$S=diag([c_1,c_2,c_3])(x-x_d)=c(x-x_d)\,. \tag{22}$$

where, $c_1 \ldots c_3$ are constant parameters, and $x-x_d$ are the tracking errors: $[T_1-T_d, P_1-P_d, F_1-F_d]^T$.

Then, Taking derivative of *S* gives:

$$\begin{aligned}\dot{S}&=c\dot{\varepsilon}\\ &=cA(x)+cB(x)u-c\dot{x}_d\end{aligned}\quad . \tag{23}$$

Thus, the control input u is designed as:

$$u=B(x)^{-1}c^{-1}[c\dot{x}_d-cA(x)-sign(S)k_c]\,. \tag{24}$$

where, $k_c=[k_{c1},k_{c2},k_{c3}]^T$ is the controller gain, and *sign* is the sign function, $sign(S)=[sign(S_1),sign(S_2),sign(S_3)]^T$.

Choose the Lyapunov function candidate as: $V=\frac{1}{2}S^TS$, then the derivative is:

$$\dot{V}=S^T\dot{S}=-S^Tsign(S)k_c=-|S|k_c\,. \tag{25}$$

Thus as long as $k_{c1}...k_{c3}$ are positive, the Lyapunov function is negative definite, the system is asymptotically stable and the states, the intake temperature, pressure and oxygen concentration will converge to the desired values.

To be noted, since the ESO is utilized to estimate the modeling error and coupling effect from the fuel path (which is much smaller), i.e. disturbance terms of $\hat{x}_2, \hat{x}_4, \hat{x}_6$ in $A(x)$ in equation (21), thus the controller design is significantly relaxed. It also means that the performance of the controller actually to a large extent depend on the performance of the ESO. In this paper, the conventional linear ESO is enhanced by the proposed super twisting ESO to deal with this MIMO system.

C. Control law of the fuel-path

For the fuel-path, considering that the effect of air-path on the combustion phasing and work out is indirect and slow, the controller is designed as follows:

$$u_{\tau_{inj}} = -\frac{1}{c_2'}(c_3' mg(k) + c_4' T_1(k) + c_5') + (c_1' - k_{c4} c_2') CA50 + k_{c5}(CA50 - CA50_d),$$
$$u_{mg} = \frac{IMEP_d - c_6' CA50 - c_8'}{c'} + k_{c6}(IMEP - IMEP_d), \tag{26}$$

where, k_{c5} and k_{c6} constant gains.

Both the controllers for the CA50 and IMEP have two parts: the first part (first two terms of $u_{\tau_{inj}}$, first term of u_{mg}) are designed based on the model (equation (10)and (11)) to compensate the effects of air-path loop; the second part (last term of $u_{\tau_{inj}}$ and u_{mg}, respectively) are designed for a fast response.

The control diagram for the whole system is drawn below.

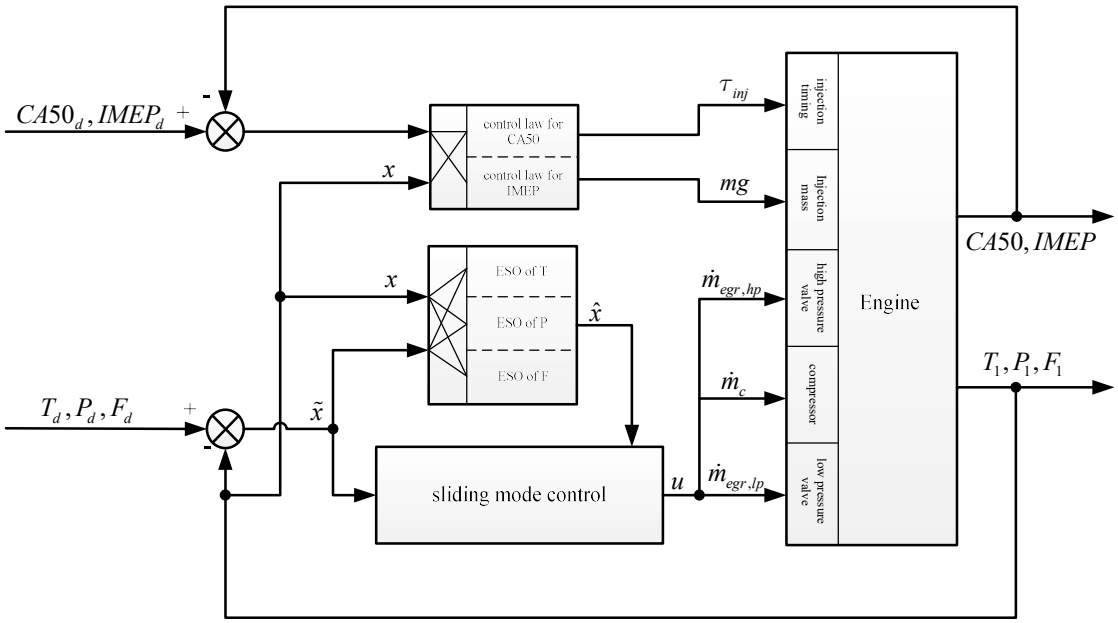

Fig.2 Control diagram for the whole system

IV. COMBUSTION MODEL CALIBRATION

A four-cylinder Diesel engine, as shown in Fig.1, was constructed in GT-Power environment. The combustion model of this engine was calibrated by the in-cylinder pressure data and injection profile information from a real engine.

A. Experiments set up

To calibrate the GT-Power model, the experimental test bench of a four-cylinder Diesel engine with displacement as 1.9L running in medium-duty is applied. The specifications of the engine are detailed in Table I.

Table I Engine Specifications Table

Items	Description
Compression ratio	17.5
Displacement (L)	1.9
Stroke (mm)	92.4
Bore (mm)	81
Rated power (kW))	93
Max. torque (Nm)	271
Fuel injection system	Common rail

As shown in Fig.3, the engine test bench equips Horiba HT250 dynamometer, Turbocharger, intercooler and DPF in the EGR loop.

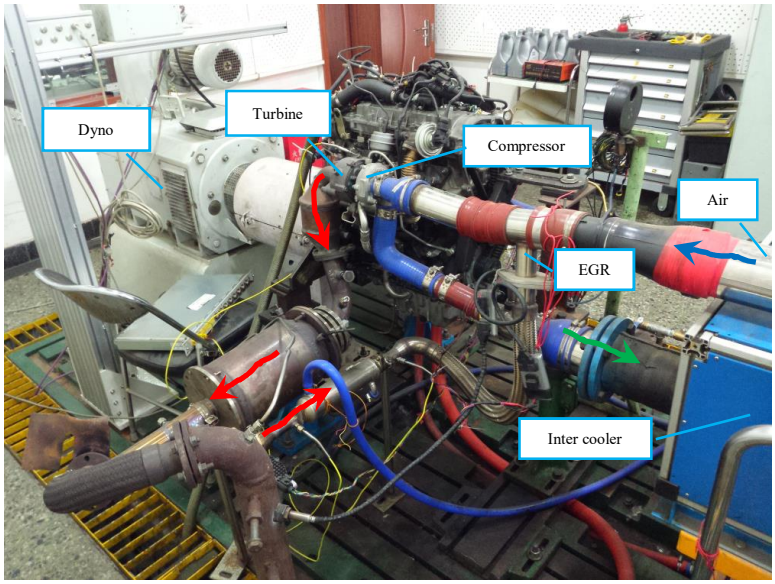

Fig.3 Engine test bench

To cover a wide range of operating conditions and make the calibration representative while the combustion is still stable, we changed the injection timing, EGR rate and injection mass as tabulated in the following table. Fixing the engine speed on 1800RPM, and 2 different injection timings, 5 EGR rates, and 6 injection masses totally 60 operating condition combinations were carried out, as tabulated in Table II.

TABLE II OPERATING CONDITIONS

Injection timing (ATDC)	EGR(%)	Injection mass(mg)
-10	10	15
		17
	15	
	20	19
		21
-15	25	
		23
	30	
		25

B. Combustion model calibration

A DI-Pulse combustion model is applied in this study. DI-Pulse combustion model is a predictive model, which tracks the fuel as it is injected, evaporates, mixes with surrounding gas and burns to predict the combustion rate and associated emissions. Hence, it is suitable for the simulations when the combustion phasing (CA50) is involved. This model requires calibration to match the combustion event as calculated from the cylinder pressure analysis[21].

The calibration for the DI-Pulse model including calibrating the injector model, TPA (three pressure analysis) and CPOA (cylinder pressure only analysis), then the model constants estimation and validation [21]. Following are the validation part of the model calibration.

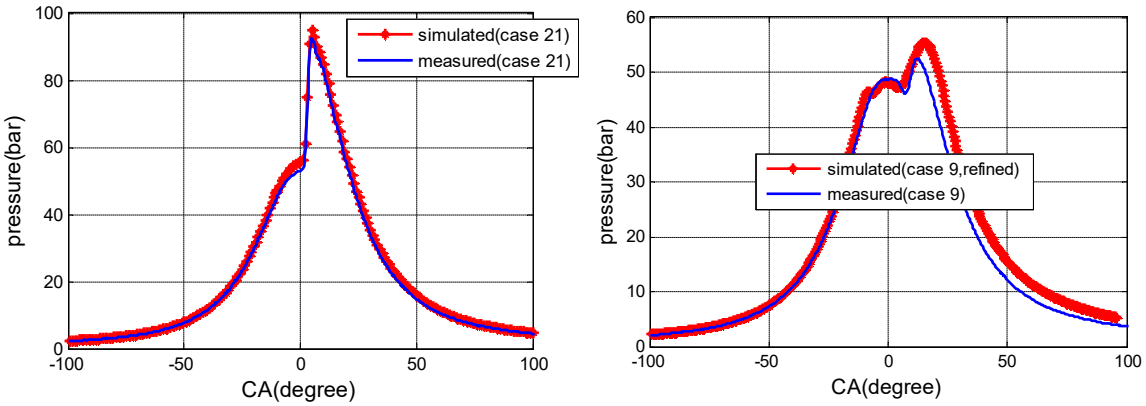

Fig.4 Two examples of the comparison between the measured and the simulated (given by the DI-Pulse combustion model) in-cylinder pressure

Two examples of the measured and the simulated in-cylinder pressure are compared in the Fig.4. Although for this two largely different operating conditions (as the distinct pressure curves in the two plots), as compared to the above figure, the in-cylinder pressure generated by the combustion model is very close to the measured pressures , which means the calibrated combustion model works well.

The CA50 calculated by the measured pressure and the simulated pressure for the whole 60 cases with different operating conditions are plotted in the following figure.

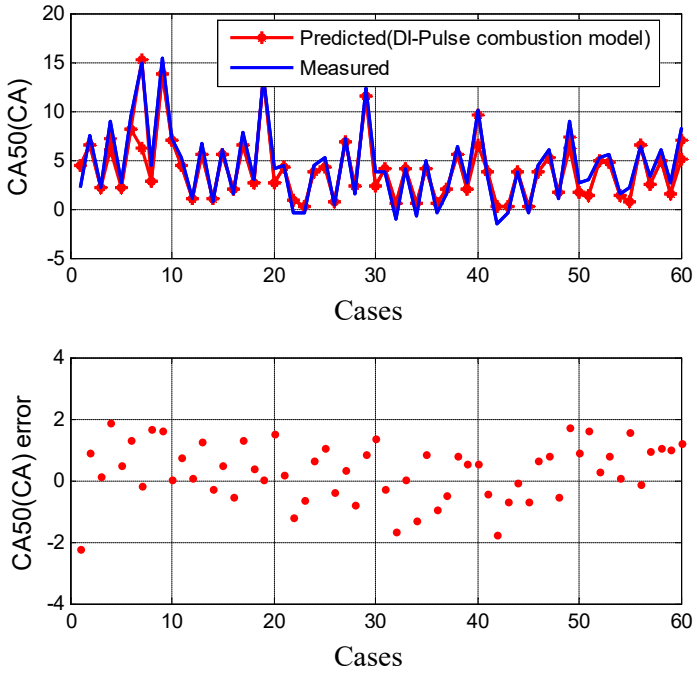

Fig.5 The comparison between the measured (calculated by the measured pressure) and the predicted(calculated by the simulated pressure) CA50

As clearly demonstrated in the Fig.5, the CA50 error given by the DI-Pulse combustion model is within 2 crank angle (CA) degrees, which lays a solid foundation for the following control simulations.

V. SIMULATION VALIDATION

To test the effectiveness of the proposed control method, the control law as demonstrated in Fig.2 was implemented in Simulink, and a series of coupling simulation between the Simulink and GT-Power are carried on.

Three scenarios are considered in the simulation: 1) apply the air-path controller only; 2）keep the IMEP and CA50 constant; 3) let the IMEP and CA50 track step trajectories. Followings are the results of the 3 scenarios.

A. Apply the air-path controller only

The injection timing and injection are fixed constantly as: -10CA ATDC (after top dead center) and 20mg, respectively. The control results given by the proposed control method is shown in Fig.6.

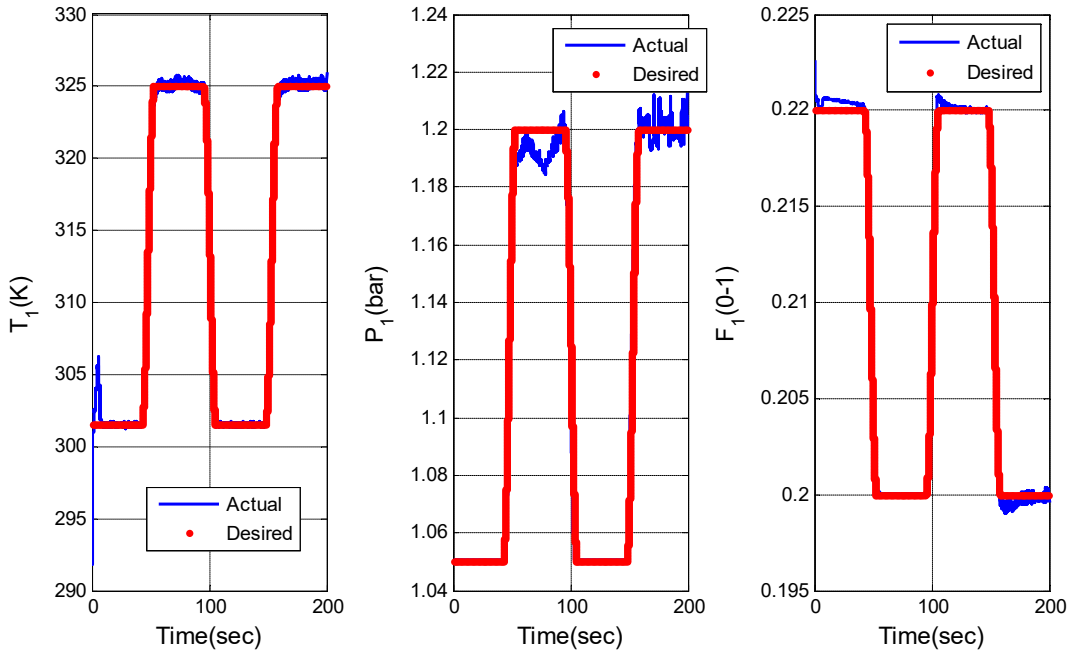

Fig.6 The air-path control results by applying the air-path controller only

The desired trajectories of temperature, pressure oxygen are selected by referring to [12][13]. Usually, for a Diesel engine switching from conventional to advanced combustion mode, the temperature and pressure need to be higher to counterbalance the effect of higher EGR to facilitate the auto-ignition. The oxygen concentration should be lower to extend the ignition delay for a better fuel and air mixing. As one can see the temperature/pressure and EGR (oxygen concentration) are competing factors for the auto-ignition and ignition delay. Therefore, the references of them need to be carefully designed on a case-by-case basis.

For the engine in Fig.3, the desired trajectories for the intake conditions are represented in red dotted lines in Fig.6. As shown in Fig.6, the actual intake conditions (the solid blue lines in Fig.6) resulted by applying the air-path controller only, track the references very well.

The change of intake conditions brings impacts on the IMEP and CA50. In this case, lower oxygen concentration tends to delay the auto-ignition and extend the combustion duration, which overshadows the effect of higher temperature and pressure, although the CA50 retards roughly only 0.5 ca, as in Fig.7 (during the periods of 50-100s and 150-200s on the red dotted lines). The later CA50 increases the IMEP, which suggests that the efficiency is increased as in Fig.7 (the red dotted lines).

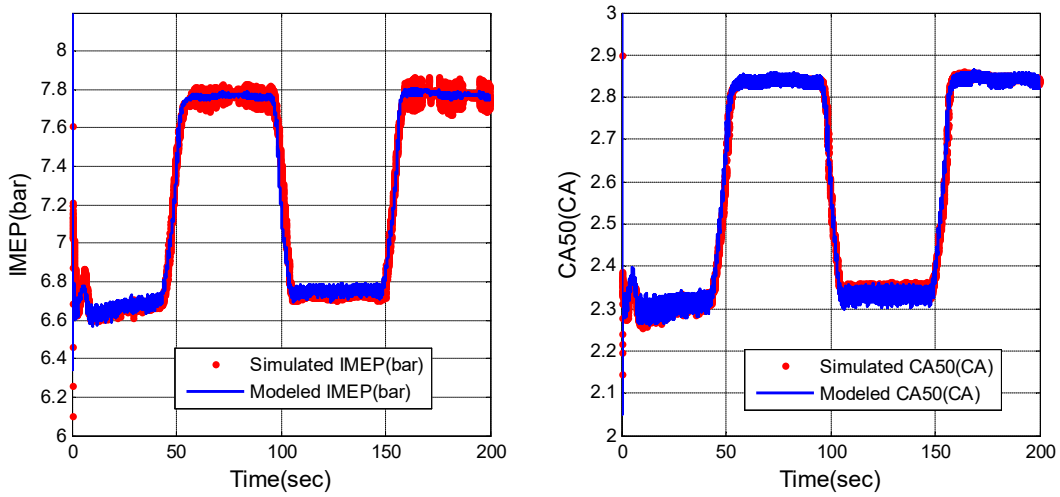

Fig.7 The IMEP and CA50 traces with injection timing and injection fixed (simulated and modeled)

The IMEP and CA50 traces as shown in the red dotted lines in the figure above are applied to calibrate their models, as equation (10) and (11). The calculated models are represented as the solid blue in Fig.7. Obviously, both models can capture the IMEP and CA50 well. The calibrated coefficients are used to design the control law.

B. Keep the IMEP and CA50 constant

In this scenario, the fuel-path controller is applied to keep the IMEP and CA50 constantly; while the air-path controller regulates the intake conditions track the same trajectories as the above scenario.

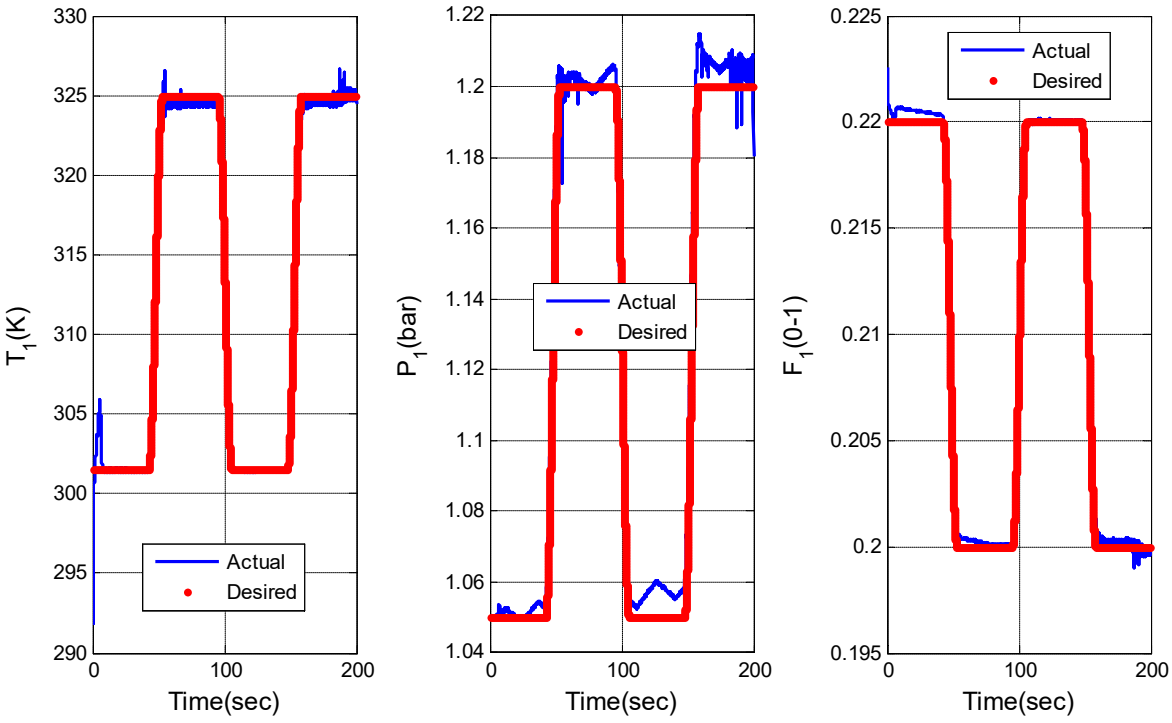

Fig.8 The air-path control results by applying both air-path and fuel-path controllers

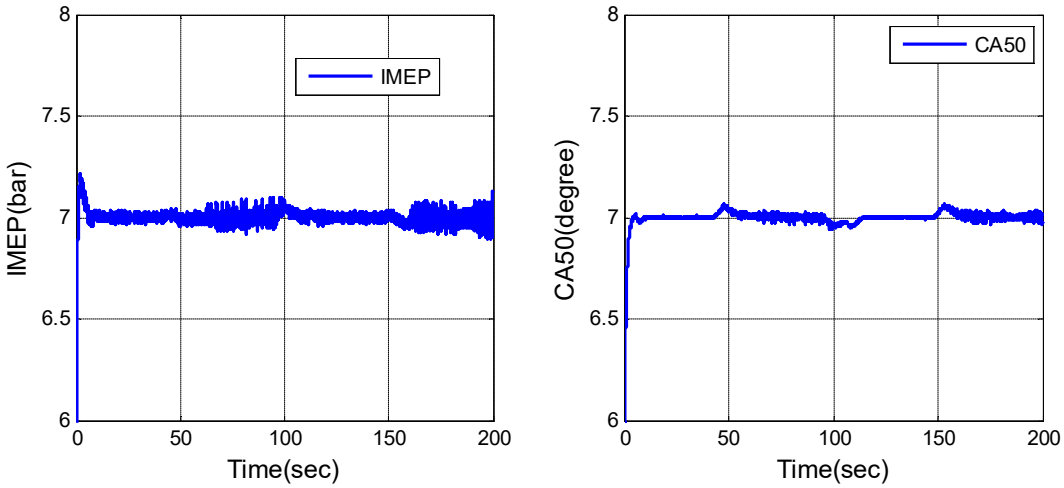

Fig.9 The IMEP and CA50 traces for scenario 2

The control results of the intake conditions and the IMEP and CA50 are showing in Fig.8, Fig.9, respectively. As told by Fig.8, although the fuel-path controller is turned on, its effect on the air-path is well compensated by the ESO and the air-path controller: all the intake conditions, including the temperature pressure and oxygen concentration can be well controlled.

The IMEP and CA50 are all successfully kept as 7 (bar and CA), as suggested by Fig.9. The corresponding control inputs are in Fig.9. As one can see, to move the CA50 to 7 CA, the injection timing is moved forward from -10 ATDC (the first scenario) to the range -5.5 to -4.5 ATDC. And the injection varies from 19mg to 21mg to maintain the IMEP as 7bar.

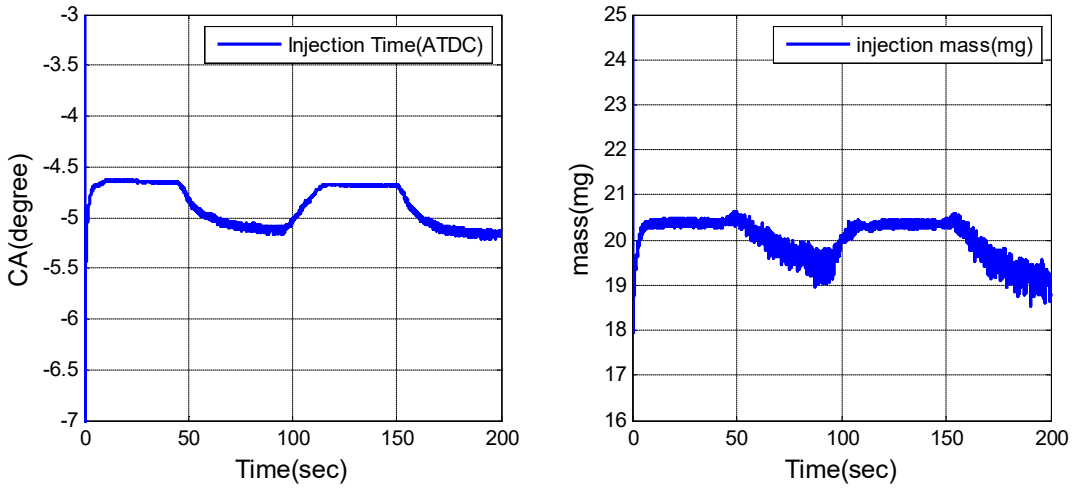

Fig.10 The injection timing and injection mass for scenario 2

This scenario is performed in the consideration that in some cases, the engine needs to keep constant work output for a stable and smooth driving experience. The simulation results in Fig.8, and Fig.9 given by the proposed control method works well.

C. IMEP and CA50 track step trajectories

The fuel-path controller can be used to improve the transient performance of the air-path controller, on account of that the effect of the intake conditions on the combustion process is critical but indirect.

As told by Fig.12, with fuel-path control, both IMEP and CA50 in transient situations (around 50s, 100s and 150s) are significantly improved: very short settling timing and small overshoot. Meanwhile, the intake conditions are also well controlled by the air-path controller, as shown in Fig.11.

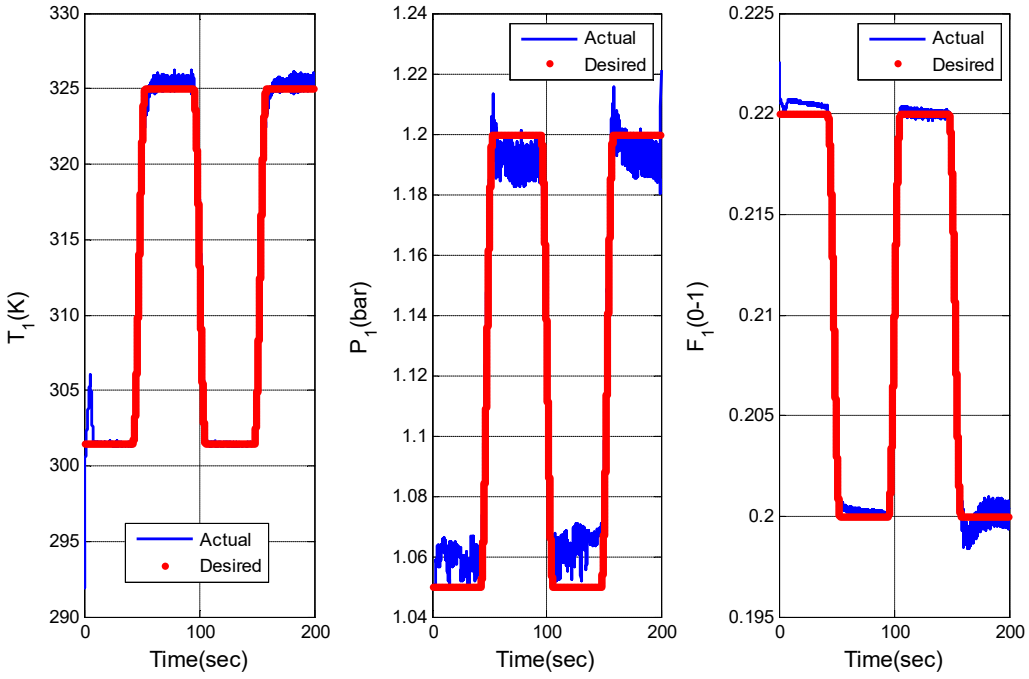

Fig.11 The air-path control results by applying both air-path and fuel-path controllers

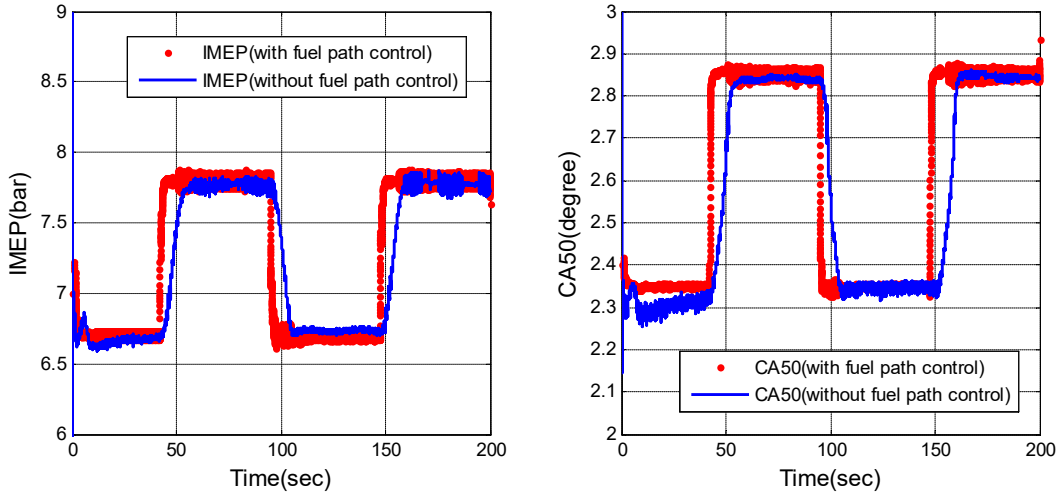

Fig.12 The comparisons of the IMEP and CA50 given by the method with and without fuel-path control

The fuel-path control inputs, as displayed in the following figure, tell that large control efforts (advanced or retarded injection timing and a large amount of injection

mass) are applied to the engine during transient situations to track the step reference. While during static periods, the control inputs reduced, which suggests that the air-path conditions take the responsibility for the combustion process control.

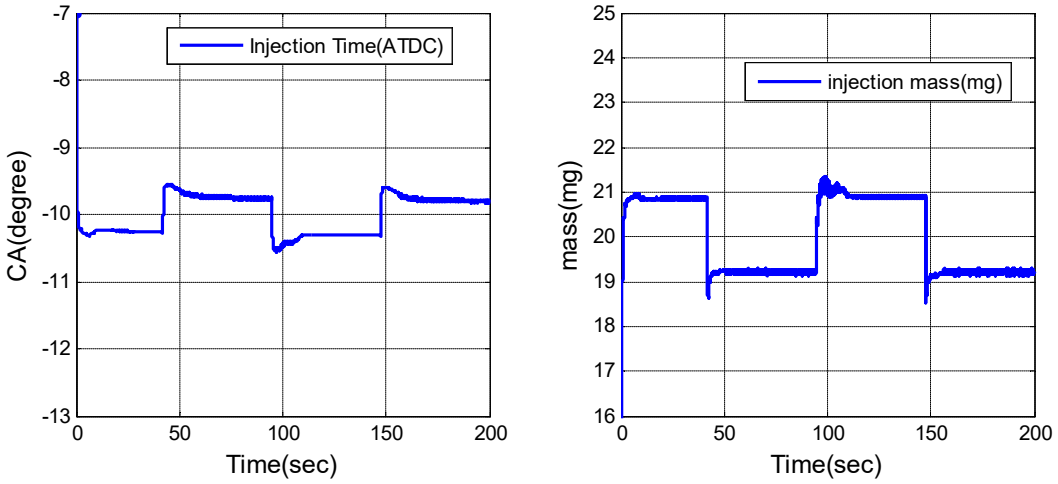

Fig.13 The fuel-path control inputs

VI. `CONCLUSIONS

In this paper, a novel air- and fuel-path control method is presented. Sliding mode control with enhanced extended state observer is applied on the air-path loop to deal with the modeling error and coupling effect from fuel-path. For the fuel-path, considering the quick and direct effect of injection timing on CA50 and injection mass on IMEP, a relatively simple control idea is adopted based on their models.

To test the effectiveness of proposed method, a four-cylinder turbocharged Diesel engine with dual-loop EGR is constructed in GT-Power and calibrated by the data from a real engine. The simulation results tell that: 1) the intake conditions can track the reference well by the air-path control law; 2) by combining with the fuel-path control law,

the CA50 and IMEP are significantly improved in transient situations and due to the ESO, the air-path can still be well controlled.

REFERENCES

[1] X.-C. Lü, W. Chen, and Z. Huang, "A fundamental study on the control of the HCCI combustion and emissions by fuel design concept combined with controllable EGR. Part 2. Effect of operating conditions and EGR on HCCI combustion," *Fuel*, vol. 84, no. 9, pp. 1084–1092, Jun. 2005.

[2] P. Borgqvist, "The Low Load Limit of Gasoline Partially Premixed Combustion (PPC) Experiments in a Light Duty Diesel Engine," Lund University, 2013.

[3] J. Wang, "Hybrid Robust Air-Path Control for Diesel Engines Operating Conventional and Low Temperature Combustion Modes," *IEEE Trans. Control Syst. Technol.*, vol. 16, no. 6, pp. 1138–1151, Nov. 2008.

[4] K. Akihama, Y. Takatori, K. Inagaki, a. M. Dean, and S. Sasaki, "Mechanism of the smokeless Rich Diesel combustion by reducing temperature," *SAE Tech. Pap.*, vol. 2001, no. 2001–01–0655, pp. 2001–01–0655, 2001.

[5] F. Yan and J. Wang, "Control of dual loop EGR air-path systems for advanced combustion diesel engines by a singular perturbation methodology," *Proc. 2011 Am. Control Conf.*, vol. 21, no. 7, pp. 1561–1566, 2011.

[6] E. Hellstr, A. G. Stefanopoulou, and L. Jiang, "Cyclic Variability and Dynamical Instabilities in Autoignition Engines with High Residuals," pp. 1–10.

[7] S. Chen and F. Yan, "Trapped Unburned Fuel Estimation and Robustness Analysis for a Turbocharged Diesel Engine With Negative Valve Overlap Strategy," *J. Dyn. Syst. Meas. Control*, vol. 137, no. 6, p. 061004, 2015.

[8] F. Willems, E. Doosje, F. Engels, and X. Seykens, "Cylinder Pressure-Based Control in Heavy-Duty EGR Diesel Engines Using a Virtual Heat Release and Emission Sensor," 2010.

[9] T. Guohong, W. Zhi, W. Jianxin, H. Xu, and S. Shijin, "Effects of Key Factors on the Engine Combustion Mode Switching Between HCCI and SI," *J. Eng. Gas Turbines Power*, vol. 131, no. 1, p. 012803, 2009.

[10] S. Chen and F. Yan, "control of a dual-loop exhaust gas recirculation system for a turbocharged diesel engine," *Int. J. Autom. Technol.*, vol. 16, no. 5, pp. 733–738, 2015.

[11] F. Yan and J. Wang, "Control of diesel engine dual-loop EGR air-path systems by a singular perturbation method," *Control Eng. Pract.*, vol. 21, no. 7, pp. 981–988, Jul. 2013.

[12] X. Zeng and J. Wang, "Control of dual-loop EGR engine air-path systems with adjustable intake manifold condition priorities," *2014 Am. Control Conf.*, pp. 208–213, Jun. 2014.

[13] F. Yan and J. Wang, "Air- and Fuel-Path Coordinated Control for Advanced Combustion Mode Transitions in Diesel Engines," in *American control conference*, 2012, pp. 2890–2895.

[14] Q. Zheng, Z. Chen, and Z. Gao, "A practical approach to disturbance decoupling control," *Control Eng. Pract.*, vol. 17, no. 9, pp. 1016–1025, Sep. 2009.

[15] J. Park, K. S. Lee, S. Song, and K. M. Chun, "Numerical Study of A Light-Duty Diesel Engine With A Dual-Loop EGR System Under Frequent Engine Operating Conditions Using The DOE Method," vol. 11, no. 5, pp. 617–623, 2010.

[16] P. Moulin and J. Chauvin, "Analysis and control of the air system of a turbocharged gasoline engine," *2008 47th IEEE Conf. Decis. Control*, pp. 5643–5649, 2008.

[17] O. Grondin, P. Moulin, and J. Chauvin, "Control of a Turbocharged Diesel Engine Fitted with High Pressure and Low Pressure Exhaust Gas Recirculation Systems," *IEEE Conf. Decis. Control Eur. Control Conf.*, pp. 6582–6589, 2009.

[18] J. B. Heywood, *Internal Combustion Engine Fundamentals*, vol. 21. McGraw-Hill,Inc., 1988.

[19] F. Yan, S. Chen, X. Zeng, J. Zhao, and J. Wang, "Modeling and Analysis of Fuel Injection Split for Diesel Engine Active Fueling Control," *J. Dyn. Syst. Meas. Control*, vol. 135, no. 6, p. 061016, 2013.

[20] J. a. Moreno and M. Osorio, "Strict lyapunov functions for the super-twisting algorithm," *IEEE Trans. Automat. Contr.*, vol. 57, no. 4, pp. 1035–1040, 2012.

[21] GT-SUITE(2013), "Engine Performance Application Manual, v 7.4," 2013.

Remarks

1) The idea introduced in this paper controls the intake conditions, the combustion phasing and the work output of a conventional Diesel engine simultaneously in a decoupled fashion. The decoupling is conducted by taking the advantage of the ESO and the different time scales of the air-path loop (slow) and fuel-path loop (fast). This method is model-based, thus, can be also applied to engines with low temperature combustion mode.

2) For advanced combustion mode, the combustion process, especially the combustion smoothness is more likely to be influenced by the intake conditions. The careful design for the air-path loop controller with the consideration of the impacts from the fuel-path loop makes the proposed method fit the requirement well.

3) The desired intake conditions should be selected carefully according to different engines running in different situations. The simulations given in this paper is under fixed engine speed. The engine speed impacts not only the combustion process, but also the air-path loop, especially the turbocharger. Although the air-path controller is model based, for different engine speeds, the gains of the ESO and controller need to be tuned accordingly. The fuel-path model, i.e. the model for CA50 and IMEP, need to be re-calibrated. Gain scheduling method can be used to deal with it.

Chaper 5. Paper 4 Trapped Unburned Fuel Estimation and Robustness Analysis for a Turbocharged Diesel Engine with Negative Valve Overlap Strategy

5.1 Citation and Main Contributor

Chen, S., & Yan, F. Trapped Unburned Fuel Estimation and Robustness Analysis for a Turbocharged Diesel Engine with Negative Valve Overlap Strategy. *Journal of Dynamic Systems, Measurement, and Control,* DOI: 10.1115/1.4028873, 2015.

The main contributor to this paper is the first author-Chen Song (contributes more than 70%).

5.2 Brief Introduction

Paper 3 deals with the Diesel engine combustion control and this paper focuses on the control quality evaluation in terms of EGR level and cyclic variations based on the estimation for the unburned fuel.

To reduce the engine out emissions, especially the particulate matter (PM), a large amount of exhaust gas will be induced (through external EGR loop) or remained (i.e. internal EGR, by utilizing negative valve overlap technique) to/in the cylinder. The dilution effect of such amount of the exhaust gas leads combustion unstable and severe cyclic variation. The cyclic variation can be quantified by calculating the heat released during combustion. It turns out the unburned fuel is a good indicator for the cyclic variation. This paper introduces a technique to estimate the unburned fuel through the estimation of the oxygen concentration.

Turbocharger and negative valve overlap strategy are widely used among advanced combustion modes for internal combustion engines. In order to achieve well

emission performance, the residual gas fraction can be up to 40%. With such amount of residual gas in the cylinder, the trapped unburned fuel is not trivial. In this paper, a novel method based on the signals of oxygen fraction is proposed to estimate it. The proposed models and methods and theoretical analysis are validated and compared to a set of simulations in high-fidelity GT-Power environment. The simulation results match well with theoretical analysis that the Smooth Variable Structure Filter has good properties of strong robustness (with a root mean square error of 0.24, comparing with 0.4 of linear parameter varying filter and 0.49 of Kalman filter, for the unburned fuel estimation).

5.3 Main contributions

1) The information of oxygen fraction is used to extract the unburned fuel in an iterative way. The direct relationship between the oxygen fraction and unburned fuel combining with the simple dynamics of oxygen fraction facilitates the estimation for unburned fuel significantly.
2) Three filters, namely KF, SVSF and LPV are designed and compared. Their robustness is analyzed theoretically. The methods introduced in this paper can be easily extended to other fields.

5.4 Full content of Paper 4

Trapped Unburned Fuel Estimation and Robustness Analysis for a Turbocharged Diesel Engine with Negative Valve Overlap (NVO) Strategy

Song Chen and Fengjun Yan*
Department of Mechanical Engineering
McMaster University
Hamilton, ON, L8S 4L7 Canada

Abstract —Turbocharger and negative valve overlap strategy are widely used among advanced combustion modes for internal combustion engines. In order to achieve well emission performance, the negative valve overlap can be as large as 100 crank angle degrees, such that the residual gas fraction can be up to 40%. With such amount of residual gas in the cylinder, the trapped unburned fuel is not trivial. It has a significant impact on the combustion process. However, the trapped unburned fuel mass is hard to be measured directly. In this paper, a novel method based on the signals of oxygen fraction is proposed to estimate it. By analyzing the combustion process, dynamic equations on the intake/ exhaust manifolds and in-cylinder oxygen fractions, as well as actual fuel mass in the cylinder are constructed. A Smooth Variable Structure Filter was designed to estimate oxygen fractions and further the trapped unburned fuel. As a comparison, Kalman filter and Linear Matrix Inequality based linear parameter-varying filter were also applied. Robustness properties of the three observers are analyzed based on the theory of input-to-state stability. The proposed models and methods and theoretical analysis are validated and compared to a set of simulations in high-fidelity GT-Power environment. The simulation results match well with theoretical analysis that the Smooth

Song Chen is with the Department of Mechanical Engineering at McMaster University, Hamilton, ON Canada, email: chens78@mcmaster.ca.
*Corresponding author. Fengjun Yan is with the Department of Mechanical Engineering at McMaster University, Hamilton, ON Canada, email: yanfeng@mcmaster.ca.

Variable Structure Filter has good properties of strong robustness (with a root mean square error of 0.24, comparing with 0.4 of linear parameter varying filter and 0.49 of Kalman filter, for the unburned fuel estimation).

Keywords: Unburned fuel, Kalman Filter, Smooth Variable Structure Filter, Linear Parameter-varying Estimation, input-to-state stability

I. INTRODUCTION

Internal and external exhaust gas recirculation (EGR) strategy offer a promising solution for reducing peak combustion temperature and adjusting combustion timing for advanced combustion modes, such as homogeneous charge compression ignition(HCCI), premixed charge compression ignition (PCCI) and low temperature combustion(LTC) [1-5].

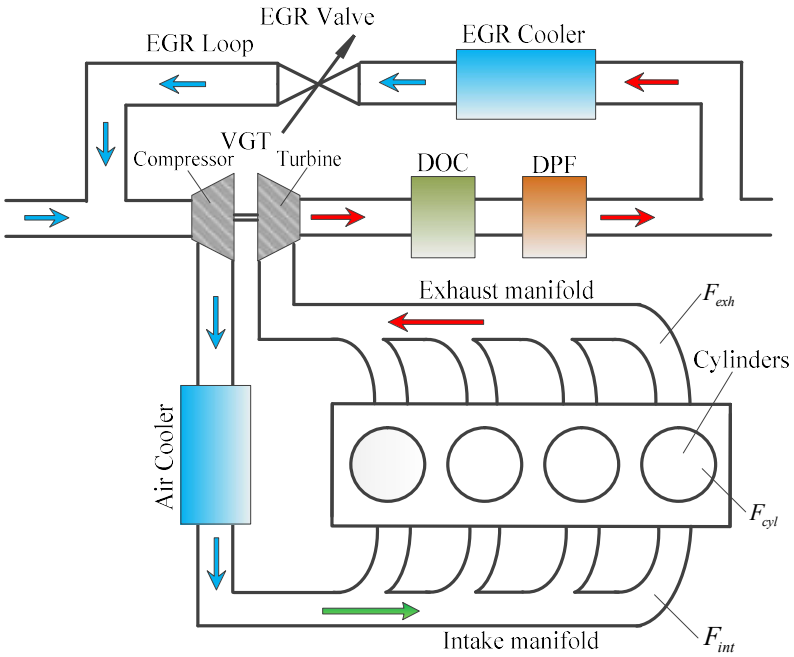

Fig.1 Engine architecture with variable geometry turbocharger and EGR loop

Typical engine architecture is shown in Fig.1 [6]. The EGR loop in the figure provides external exhaust for the engine. The external exhaust gas drives the VGT (variable geometry turbocharger) as indicated in Fig.1. VGT combines with the EGR valve can conveniently and flexibly control the total and exhaust gas mass inhaled to the intake manifold. By closing the exhaust valves early, well before top dead center (TDC), to trap residual gas in the cylinder, and meanwhile, to avoid large amount of backflow to the intake manifold, the inlet valves have to be opened later, well after TDC, this called negative valve overlap (NVO) [7], which provides internal exhaust for the engine.

In order to achieve well emission performance and high thermal efficiency, the NVO can be as large as over 100 crank angles (CA), such that the residual gas fraction can be up to 40%-50%[8,9]. With such amount of residual gas in the cylinder, the trapped unburned fuel is not trivial. Furthermore, it has a significant impact on the combustion process[10]; on the other hand, the trapped unburned fuel introduces severe cyclic variability to the engines[11].

However, the trapped unburned fuel is very hard to be measured directly in commercial applications. [10] introduced a method based on calculating the heat release. This approach is sensitive to the noise of the pressure signal and relies on an accurate model of the cylinder wall temperature. The simulation results show that it falls in severe vibration and low accuracy, especially in the case of cold start.

In this paper, a novel method based on the oxygen fraction is proposed to estimate the trapped unburned fuel. The in-cylinder oxygen fraction well indicates the combustion efficiency which has a direct relationship with the mass of unburned fuel. The oxygen

and/or air fraction estimation issues were investigated in some literature. [12] provided an estimation method for the oxygen concentration of the charge gas when the residual gas is negligible. A physically-based strategy was outlined in [13], the estimation algorithm was developed and proven to be robust to turbine flow errors. A Luenberger-like observer was designed to estimate the air fractions in all engine sections for a light-duty diesel engine in [14]. Maps and lookup tables based models for air flow and residual gas were presented for a variable valve timing simulation engine in [15].

As for the engine with VGT and dual-loop EGR system in Fig.1, by analyzing the combustion process, we constructed dynamic equations for the intake/ exhaust manifolds and in-cylinder oxygen fraction, as well as actual fuel mass in the cylinder. A Smooth Variable Structure Filter (SVSF) was utilized for the purpose of estimating the in-cylinder oxygen fraction. As a comparison, two other observers, specifically as the Kalman filter and Linear Matrix Inequality (LMI) based linear parameter-varying filter (LPV) were designed for the same estimation. For every cycle, the in-cylinder oxygen fraction can be roughly estimated by applying the previous combustion efficiency, and then refined in an iterative way until they reach stable. Then, the unburned fuel mass can be updated by the refined combustion efficiency and actual fuel mass in the cylinder.

To compare the three filters' properties on uncertainties rejection, the robustness of the 3 observers were analyzed based on input-to-state-stability (ISS) theory. By rearranging the terms of the three observers and applying the ISS theory, their robustness properties can be compared in a quantified way. Through simulating a high-fidelity GT-Power model, the proposed models and observers are validated and the simulation results show good consistent with the theory analysis.

The arrangement of the rest of this paper is as follows. In section II, the system dynamic models are proposed. The three filters are designed in section III. Robustness analyses based on ISS theory are summarized in section IV. The proposed models, observers, and robustness analysis are validated by a set of simulation in GT-Power environment in section V. Conclusive remarks are given in section VI.

II. SYSTEM MODELING

In this section, the models for the residual gas mass, the oxygen fractions in the cylinder, and in the intake and exhaust manifolds, as well as for the fuel mass are introduced.

A. Variable geometry turbocharger (VGT)

The VGT consists of a compressor connected to a turbine via a shaft. The turbine is driven by the exhaust gas, and thus part of the energy kept in the exhaust system is transferred to the compressor through the shaft. The turbocharger rotational speed (N) is derived from the power balance between the turbine and compressor [16].

$$JN\frac{dN}{dt} = P_{turbine} - P_{comp}, \tag{1}$$

where, J is the moment of inertia of the rotating parts; $P_{turbine}, P_{comp}$ are the power of the turbine and the compressor, they can be expressed as follow[17,18]:

$$\begin{cases} P_{turbine} = \dot{m}_{turbine} C_p \eta_{turbine} T_{exh} \left[1 - \left(\dfrac{1}{PR_{turbine}} \right)^{\frac{\gamma-1}{\gamma}} \right], \\ P_{comp} = \dot{m}_{comp} C_p \dfrac{1}{\eta_{comp}} T_{uc} \left(PR_{comp}^{\ \frac{\gamma-1}{\gamma}} - 1 \right) \end{cases} \tag{2}$$

where, $\dot{m}_{comp}$ and $\dot{m}_{turbine}$ are the mass flow rate of the compressor and turbine, by integrating them the gas mass through compressor and turbine, m_{comp} and $m_{turbine}$ can be obtained; $\eta_{turbine}$ and η_{comp} are the efficiency of the turbine and compressor, $PR_{turbine}$ and PR_{comp} stand for the pressure ratio of turbine and compressor, T_{exh} and T_{uc} are the exhaust manifold temperature and the upstream temperature of the compressor; C_p is the heat specific ratio at constant pressure. The compressor efficiency and pressure ratio are given by maps, which depend on compressor speed and mass flow.

B. Residual gas and trapped unburned fuel

Here, we take the time of the end of injection as the as the boundary point for adjacent cycles. The fuel mass in the next cycle (k+1) before combustion is the trapped fuel in present cycle (k) plus the injection:

$$m_f(k+1)=m_{unburned}(k)+m_i(k), \tag{3}$$

where, m stands for mass; subscript *f*, *unburned* and *i* represent fuel, trapped unburned fuel and injected fuel, respectively; *k* is the cycle index.

The trapped unburned fuel is contained in the residual gas:

$$m_{unburned}(k)=\frac{m_r(k)}{m_{cyl}(k)}[1-\hat{\eta}(k)]m_f(k), \tag{4}$$

where, m_{cyl} means the total mass of the in-cylinder gas after injection; $\hat{\eta}$ is an approximated combustion efficiency and can be assumed roughly equals to the refined previous value:

$$\hat{\eta}(k) = \eta(k-1) . \tag{5}$$

Note, $\eta(k)$, the exact combustion efficiency, is needed rather than $\hat{\eta}(k)$ to calculate the $m_{unburned}(k)$, in equation (4). The approximated combustion efficiency; $\hat{\eta}$ will be updated and refined in an iterative way by using the estimated in-cylinder oxygen fraction which was detailed in subsection D.

The aspirated gas from intake manifold to the cylinder, $m_{int\text{-}c}$, can be obtained by integrating the speed-density model:

$$\dot{m}_{int\text{-}c} = \frac{\lambda_v P_{int} V_d N_e}{120 R T_{int}}, \tag{6}$$

where λ_v is the volumetric efficiency was mapped as a function of combustion efficiency and EGR valve opening, N_e is the engine speed and V_d is the swept volume.

Applying the ideal gas law:

$$\frac{m_r(k)}{m_{cyl}(k)} = \frac{P_{evc}(k)}{P_{evo}(k)} \frac{V_{evc}(k)}{V_{evo}(k)} \frac{T_{evo}(k)}{T_{evc}(k)}, \tag{7}$$

where, *P* and *V* stand for the pressure and volume, subscript *evc* and *evo* are the crank angle degree of exhaust valve closing and opening.

Assuming the exhaust process is isentropic, the residual mass, $m_r(k)$, can be estimated as:

$$m_r(k) = m_{cyl}(k) \left(\frac{V_{evc}(k)}{V_{evo}(k)} \right) \left(\frac{P_{evc}(k)}{P_{evo}(k)} \right)^{\frac{1}{\gamma}} . \tag{8}$$

C. Cylinder, intake and exhaust manifolds oxygen fraction

The in-cylinder gas in the next cycle is composed of the residual gas plus the injection and the aspirated gas from the intake manifold in the present cycle:

$$m_{cyl}(k+1) = m_{cyl}(k) - m_{c-e}(k) + m_{int\text{-}c}(k) + m_i(k), \tag{9}$$

where , subscript *r* and *int-c* are the residual gas and aspirated gas from the intake manifold into the cylinders.

Applying the oxygen conservation, the next in-cylinder oxygen is composed of present in-cylinder oxygen plus aspirated minus the consumed and the exhaled and then divided by next in-cylinder gas mass:

$$F_{cyl}(k+1) = \frac{F_{cyl}(k)m_{cyl}(k) - \hat{\eta}(k)m_f(k)\lambda_s - m_{c-e}(k)F_{c-e}(k) + F_{int}(k)m_{int\text{-}c}(k)}{m_{cyl}(k+1)}, \tag{10}$$

where, *F* represents the oxygen fraction, subscript *cyl* means the cylinder and *c-e* ; λ_s is the stoichiometric oxygen fuel ratio.

The oxygen mass fraction of the gas exhales from cylinder to the exhaust manifold, or the oxygen concentration after combustion, F_{c-e}, is computed by the in-cylinder oxygen before combustion minus the consumed oxygen and then divided by the total gas mass:

$$F_{c-e}(k) = \frac{F_{cyl}(k)m_{cyl}(k) - \hat{\eta}(k)m_f(k)\lambda_s}{m_{cyl}(k)}. \tag{11}$$

The in-cylinder gas minus the residual gas is the gas exhales from cylinder to the exhaust manifold:

$$m_{c-e}(k) = m_{cyl}(k) - m_r(k). \tag{12}$$

The oxygen fraction dynamic equations for intake manifold can be computed as follows. The next intake manifold oxygen can be computed as the present oxygen in the manifold minus the aspirated gas, plus the turbocharged EGR gas and the fresh air:

$$F_{int}(k+1) = \frac{F_{int}(k)[m_{int}(k) - m_{int\text{-}c}(k)] + m_{egr}(k)F_{exh}(k) + F_{air}[m_{comp}(k) - m_{egr}(k)]}{m_{int}(k) + m_{comp}(k) - m_{int\text{-}c}(k)}. \tag{13}$$

Similarly, the current exhaust manifold oxygen can be computed as the previous oxygen in the manifold minus the turbocharged gas, plus the gas exhaled from cylinder:

$$F_{exh}(k+1) = \frac{F_{exh}(k)[m_{exh}(k) - m_{turbine}(k)] + F_{c-e}(k)m_{c-e}(k)}{m_{exh}(k) + m_{c-e}(k) - m_{turbine}(k)}. \tag{14}$$

where, F_{air} and F_{exh} are the oxygen fraction of the fresh air and in the exhaust manifold; m_{comp} and $m_{turbine}$ are the gas mass go through compressor and turbine of the VGT respectively. The intake and exhaust manifolds oxygen concentrations, F_{int} and F_{exh} are the two measurements in the observers to estimate the in-cylinder oxygen concentration and total fuel mass.

The gas mass of the EGR valve, m_{egr} is calculated by the following orifice equation:

a) When the flow is not choked ($\frac{p_d}{p_u} > \left(\frac{2}{\gamma+1}\right)^{\gamma/(\gamma-1)}$),

$$\dot{m} = \frac{C_D A_R p_u}{\sqrt{RT_u}} \left(\frac{p_d}{p_u}\right)^{1/\gamma} \left\{\frac{2\gamma}{\gamma-1}\left[1 - \left(\frac{p_d}{p_u}\right)^{(\gamma-1)/\gamma}\right]\right\}^{1/2}, \tag{15}$$

b) When the flow is choked ($\frac{p_d}{p_u} \le \left(\frac{2}{\gamma+1}\right)^{\gamma/(\gamma-1)}$),

$$\dot{m} = \frac{C_D A_R p_u}{\sqrt{RT_u}} \sqrt{\gamma} \left(\frac{2}{\gamma+1}\right)^{(\gamma+1)/2(\gamma-1)}, \tag{16}$$

where C_D is the discharge coefficient, which is experimentally determined, subscript u and d stand for upstream and downstream respectively, A_R is the valve reference area, γ is the specific heat ratio.

The gas mass in the intake (exhaust) manifold, $m_{int(exh)}(k)$, can be computed by the ideal gas law:

$$m_{int(exh)}(k) = \frac{\overline{P}_{int(exh)}(k) V_{int(exh)}}{R\overline{T}_{int(exh)}}, \tag{17}$$

where, $\overline{P}_{int(exh)}$ and $\overline{T}_{int(exh)}$ are the mean pressure and temperature of the intake (exhaust).

D. Model validation

To validate the dynamic models derived above, an engine model like Table I was constructed in GT-Power environment. The settings of the actuators were tabulated in Table I, where the EGR valve opening began from 5% and then increased to 50% gradually as plotted in Fig.2 (a).

Table I validation Settings

Engine speed(RPM)	Rack position of VGT	EGR valve opening	Injection(mg)	η
2000	0.7	5% to 50%	20	100%

The simulation ran 90 continuously cycles; all data were sampled on engine cycle basis. Residual gas mass was calculated by applying equation (8); the mass of total gas

and in-cylinder, intake manifold, exhaust manifold oxygen concentrations were computed by applying dynamic equations (9)(10)(13)(14), respectively. These modeled variables are compared with real values directly given by GT-Power in the following figures.

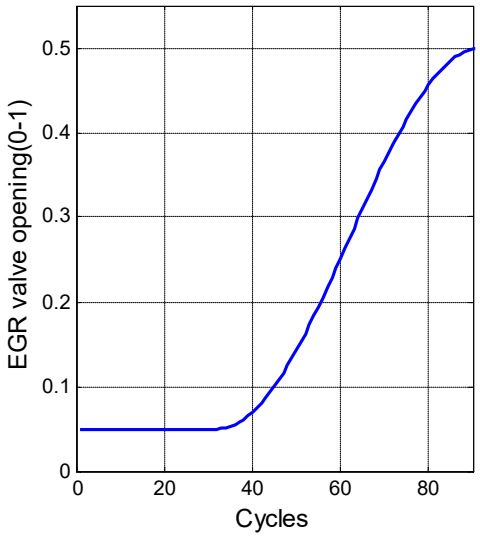

a) EGR validate opening

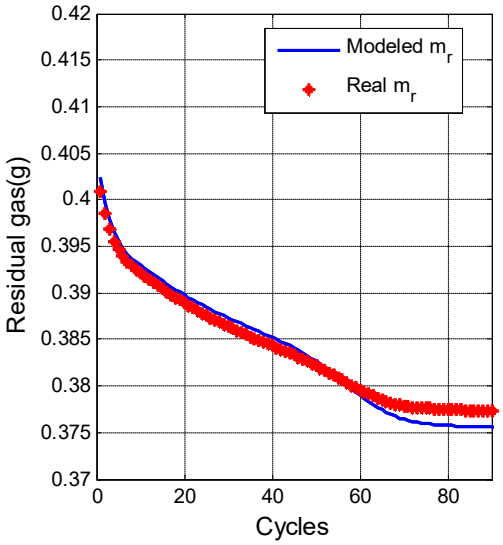

b) m_r model validation

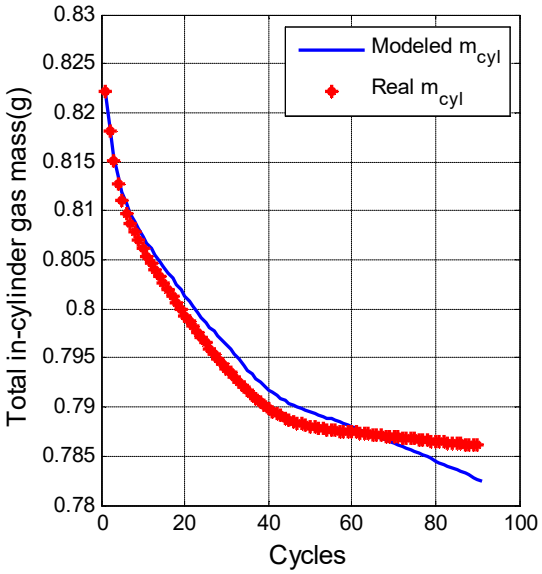

c) m_{cyl} model validation

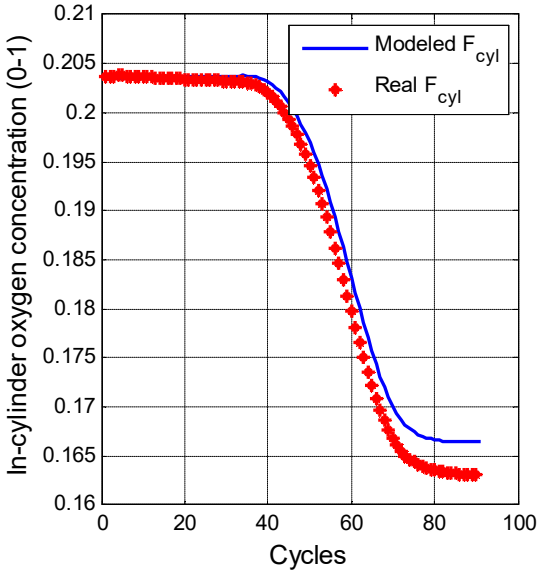

d) F_{cyl} model validation

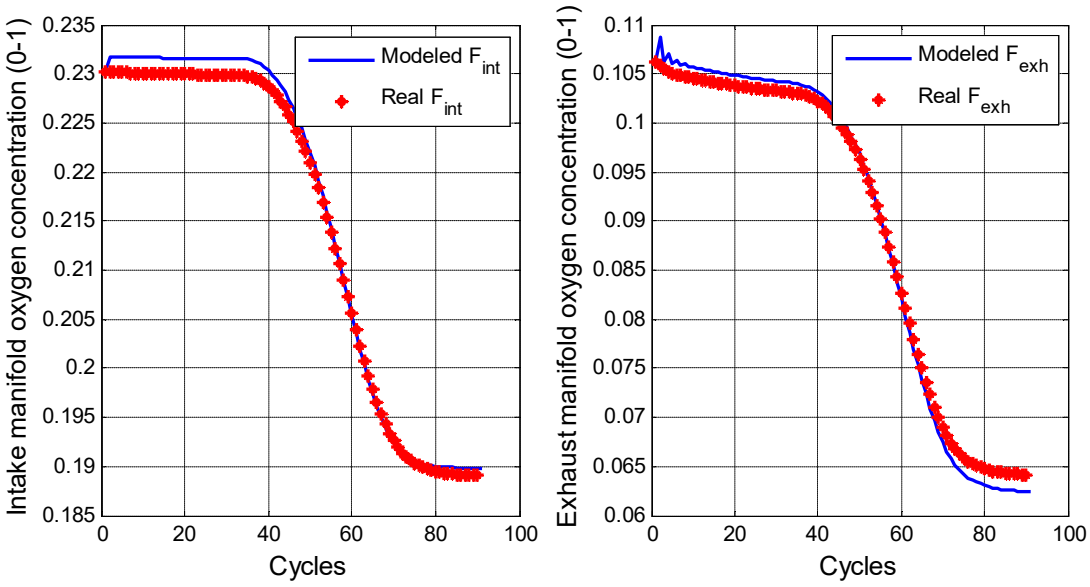

e) F_{int} **model validation** **f)** F_{exh} **model validation**

Fig.2 EGR valve opening and models validation

As told by Fig.2 (b)-(f), the proposed models can well capture the dynamic properties of the residual gas, the total in-cylinder gas mass as well as oxygen concentrations in different locations.

A. Combustion efficiency

Once the present values for the oxygen fraction of the intake manifold and cylinder, and the fuel mass have been obtained by the above equations, the updating law for the combustion efficiency is therefore derived as:

$$\hat{\eta}_m(k) = \frac{F_{cyl}(k+1)m_{cyl}(k+1) - m_{cyl}(k+1)F_{c-e}(k)}{\lambda_s m_f(k+1)}. \tag{18}$$

The updated combustion efficiency in equation (18) will be taken into equation (11) and the following equations to refine the four states. Then a newer combustion can be calculated by equation (18), the refining loop will conduct again. Therefore, the

combustion efficiency can be estimated in an iterative way until it gets stable as shown in the following figure.

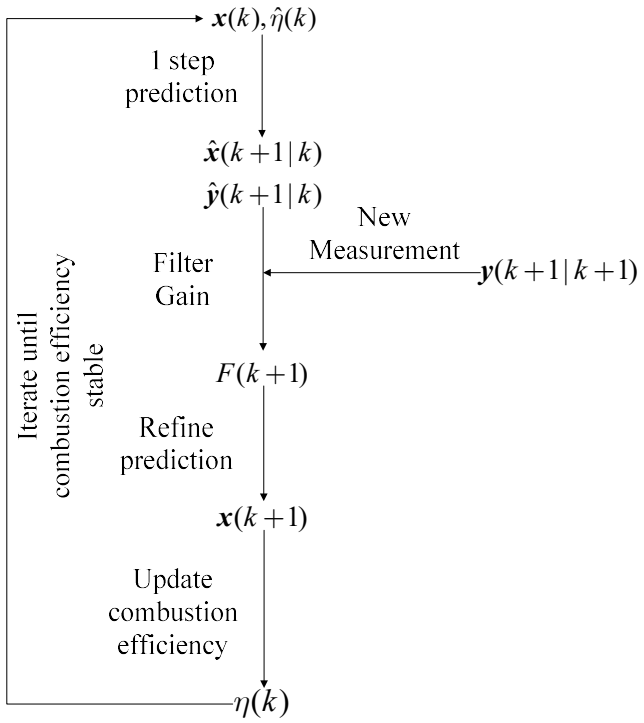

Fig.3 Estimation flow chart

III. FILTERS DESIGN

Taking the oxygen fractions in the intake, exhaust manifolds, and the cylinder, as well as the fuel mass as 4 states, the injection as the input, the system dynamics can be expressed in a state-space form:

$$\underbrace{\begin{bmatrix} F_{int}(k+1) \\ F_{exh}(k+1) \\ F_{cyl}(k+1) \\ m_f(k+1) \end{bmatrix}}_{\boldsymbol{x}(k+1)} = \underbrace{\begin{bmatrix} A_1(\rho_1(k)) & A_2(\rho_2(k)) & 0 & 0 \\ 0 & A_3(\rho_3(k)) & A_4(\rho_4(k)) & A_5(\rho_5(k)) \\ A_6(\rho_6(k)) & 0 & A_7(\rho_7(k)) & A_8(\rho_8(k)) \\ 0 & 0 & 0 & A_9(\rho_9(k)) \end{bmatrix}}_{\boldsymbol{A}(\rho(k))} \underbrace{\begin{bmatrix} F_{int}(k) \\ F_{exh}(k) \\ F_{cyl}(k) \\ m_f(k) \end{bmatrix}}_{\boldsymbol{x}(k)} + \underbrace{\begin{bmatrix} \rho_{10}(k) \\ 0 \\ 0 \\ \rho_{11}(k) \end{bmatrix}}_{\boldsymbol{B}(\rho(k))}, \tag{19}$$

where, $\rho_i, i = 1,...9$ refer to varying parameters,

$$A_1(\rho_1(k)) = \frac{m_{int}(k) - m_{int\text{-}c}(k)}{m_{int}(k) + m_{comp}(k) - m_{int\text{-}c}(k)};\ A_2(\rho_2(k)) = \frac{m_{egr}(k)}{m_{int}(k) + m_{comp}(k) - m_{int\text{-}c}(k)};$$

$$A_3(\rho_3(k)) = \frac{m_{exh}(k) - m_{turbine}(k)}{m_{exh}(k) + m_{c-e}(k) - m_{turbine}(k)};$$

$$A_4(\rho_4(k)) = \frac{m_{c-e}(k) m_{cyl}(k)}{(m_{exh}(k) + m_{c-e}(k) - m_{turbine}(k)) m_{cyl}(k)};$$

$$A_5(\rho_5(k)) = -\frac{m_{c-e}(k)\hat{\eta}(k)\lambda_s}{(m_{exh}(k) + m_{c-e}(k) - m_{turbine}(k)) m_{cyl}(k)};$$

$$A_6(\rho_6(k)) = \frac{m_{int\text{-}c}(k)}{m_{cyl}(k) - m_{c-e}(k) + m_{int\text{-}c}(k) + m_i(k)};$$

$$A_7(\rho_7(k)) = 1 - \frac{m_{c-e}(k)}{m_{cyl}(k) + m_i(k)};\ A_8(\rho_8(k)) = -\frac{\hat{\eta}(k)\lambda_s}{m_{cyl}(k)} + \frac{m_{c-e}(k)\hat{\eta}(k)\lambda_s}{m_{cyl}(k)[m_{cyl}(k) + m_i(k)]};$$

$$A_9(\rho_9(k)) = \frac{m_r(k)}{m_{cyl}(k)}(1 - \hat{\eta}(k));\ \rho_{10} = \frac{F_{air}(m_{comp}(k) - m_{egr}(k))}{m_{int}(k) + m_{comp}(k) - m_{int\text{-}c}(k)};\ \rho_{11} = m_i(k).$$

Assume intake and exhaust magnitude oxygen fractions can be measured directly, then the measurement matrix equation is:

$$\mathbf{Y}(k) = \begin{bmatrix} 1 & 0 & 0 & 0 \\ 0 & 1 & 0 & 0 \end{bmatrix} \begin{bmatrix} F_{int}(k) \\ F_{exh}(k) \\ F_{cyl}(k) \\ m_f(k) \end{bmatrix}, \tag{20}$$

where, ***H*** is the measurement matrix.

One can see from equation (19), this is a linear parameter time-varying system. An SVSF and two comparing filers, specifically as Kalman filter and Linear Parameter-Varying (LPV) filter will be presented as follows.

A. Smooth Variable Structure Filter

The SVSF estimates the states in prediction-correction fashion. The core idea is to find a vector $\boldsymbol{K}(k+1)$ to correct the predicted states:

$$\hat{\boldsymbol{x}}(k+1|k+1)=\hat{\boldsymbol{x}}(k+1|k)+\boldsymbol{K}(k+1), \tag{21}$$

where, $\hat{\boldsymbol{x}}(k+1|k)$ is the predicted states by equation (19).

Denote the oxygen fractions of intake and exhaust manifolds, which have a direct relationship with the output, as $\boldsymbol{z}$: $\boldsymbol{z}=\begin{bmatrix}F_{int}\\F_{exh}\end{bmatrix}$, the other two states, which are the in-cylinder oxygen fraction and the fuel mass as: $\boldsymbol{y}=\begin{bmatrix}F_{cyl}\\m_f\end{bmatrix}$. Then, the system can be presented as:

$$\begin{bmatrix}\boldsymbol{z}(k+1)\\\boldsymbol{y}(k+1)\end{bmatrix}=\begin{bmatrix}\boldsymbol{\Phi}_{11}(k) & \boldsymbol{\Phi}_{12}(k)\\\boldsymbol{\Phi}_{21}(k) & \boldsymbol{\Phi}_{22}(k)\end{bmatrix}\begin{bmatrix}\boldsymbol{z}(k)\\\boldsymbol{y}(k)\end{bmatrix}+\begin{bmatrix}\boldsymbol{G}_1(k)\\\boldsymbol{G}_2(k)\end{bmatrix}, \tag{22}$$

where,

$$\boldsymbol{\Phi}_{11}(k)=\begin{bmatrix}0 & \dfrac{m_{int}(k)-m_{asp}(k)}{m_{int}(k)+m_{comp}(k)-m_{asp}(k)}\\\dfrac{m_{c-e}(k)m_{cyl}(k)}{[m_{exh}(k)+m_{c-e}(k)-m_{turbine}(k)]m_{cyl}(k)} & 0\end{bmatrix}, \tag{23}$$

$$\boldsymbol{\Phi}_{12}(k)=\begin{bmatrix}\dfrac{m_{egr}(k)}{m_{int}(k)+m_{comp}(k)-m_{asp}(k)} & 0\\ \dfrac{m_{exh}(k)-m_{turbine}(k)}{m_{exh}(k)+m_{c-e}(k)-m_{turbine}(k)} & -\dfrac{m_{c-e}(k)\eta(k)\lambda_s}{[m_{exh}(k)+m_{c-e}(k)-m_{turbine}(k)]m_{cyl}(k)}\end{bmatrix}, \tag{24}$$

$$\boldsymbol{\Phi}_{21}(k)=\begin{bmatrix}1-\dfrac{m_{c-e}(k)}{m_{cyl}(k)+m_i(k)} & \dfrac{m_{asp}(k)}{m_{cyl}(k)}\\ 0 & 0\end{bmatrix}, \tag{25}$$

$$\boldsymbol{\Phi}_{22}(k)=\begin{bmatrix}0 & \dfrac{-\eta(k)\lambda_s}{m_{cyl}(k)}+\dfrac{m_{c-e}(k)\eta(k)\lambda_s}{m_{cyl}(k)m_{cyl}(k)}\\ 0 & \dfrac{m_r(k)}{m_{cyl}(k)}[1-\eta(k)]\end{bmatrix}, \tag{26}$$

$$\boldsymbol{G}_1(k)=\begin{bmatrix}\dfrac{F_{air}[m_{comp}(k)-m_{egr}(k)]}{m_{int}(k)+m_{comp}(k)-m_{asp}(k)}\\ 0\end{bmatrix}, \boldsymbol{G}_2(k)=\begin{bmatrix}0\\ m_i(k)\end{bmatrix}. \tag{27}$$

Given the partitioned state space equation as above, the filter correcting vector in equation (21)can be similarly partitioned as:

$$\boldsymbol{K}(k+1)=\begin{bmatrix}\boldsymbol{K}_u(k+1)\\ \boldsymbol{K}_l(k+1)\end{bmatrix}. \tag{28}$$

Then the upper corrective vector can be designed as[19,20]:

$$\boldsymbol{K}_u(k+1)=(\left|e_z(k+1\,|\,k)\right|_{ABS}+\boldsymbol{\gamma}\left|e_z(k\,|\,k)\right|_{ABS})\circ sat\left(e_z(k+1\,|\,k),\boldsymbol{\psi}_z\right), \tag{29}$$

where, $\boldsymbol{\gamma}$ is a diagonal matrix with elements such that $0\le\gamma_{ii}\le 1, i=1,2$;*sat(**a**,**b**)* is a saturation function to mitigate the chattering effect of SVSF, it has the following structure:

$$sat_i(\boldsymbol{a},\boldsymbol{b}) = \begin{cases} a_i / b_i & for \left|a_i / b_i\right| \le 1 \\ sign(a_i / b_i)\, for \left|a_i / b_i\right| > 1 \end{cases}. \tag{30}$$

The measurement error vector $e_z(k+1|k)$ can be calculated:

$$e_z(k+1|k) = \boldsymbol{z}(k+1) - \hat{\boldsymbol{z}}(k+1|k). \tag{31}$$

After corrected, the measurement error turns to be:

$$e_z(k+1|k+1) = \boldsymbol{z}(k+1) - \hat{\boldsymbol{z}}(k+1|k+1). \tag{32}$$

The upper corrective vector can be designed as[19,20]:

$$\boldsymbol{K}_u(k+1) = (\left|\boldsymbol{\Phi}_{22}\boldsymbol{\Phi}_{12}^{-1} e_z(k+1|k)\right|_{ABS} + \boldsymbol{\gamma}\left|\boldsymbol{\Phi}_{12}^{-1} e_z(k|k)\right|_{ABS}) \circ sat(\boldsymbol{\Phi}_{22}\boldsymbol{\Phi}_{12}^{-1} e_z(k+1|k), \boldsymbol{\psi}_y). \tag{33}$$

Together with equation (29), the filter correction vector can be obtained.

B. Kalman Filter

The estimation procedure for Kalman filter contains the following 6 steps[21,22].

1) State prediction:

$$\begin{bmatrix} \hat{F}_{int}(k+1,k) \\ \hat{F}_{exh}(k+1,k) \\ \hat{F}_{cyl}(k+1,k) \\ \hat{m}_f(k+1,k) \end{bmatrix} = \boldsymbol{A}(\rho(k)) \begin{bmatrix} F_{int}(k,k) \\ F_{exh}(k,k) \\ F_{cyl}(k,k) \\ m_f(k,k) \end{bmatrix} + \boldsymbol{B}(\rho(k)), \tag{34}$$

2) State prediction covariance:

$$\boldsymbol{P}(k+1,k) = \boldsymbol{A}(\rho(k))\boldsymbol{P}(k,k)\boldsymbol{A}(\rho(k))^T + \boldsymbol{Q}, \tag{35}$$

3) Innovation covariance:

$$\boldsymbol{S}(k+1) = \boldsymbol{R} + \boldsymbol{H}\boldsymbol{P}(k+1,k)\boldsymbol{H}^T, \tag{36}$$

4) Filter gain:

$$\boldsymbol{W}(k+1)=\boldsymbol{P}(k+1,k)\boldsymbol{H}^{T}\boldsymbol{S}(k+1)^{-1}, \tag{37}$$

5) Update state estimation:

$$\begin{bmatrix} F_{int}(k+1,k+1) \\ F_{exh}(k+1,k+1) \\ F_{cyl}(k+1,k+1) \\ m_f(k+1,k+1) \end{bmatrix} = \begin{bmatrix} \hat{F}_{int}(k+1,k) \\ \hat{F}_{exh}(k+1,k) \\ \hat{F}_{cyl}(k+1,k) \\ \hat{m}_f(k+1,k) \end{bmatrix} + \boldsymbol{W}(k+1)\left(\boldsymbol{Y}(k+1) - \boldsymbol{H}\begin{bmatrix} \hat{F}_{int}(k+1,k) \\ \hat{F}_{exh}(k+1,k) \\ \hat{F}_{cyl}(k+1,k) \\ \hat{m}_f(k+1,k) \end{bmatrix} \right), \tag{38}$$

6) Updated state covariance:

$$\boldsymbol{P}(k+1,k+1)=\boldsymbol{A}(\rho(k))\boldsymbol{P}(k,k)\boldsymbol{A}(\rho(k))^{T}+\boldsymbol{Q}, \tag{39}$$

The Kalman filter was, therefore, developed by repeating the above procedures for each cycle.

C. Linear Matrix Inequality (LMI) based, linear parameter-varying filter

The observer to be designed in the following form:

$$\begin{aligned} \hat{\boldsymbol{x}}(k+1) &= \boldsymbol{A}(\rho(k))\hat{\boldsymbol{x}}(k)+\boldsymbol{B}(\rho(k))+\boldsymbol{L}(\rho(k))(\boldsymbol{Y}(k)-\hat{\boldsymbol{Y}}(k)) \\ \hat{\boldsymbol{y}}(k) &= \boldsymbol{C}\hat{\boldsymbol{x}}(k) \end{aligned}. \tag{40}$$

The estimation error can be defined as:

$$\tilde{\boldsymbol{x}}=\boldsymbol{x}-\hat{\boldsymbol{x}}. \tag{41}$$

Whose dynamics is given as:

$$\begin{aligned} \tilde{\boldsymbol{x}}(k+1) &= \boldsymbol{x}(k+1)-\hat{\boldsymbol{x}}(k+1) \\ &= \boldsymbol{A}(\rho(k))\boldsymbol{x}(k)+\boldsymbol{B}(\rho(k))-[\boldsymbol{A}(\rho(k))\hat{\boldsymbol{x}}(k)+\boldsymbol{B}(\rho(k))+\boldsymbol{L}(\rho(k))(\boldsymbol{Y}(k)-\hat{\boldsymbol{Y}}(k))]. \\ &= [\boldsymbol{A}(\rho(k))-\boldsymbol{L}(\rho(k))\boldsymbol{C}]\tilde{\boldsymbol{x}}(k) \end{aligned} \tag{42}$$

The idea is to find a proper filter gain matrix, $\boldsymbol{L}(\rho(k))$, such that the state estimation error, $\tilde{\boldsymbol{x}}(k+1)$ can be asymptotically stable.

The structure of the dynamical matrix A is assumed to be the form of:

$$A(\rho(k)) = \sum_{i=1}^{N} \xi_i(k) A_i \,. \tag{43}$$

where $\xi_i(k) \geq 0,\ \sum_{i=1}^{N} \xi_i(k) = 1$. (44)

There are 8 time-varying parameters in A: $\rho_1(k), \rho_2(k), \rho_3(k), \rho_5(k), \rho_6(k), \rho_7(k), \rho_8(k), \rho_9(k)$. Assume they are bounded by:

$$\rho_{i,min} \leq \rho_i(k) \leq \rho_{i,max}, \quad i = 1,2,3,5,6,7,8,9, \tag{45}$$

where $\rho_{i,min}$ and $\rho_{i,max}$ are constants.

Define $\xi_j(k)$ as:

$$\xi_{2j-1}(k) = \frac{\rho_{i,max} - \rho_i}{8(\rho_{i,max} - \rho_{i,min})}, \tag{46}$$

$$\xi_{2j}(k) = \frac{\rho_i - \rho_{i,min}}{8(\rho_{i,max} - \rho_{i,min})},\ j = 1,2,...,8.. \tag{47}$$

Therefore, the A_i can be accordingly derived as:

$$A_{2j-1} = \begin{bmatrix} 0 \text{ or } 8\rho_{1,min} \text{ if } j=1 & 0 \text{ or } 8\rho_{2,min} \text{ if } j=2 & 0 & 0 \text{ or } 8\rho_{3,min} \text{ if } j=3 \\ 0 & \frac{\rho_4}{8} & 0 \text{ or } 8\rho_{5,min} \text{ if } j=4 & 0 \\ 0 \text{ or } 8\rho_{6,min} \text{ if } j=5 & 0 & 0 \text{ or } 8\rho_{7,min} \text{ if } j=6 & 0 \text{ or } 8\rho_{8,min} \text{ if } j=7 \\ 0 & 0 & 0 & 0 \text{ or } 8\rho_{9,min} \text{ if } j=8 \end{bmatrix}, \tag{48}$$

$$A_{2j} = \begin{bmatrix} 0 \text{ or } 8\rho_{1,max} \text{ if } j=1 & 0 \text{ or } 8\rho_{2,max} \text{ if } j=2 & 0 & 0 \text{ or } 8\rho_{3,max} \text{ if } j=3 \\ 0 & \frac{\rho_4}{8} & 0 \text{ or } 8\rho_{5,max} \text{ if } j=4 & 0 \\ 0 \text{ or } 8\rho_{6,max} \text{ if } j=5 & 0 & 0 \text{ or } 8\rho_{7,max} \text{ if } j=6 & 0 \text{ or } 8\rho_{8,max} \text{ if } j=7 \\ 0 & 0 & 0 & 0 \text{ or } 8\rho_{9,max} \text{ if } j=8 \end{bmatrix}. \tag{49}$$

Theorem 1: if there exist symmetric positive definite matrices S_i , S_j , G_i , R_i of appropriate dimensions such that the following LMI holds,

$$\begin{bmatrix} G_i + G_i^T - S_i & (\bullet)^T \\ A_i G_i - R_i & S_j \end{bmatrix} > 0 , \tag{50}$$

then the equation (42) is poly-quadratically stable and the filter gain is given by:

$$L_i = R_i (C G_i)^+ . \tag{51}$$

Proof: Let the matrix $R_i = L_i C G_i$, then the above LMI turns to be:

$$\begin{bmatrix} G_i + G_i^T - S_i & (\bullet)^T \\ (A_i - L_i C) G_i & S_j \end{bmatrix} > 0 . \tag{52}$$

Therefore, directly apply the theorem 3 in [23], if S_i , S_j , G_i , R_i exist, the system is stable and the theorem 1 holds.

IV. ROBUSTNESS ANALYSIS

The three aforementioned observers were designed with the assumption that there are no parametric inaccuracies. However, in practical applications, parametric uncertainties are ubiquitous included during device calibrations or measurements. Particularly, for the estimation and control of Diesel engines, volumetric efficiency is usually cannot be accurately obtained as the engine speed and in-cylinder temperature/pressure vary. Also, the accuracy of temperatures of the manifolds always suffers from the temperature sensor dynamics, which is typically seen as a first-order system with a varying time-constant.

In order to analyze the robustness of the above 3 filters in a quantified way, the structure of the estimation system can be rearranged as follows.

Denote the filter gain as, $G_f(\rho(k))$ which can represent $\begin{bmatrix} \boldsymbol{K}_u(k+1) \\ \boldsymbol{K}_l(k+1) \end{bmatrix}$ (SVSF), $\boldsymbol{W}(k+1)$ (KF), and $\boldsymbol{L}(\rho(k))$ (LPV). Then, for the KF and LPV, with the parametric uncertainties, the dynamical equation of the estimated states can be derived as:

$$\hat{\boldsymbol{x}}(k+1) = \boldsymbol{A}(\hat{\rho}(k))\hat{\boldsymbol{x}}(k) + \boldsymbol{B}(\hat{\rho}(k)) + \boldsymbol{G}_f(k)[\boldsymbol{Y}(k) - \hat{\boldsymbol{Y}}(k)]. \tag{53}$$

Therefore, the dynamics of the state error, $e(k)$, can be written as:

$$\begin{aligned} \boldsymbol{e}(k+1) &= \boldsymbol{x}(k+1) - \hat{\boldsymbol{x}}(k+1) \\ &= \boldsymbol{A}(\rho(k))\boldsymbol{x}(k) + \boldsymbol{B}(\rho(k)) - \{\boldsymbol{A}(\hat{\rho}(k))\hat{\boldsymbol{x}}(k) + \boldsymbol{B}(\hat{\rho}(k)) + \boldsymbol{G}_f(\hat{\rho}(k))[\boldsymbol{Y}(k) - \hat{\boldsymbol{Y}}(k)]\} \\ &= \underbrace{[\boldsymbol{A}(\rho(k)) - \boldsymbol{G}_f(\hat{\rho}(k))\boldsymbol{H}]}_{\boldsymbol{\Gamma}(\hat{\rho}(k))}\boldsymbol{e}(k) + \underbrace{[\boldsymbol{A}(\rho(k)) - \boldsymbol{A}(\hat{\rho}(k))]\boldsymbol{x}(k) + \boldsymbol{B}(\rho(k)) - \boldsymbol{B}(\hat{\rho}(k))}_{\boldsymbol{u}(k)}. \\ &= \boldsymbol{\Gamma}(\hat{\rho}(k))\boldsymbol{e}(k) + \boldsymbol{u}(k). \end{aligned} \tag{54}$$

Theorem 2: System (54) is input-to-state stable (ISS) [24,25], i.e. there exists a $\mathcal{KL}$ function $\beta : \mathbb{R} \times \mathbb{R} \to \mathbb{R}$ and a strictly positive number α, such that

$$\| \boldsymbol{e}(k) \| \leq \beta(\| \boldsymbol{e}(0) \|, k) + \alpha \| \boldsymbol{u} \|_\infty, \tag{55}$$

where $\| \bullet \|$ is the Euclidean norm and $\| \bullet \|_\infty$ is the supremum norm; $\alpha = 1/(1-c)$, with $c = \sup\{ | \lambda_{\max}(\boldsymbol{\Gamma}(\hat{\rho}(k))) | \}, \forall k$, and $\lambda_{\max}(\boldsymbol{\Gamma}(\hat{\rho}(k)))$ is the maximum eigenvalue of the matrix $\boldsymbol{\Gamma}(\hat{\rho}(k))$, if 0<c<1.

Proof: For the KF, as proved in[26], the estimated error is exponentially stable and Theorem 1 tells that the LMI based PLV is also stable. Therefore, the estimation error

without uncertainties, $\hat{e}(k+1)=\boldsymbol{\Gamma}(\hat{\rho}(k))\hat{e}(k)$, will decrease to zero within finite time for both observers. Then, applying **Theorem 2** in [27], the function β can be constructed as:

$$\beta(\|\boldsymbol{e}(0)\|,k)=\|\hat{\boldsymbol{e}}(k)\|. \tag{56}$$

Then,

$$\|\boldsymbol{e}(k)\|\leq\|\hat{\boldsymbol{e}}(k)\|+\alpha\|\boldsymbol{u}\|_{\infty}=\beta(\|\boldsymbol{e}(0)\|,k)+\alpha\|\boldsymbol{u}\|_{\infty}. \tag{57}$$

Therefore, system (54) is ISS. Detailed proof can be found in [27].

Similarly, for the SVSF, by taking (29) and (33) into $\begin{bmatrix}\boldsymbol{K}_u(k+1)\\ \boldsymbol{K}_l(k+1)\end{bmatrix}$, and recalling $e_z(k)=\gamma\left|e_z(k-1)\right|_{ABS}\circ sgn(e_z(k-1))$,then the filter gain turns to be:

$$\begin{bmatrix}\boldsymbol{K}_u(k+1)\\ \boldsymbol{K}_l(k+1)\end{bmatrix}=\begin{bmatrix}(1+\gamma^2)\boldsymbol{I} & \boldsymbol{0}\\ \boldsymbol{0} & \boldsymbol{\Phi}_{22}\boldsymbol{\Phi}_{12}^{-1}+\gamma\left|\boldsymbol{\Phi}_{12}^{-1}\right|_{ABS}\circ sgn(\boldsymbol{\Phi}_{22}\boldsymbol{\Phi}_{12}^{-1})\end{bmatrix}\boldsymbol{e}(k)=\boldsymbol{G}_f(\hat{\rho}(k))\boldsymbol{e}(k). \tag{58}$$

Then, the dynamical equation of the estimated states can be written as:

$$\begin{aligned}\boldsymbol{e}(k+1)&=\boldsymbol{A}(\rho(k))\boldsymbol{e}(k)-\boldsymbol{G}_f(\hat{\rho}(k))+\boldsymbol{A}(\rho(k))-\boldsymbol{A}(\hat{\rho}(k))]\boldsymbol{x}(k)+\boldsymbol{B}(\rho(k))-\boldsymbol{B}(\hat{\rho}(k))\\&=\underbrace{[\boldsymbol{A}(\rho(k))-\boldsymbol{G}_f(\hat{\rho}(k))]}_{\boldsymbol{\Gamma}'(\hat{\rho}(k))}\boldsymbol{e}(k)+\underbrace{[\boldsymbol{A}(\rho(k))-\boldsymbol{A}(\hat{\rho}(k))]\boldsymbol{x}(k)+\boldsymbol{B}(\rho(k))-\boldsymbol{B}(\hat{\rho}(k))}_{\boldsymbol{u}(k)}.\\&=\boldsymbol{\Gamma}'(\hat{\rho}(k))\boldsymbol{e}(k)+\boldsymbol{u}(k),\end{aligned} \tag{59}$$

[20] tells it is stable if the error of the estimation for the SVSF satisfies $\left|e(k)\right|_{ABS}<\left|e(k-1)\right|_{ABS}$ which can be guaranteed by selecting $0<\gamma\leq 1$ for our system. Therefore, applying Theorem 2, the system (59) is ISS and the $\mathcal{KL}$ function β and the function can be constructed as (57).

Note, the estimation error dynamics with uncertainties is proved to be ISS with the same equation structure, as (57), and the same excitation source, the model error $\boldsymbol{u}$. Although these three observers have difference estimation strategy, their robustness property can be compared based on (57) and further quantified by the indicator α in (57). It can be easily got that a smaller α indicates a better robustness property. For the observer 1, the SVSF, $c=0.526$, $\alpha=2.08$. For the observer 2, the KF, $c=0.825$, $\alpha=5.73$ For the observer 3, the LMI based LPV, $c=0.786$, $\alpha=4.69$. Therefore the SVSF is the most robust one among the three. In section V, their performance will be investigated in simulations.

V. SIMULATION STUDIES

A medium-load situation is mimicked in the simulation. Simulation settings are tabulated in Table II. The NVO, in this case, is set as 100 CA. White noises with an amplitude of 0.01 are added to the measurement, i.e. the oxygen fractions of intake and exhaust manifolds.

TABLE II SIMULATION SETTINGS

Engine speed(RPM)	Rack position of VGT	EGR valve opening	Injection(mg)	η
2000	0.5	50%	20	94%-98%

A high-fidelity engine model with 4 cylinders as shown in Fig.1 was constructed in GT-Power environment. The engine was operated from cold start; therefore, the combustion efficiency was set as started from 94%, and then jumped to 98% in the middle of the simulation as shown in table I and the following figures. The settings and performances of the 3 filters are detailed in follows.

A. Filters settings

Smooth Variable Structure Filter (SVSF)

γ_{ii} was tuned as 0.3 , $i = 1,2$ and :

$$\boldsymbol{\psi}_z = \begin{bmatrix} 0.02 \\ 0.02 \end{bmatrix}, \boldsymbol{\psi}_y = \begin{bmatrix} 0.02 \\ 2\times 10^{-7} \end{bmatrix}. \tag{60}$$

Kalman Filter (KF)

Generally, the measurement covariance matrix, ***R***, can be picked up by the sensors' noise variance. Assuming the oxygen sensors mounted at intake and exhaust manifolds are independent, then to make the filter work the noise can be added to the simulated two outputs separately. The noise is white noise with variance of 0.01^2, thus, the ***R*** can be set as:

$$R = \begin{bmatrix} 0.01^2 & 0 \\ 0 & 0.01^2 \end{bmatrix}, \tag{61}$$

The system process covariance matrix, ***Q***, was tuned as:

$$Q = \begin{bmatrix} 0.01^2 & 0 & 0 & 0 \\ 0 & 0.005^2 & 0 & 0 \\ 0 & 0 & 0.005^2 & 0 \\ 0 & 0 & 0 & 0.000001^2 \end{bmatrix}, \tag{62}$$

LMI based LPV Filter

Based on (51), L_i were calculated as:

$$L_1 = L_2 = \begin{bmatrix} 0 & 0 \\ 0.0804 & 0 \\ 0 & 0 \\ 0 & 0 \end{bmatrix},\ L_3 = \begin{bmatrix} 2.347 & 0 \\ 0.117 & 0 \\ 0 & 0 \\ 0 & 0 \end{bmatrix},\ L_4 = \begin{bmatrix} 2.986 & 0 \\ 0.199 & 0 \\ 0 & 0 \\ 0 & 0 \end{bmatrix},\ L_5 = \begin{bmatrix} 0 & -1.362\times10^4 \\ 0 & 0 \\ 0 & 0.056\times10^4 \\ 0 & 0 \end{bmatrix},$$

$$L_6 = \begin{bmatrix} 0 & -1.212\times10^3 \\ 1 & 0 \\ 0 & 0.118\times10^4 \\ 0 & 0 \end{bmatrix},\quad L_7 = \begin{bmatrix} 0 & 0 \\ 0.058 & 0 \\ 0 & 0 \\ 0.131 & 0 \end{bmatrix},\quad L_8 = \begin{bmatrix} 0 & 0 \\ 0.0148 & 0 \\ 0 & 0 \\ 0.2117 & 0 \end{bmatrix},$$

$$L_9 = \begin{bmatrix} 0 & 0.2478 \\ 0.0804 & 0 \\ 0 & -0.0958 \\ 0 & 0 \end{bmatrix},\quad L_{10} = \begin{bmatrix} 0 & 0.228 \\ 0.0804 & 0 \\ 0 & -0.1051 \\ 0 & 0 \end{bmatrix},\quad L_{11} = \begin{bmatrix} 0 & 0 \\ 0.0804 & 0 \\ 0 & 5.323 \\ 0 & 0 \end{bmatrix}, \quad (63)$$

$$L_{12} = \begin{bmatrix} 0 & 0 \\ 0.0804 & 0 \\ 0 & 6.016 \\ 0 & 0 \end{bmatrix},\quad L_{13} = \begin{bmatrix} 0 & 0 \\ 0.0706 & 0 \\ 0 & 2.143 \\ 0 & -0.088 \end{bmatrix},\quad L_{14} = \begin{bmatrix} 0 & 0 \\ 0.0655 & 0 \\ 0 & 1.507 \\ 0 & -0.1524 \end{bmatrix},$$

$$L_{15} = \begin{bmatrix} 0 & 0 \\ 0.0804 & 0 \\ 0 & 0 \\ 0 & 0 \end{bmatrix},\ L_{16} = \begin{bmatrix} 0 & 0 \\ 0 & 0 \\ 0 & 0 \\ 0 & 0 \end{bmatrix}.$$

B. Filters evaluation without parameter uncertainties

Only noises are considered in this case as plotted in Fig.4-Fig.9, no parameter uncertainties or measurement disturbances were introduced.

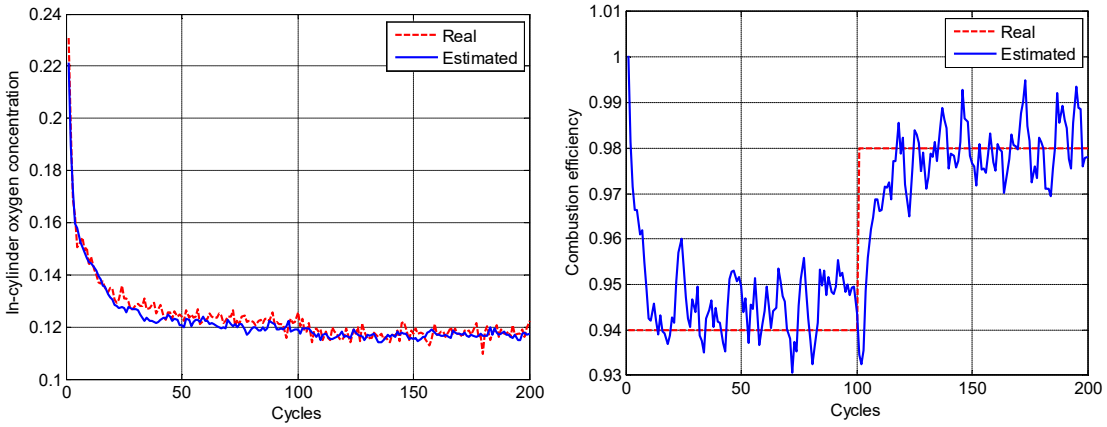

a) in-cylinder oxygen concentration **b) combustion efficiency**

Fig.4 In-cylinder oxygen concentration and combustion efficiency estimated by SVSF

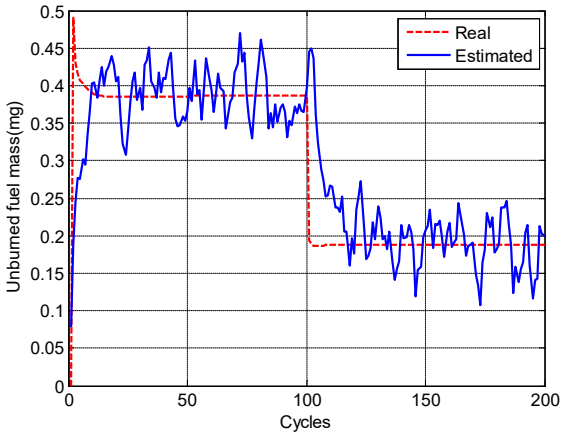

Fig.5 Unburned fuel mass estimated by SVSF

As can be seen from the above two figures, for the SVSF, the convergence time of the combustion efficiency and the unburned fuel mass are around 20 cycles with the noise magnitude of 0.02 for the former one, and 0.15mg for the later one.

Similarly, the performance of the Kalman Filter and LPV are plotted in Fig.6, Fig.7 and Fig.8, Fig.9, respectively.

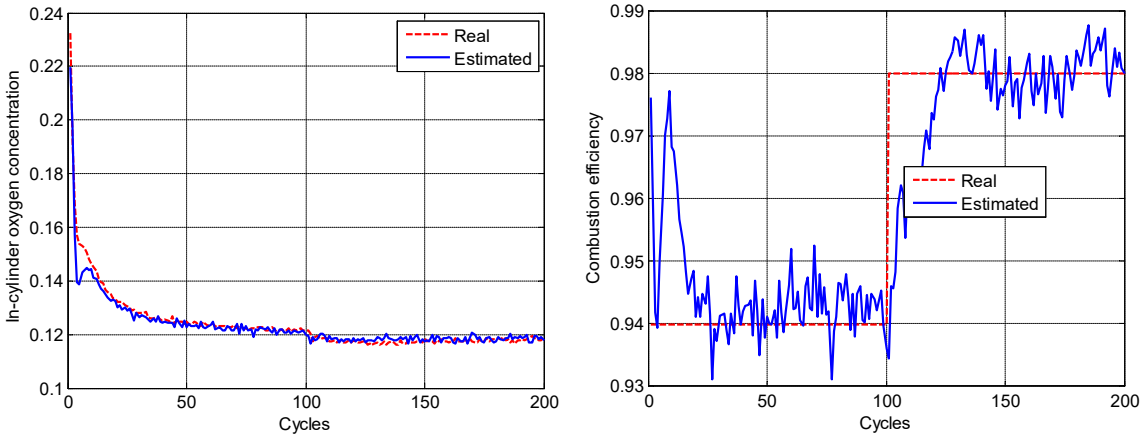

a) in-cylinder oxygen concentration **b) combustion efficiency**

Fig.6 In-cylinder oxygen concentration and combustion efficiency estimated by KF

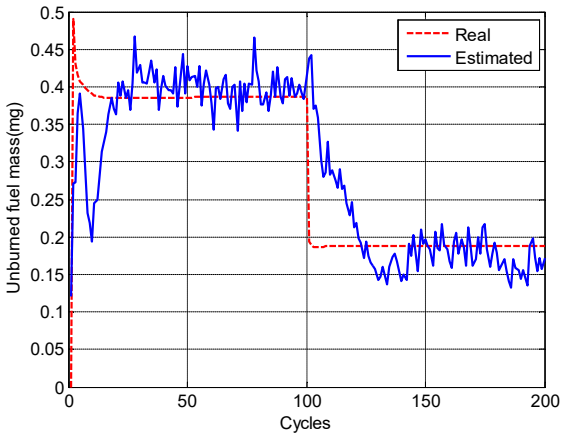

Fig.7 Unburned fuel mass estimated by KF

Fig.6 and Fig.7 tell us that the combustion efficiency and unburned fuel mass can be estimated in around 30 cycles by KF. The noise magnitude of unburned fuel mass is less than 0.1mg.

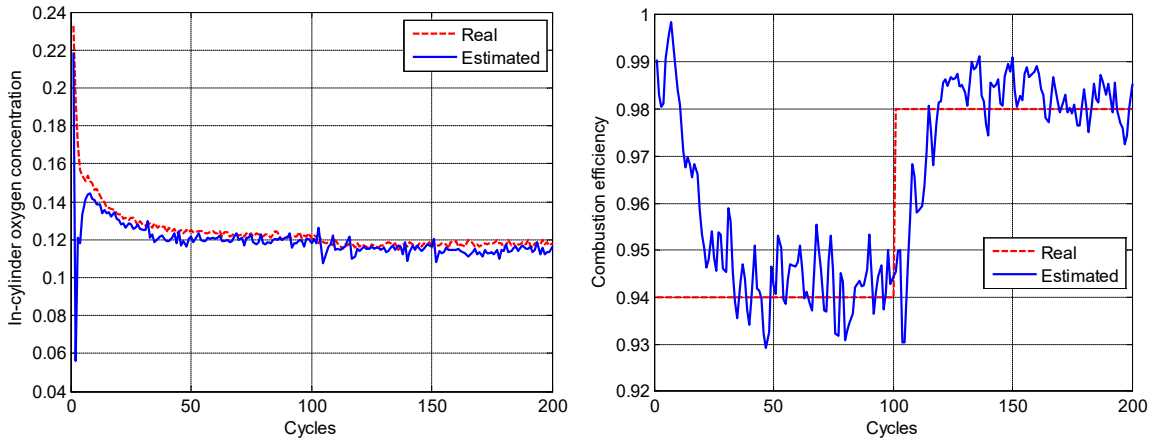

a) in-cylinder oxygen concentration **b) combustion efficiency**

Fig.8 In-cylinder oxygen concentration and combustion efficiency estimated by LPV

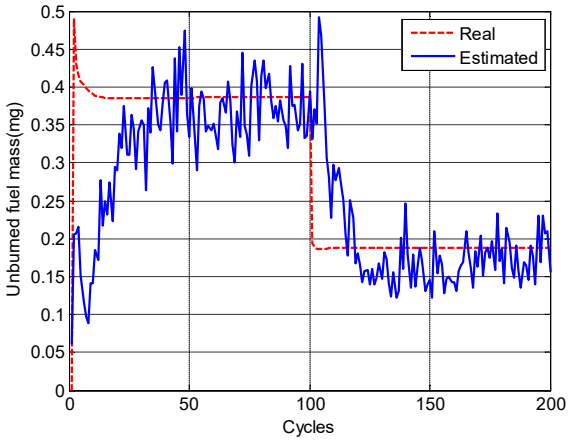

Fig.9 Unburned fuel mass estimated by LPV

As one can see from Fig.9 the performance of LPV ranking in the middle among the three filters in terms of convergence time, while the noise magnitude is the largest one.

To evaluate their property on noise rejection, the root mean square error (RMSE) of the estimated in-cylinder oxygen fraction, the combustion efficiency and unburned fuel for the 3 observers were computed and tabulated in Table III.

TABLE III ROOT MEAN SQUARE ERROR (RMSE) OF 3 FILTERS

RMSE	F_{cyl}	η	$m_{unburned}$
SVSF	0.0053	0.012	0.086
KF	0.0027	0.011	0.067
LPV	0.0038	0.019	0.167

The above estimation results in figures and Table III tell that the KF shows good property on noise rejection and it is the best one, the LPV is the worse one among them. It is reasonable since the KF is the only observer that requires the system's stochastic properties which are the measurement covariance and the process covariance matrices. And the SVSF shows quicker convergence time than the other two filters.

C. Filters evaluation with parameter uncertainties

To evaluate the property on uncertainties rejection, the error of volumetric efficiency was introduced to the system. From the measurement point of view, the volumetric efficiency is varying with different pressure and temperature and will affect the total mass of the inhaled gas. Here we assume the calculated or mapped volumetric efficiency is 10% less than the true value. The according performances of the 3 observers are plotted in the following Fig.10-Fig.15.

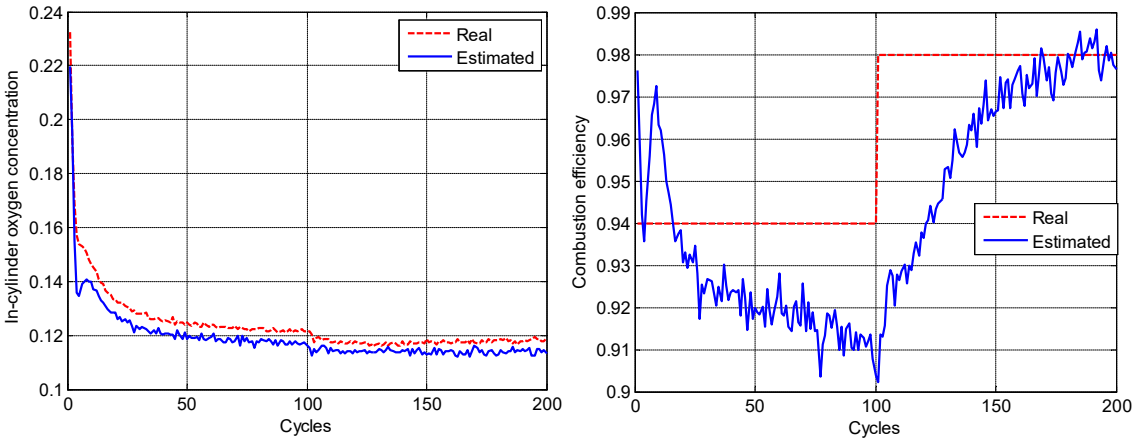

a) in-cylinder oxygen concentration **b) combustion efficiency**

Fig.10 In-cylinder oxygen fraction and combustion efficiency estimated by KF with parameter uncertainty

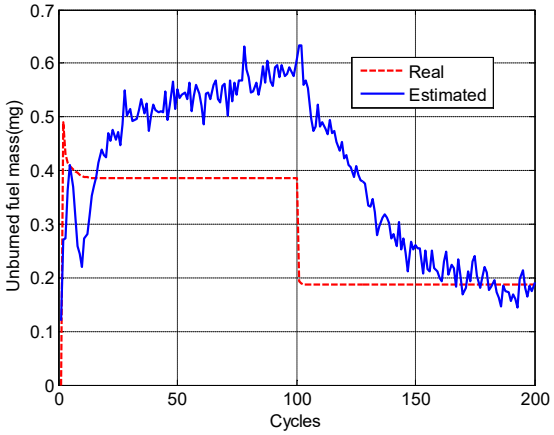

Fig.11 Unburned fuel mass estimated by KF with parameter uncertainty

The in-cylinder oxygen concentration cannot be estimated accurately, as shown in Fig.10 and it takes more than 100 cycles for the combustion efficiency and unburned fuel mass to converge, as shown in Fig.10 and Fig.11.

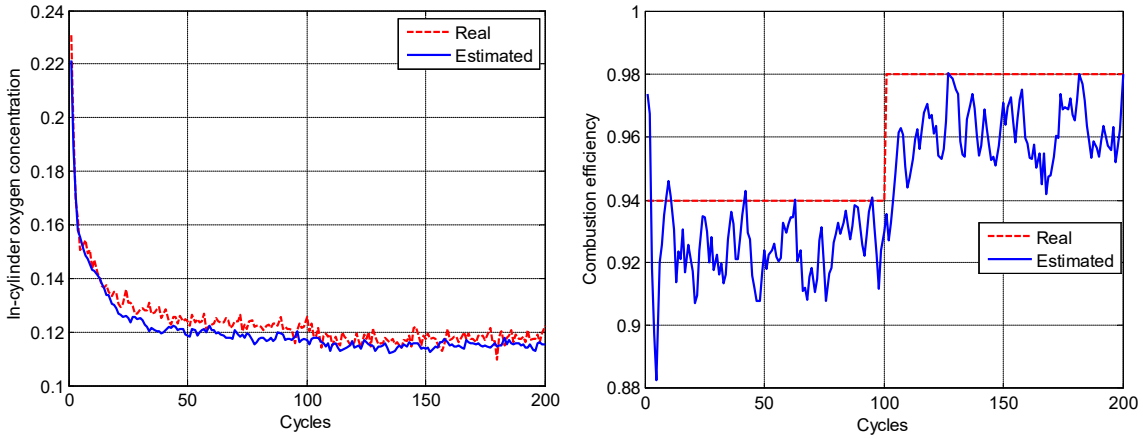

a) in-cylinder oxygen concentration **b) combustion efficiency**

Fig.12 In-cylinder oxygen fraction and combustion efficiency estimated by SVSF with parameter uncertainty

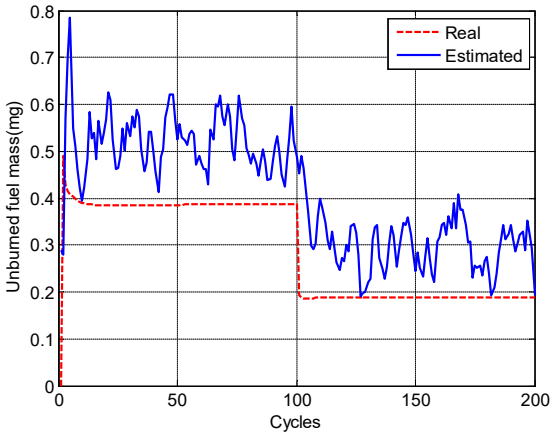

Fig.13 Unburned fuel mass estimated by SVSF with parameter uncertainty

The convergence time and the noise level remained almost the same when there is no uncertainty of volumetric efficiency. However, bias exists for the estimated of in-cylinder oxygen concentration and combustion efficiency and calculated unburned fuel mass by SVSF with parameter uncertainty.

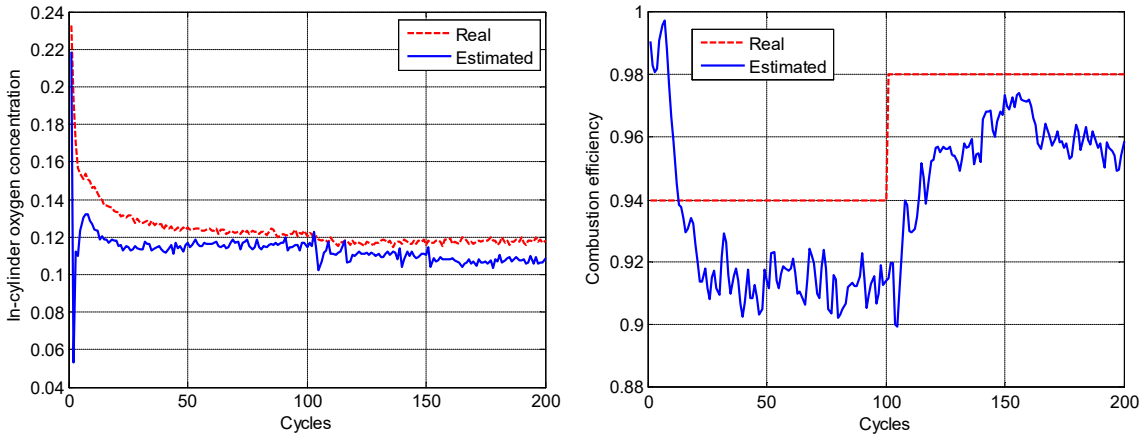

a) in-cylinder oxygen concentration **b) combustion efficiency**

Fig.14 In-cylinder oxygen fraction and combustion efficiency estimated by LPV with parameter uncertainty

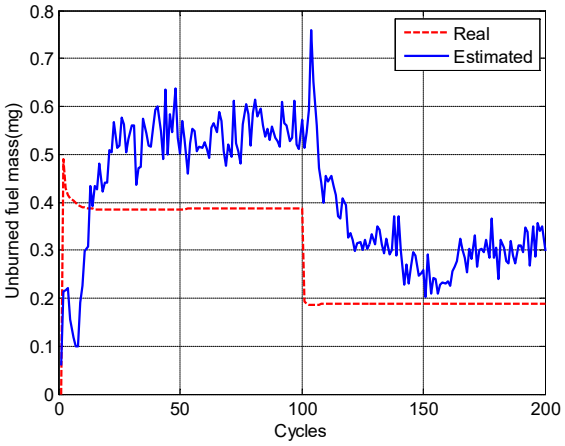

Fig.15 Unburned fuel mass estimated by LPV with parameter uncertainty

Fig.14 and Fig.15 show that the performance of LPV is better than KF, worse than SVSF in terms of convergence time and noise level.

TABLE IV. ROOT MEAN SQUARE ERROR (RMSE) OF 3 FILTERS

RMSE	F_{cyl}	η	$m_{unburned}$
KF	0.009	0.045	0.49
SVSF	0.006	0.021	0.24
LPV	0.015	0.038	0.40

As one can see from the figures and TABLE IV. above, the SVSF has the best performance (in Fig.13) by which the estimated unburned fuel is the closest to the real value when the parameter uncertainties exist, and the LPV (in Fig.15) is better than the KF (in Fig.11) in terms of uncertainties rejection. These results are consistent with the analysis in section IV, i.e., SVSF has the smallest α, i.e. best property on uncertainties rejection, while the KF has the largest one and LPV is in second place.

Note, only standard SVSF was considered in this paper, some advanced techniques, such as the bias removing strategy [20] and combining strategy[28], have been developed in recent years although it is a relatively new filter. The research for SVSF is in the process, but comparing with KF and LPV, standard SVSF shows promising results.

CONCLUSIONS

In this paper, the models and estimation strategy for estimating the unburned fuel for Diesel engines is proposed. Three observers, specifically, Smooth Variable Structure Filter, Kalman filter, and Linear Matrix Inequality based linear parameter-varying filter are designed to estimate it. Robustness properties based on Input-to-State Stability are analyzed in a quantified way for the 3 filters. A set of simulations in GT-Power

environment show the effectiveness of the designed observers. By comparisons, the SVSF shows good rejection on parameter uncertainties and quick convergence time, while KF has better property on noise. The simulation results match with the observer theoretical robustness analyzes well.

REFERENCES

[1] Dec, E., 2009. "Advanced Compression-Ignition Engines—understanding the in-Cylinder Processes." Proceedings of the Combustion Institute., **32** (2), pp.27–42.

[2] Rausen, D. J., Stefanopoulou, A. G., Kang, J.M., Eng, J. A., and Kuo, T. W., 2005. "A Mean-Value Model for Control of Homogeneous Charge Compression Ignition (HCCI) Engines." Journal of Dynamic Systems, Measurement, and Control., **127** (3), pp. 355-362.

[3] Ravi, N., Matthew, J. R., Liao ,H., Adam, F. J., Chang, C., Park, S., and Gerdes, J. C., 2010. "Model-Based Control of HCCI Engines Using Exhaust Recompression." IEEE Transactions on Control Systems Technology., **18** (6), pp.1289–1302.

[4] Swami N.S., Mallikarjuna, J.M., and Ramesh. A., 2010. "Effects of Charge Temperature and Exhaust Gas Re-Circulation on Combustion and Emission Characteristics of an Acetylene Fuelled HCCI Engine." Fuel., **89** (2),pp. 15–21.

[5] Stuart, D., Robert, C.M., Wagner, K., Dean, E., and Johney B. G., 2007. "Understanding the Transition between Conventional Spark-Ignited Combustion and HCCI in a Gasoline Engine." Proceedings of the Combustion Institute., **31** (2), pp.2887–94.

[6] Stefnanopoulou, A.G., Kolmanovsky, I., and Freudenberg, J. S., 2000. "Control of Variable Geometry Turbocharged Diesel Engines for Reduced Emissions." IEEE Transactions on Control Systems Technology., **8** (4), pp.733–45.

[7] Sellnau, M., James, S., and Larry, O., 2009. "Development of a Practical Tool for Residual Gas Estimation in IC Engines Carroll Dase , Matthew Viele and Kris Quillen John Silvestri and Iakovos Papadimitriou." SAE Technical Paper, No.2009-01-0695.

[8] Albert, B.P., 2004. "RESIDUAL GAS EFFECTS ON COMBUSTION IN AN AIR-COOLED UTILITY ENGINE," Thesis for the degree of Master of Science (Mechanical Engineering), UNIVERSITY OF WISCONSIN-MADISON.

[9] Giansetti, P., Colin.G., Higelin. P., and Chamaillard.Y., 2007. "Residual Gas Fraction Measurement and Computation." International Journal of Engine Research., **8** (4), pp.347–64.

[10] Hellström, E., Stefanopoulou, A., Jiri, V., Aristotelis, B., Dennis, A., Jiang, L., and Yilmaz, H., 2012. "Understanding the Dynamic Evolution of Cyclic Variability at the Operating Limits of HCCI Engines with Negative Valve Overlap." SAE Technical Paper, No.2012-01-1106.

[11] Karagiorgis, S., Nick, C., Keith, G., Neil, C., and Petridis, A., 2006. "Residual Gas Fraction Measurement and Estimation on a Homogeneous Charge Compression Ignition Engine Utilizing the Negative Valve Overlap Strategy." SAE Technical Paper, No.2006-01-3276.

[12] Nakayama, S., Takao, F., Akio, M., Teruhiko, Mi., and Toru, W., 2003. "A New Dynamic Combustion Control Method Based on Charge Oxygen Concentration for Diesel Engines." SAE Technical Paper, No. 2003-01-3181.

[13] Kocher, L., Karla, S., Daniel, V.A., and Gregory, M.S., 2012. "Robust Oxygen Fraction Estimation for Diesel Engines Utilizing Variable Intake Valve Actuation." In Engine and Powertrain Control, Simulation and Modeling, **3**, pp.310–17.

[14] Wang, J., 2008. "Air Fraction Estimation for Multiple Combustion Mode Diesel Engines with Dual-Loop EGR Systems." Control Engineering Practice., **16** (12),pp. 1479–86.

[15] Leroy, T., Alix, G., Chauvin, J., Duparchy, A., and Le Berr, F., 2008. "Modeling Fresh Air Charge and Residual Gas Fraction on a Dual Independent Variable Valve Timing SI Engine." SAE Technical Paper, No. 2008-01-0983.

[16] Kolmanovsky, I., Morall, P., and Van, N.M., 1999. "Issues in Modeling and Control of Intake Flow in Variable Geometry Turbocharged Engines". Chapman and Hall CRC research notes in mathematics. pp. 436–445.

[17] Wang, J., 2008. "Hybrid Robust Air-Path Control for Diesel Engines Operating Conventional and Low Temperature Combustion Modes." IEEE Transactions on Control Systems Technology., **16** (6),pp.1138–51.

[18] Grondin, O., Philippe, M., and Jonathan, C., 2009. "Control of a Turbocharged Diesel Engine Fitted with High Pressure and Low Pressure Exhaust Gas

Recirculation Systems." IEEE Conference on Decision and Control and European Control Conference, pp.6582–89.

[19] Habibi, S. R., 2007. "The Smooth Variable Structure Filter." Proceedings of the IEEE., **95** (5),pp.1026–59.

[20] Habibi, S. R., and Burton,R., 2003. "The Variable Structure Filter." Journal of Dynamic Systems, Measurement, and Control., **125** (3),pp. 287-293.

[21] Welch, G., Gary, B., and Chapel, H., "An Introduction to the Kalman Filter" ,pp.1–16.

[22] Barbarisi, O., Alessandro, G., and Luigi, G., 2002. "An Extended Kalman Observer for the In-Cylinder Air Mass Flow Estimation." Proceedings of MECA02 International Workshop on Diagnostics in Automotive Engines and Vehicles.

[23] Daafouz, J., and Jacques, B., 2001. "Parameter Dependent Lyapunov Functions for Discrete Time Systems with Time Varying Parametric Uncertainties." Systems & Control Letters., **43** (5),pp. 355–59.

[24] Jiang, Z.P., and Yuan,W., 2001. "Input-to-State Stability for Discrete-Time Nonlinear Systems." Automatica., **6** (37),pp. 857–69.

[25] Sontag, E. D., 1995. "On the Input-to-State Stability Property." European Journal of Control, **1** (1),pp. 24–36.

[26] Cao, L, and Howard M. S., 2003. "Exponential Convergence of the Kalman Filter Based Parameter Estimation Algorithm." International Journal of Adaptive Control and Signal Processing, **17** (10),pp.763–83.

[27] Yan, F., and Wang, J., 2012. "Design and Robustness Analysis of Discrete Observers for Diesel Engine In-Cylinder Oxygen Mass Fraction Cycle-by-Cycle Estimation." IEEE Transactions on Control Systems Technology, **20** (1),pp. 72–83.

[28]Habibi, S. R., 2008. "Combined Variable Structure and Kalman Filtering Approach." *2008* American Control Conference, pp.1855–62.

5.5 Remarks

1) The volumetric efficiency in equation (6) plays an important role for calculating the oxygen fraction and further the unburned fuel. Usually, volumetric efficiency is given by a lookup table. For this specific system, the volumetric efficiency can be mapped as a function of combustion efficiency and EGR valve opening. The map is generated from steady-state data and used to predict the air flow in transient situations. Therefore in steady-state operating conditions, it is not necessary to validate the volumetric efficiency map, in transient cycles, the effectiveness can be indirectly observed from the performance of the proposed models.
2) The method introduced in this paper is aiming the engine with NVO strategy. However, the characteristics of the system dynamics remain the same for a system with EGR loop. Thus, the technique can be easily applied to the Diesel engine with dual-loop EGR system, as the system model in paper 2 and paper 3.

Chaper 6. Conclusions and Future Work

In this chapter, conclusions of this thesis are presented and the potential future directions are proposed

6.1 Conclusions

In this thesis, to overcome the obstacles to applying the advanced combustion modes practically, the techniques, including the modeling and estimation for in-cylinder temperature and oxygen concentration, the control for air- and fuel-path coordinately, and the control quality evaluation in terms of smoothness and the cyclic variation by estimating the mass unburned fuel, are proposed in four papers, respectively.

As one of the essential issues, the difficulty of controlling the combustion phasing makes the advanced combustion mode unfeasible. The in-cylinder conditions, such as the in-cylinder pressure, temperature and oxygen concentration are critical to understanding the auto-ignition process and further to stabilize the combustion phasing. The system dynamics for in-cylinder temperature and in-cylinder oxygen concentration derived in paper 1 and paper 2 provide a systematical way to estimate these two unmeasurable states.

The EKF is utilized to estimate the in-cylinder temperature with the measurement of intake and exhaust manifold temperature. The measurement error caused by the thermocouple lag is also addressed by re-deriving the measurement and process covariance matrices.

To obtain a robust and more accurate estimation, the in-cylinder oxygen concentration is also calculated from the ignition delay. SVSF is applied to extract the in-cylinder oxygen concentration from two sources: the system dynamics and ignition delay.

The experimental results tell that the accuracy is improved comparing to estimation from each single source.

For Diesel engine combustion control, models of air- and fuel- path loops are presented in paper 3. The air-path loop dynamics are combined with the dynamics of the intake manifold, the turbocharging system and the intake and inter-cooling system. The control-oriented models of the IMEP and CA50 for fuel path loop is presented as functions of injection mass, injection timing and intake temperature.

The air/fuel path coordinated control is achieved by the enhanced disturbance rejection control with the extended state observer based on the super twisting concept and the model based injection compensation. The control objectives are to track the desired intake conditions accurately which are critical to for the advanced combustion mode running smoothly, and the desired CA50 and IMEP which are aiming at a good transient performance. The results on a calibrated engine model by real experimental data tell the advantage for the coordinated control comparing to the one with only air-path loop control. This control method can be potentially applied to the Diesel engine advanced combustion mode transient control as well as the operating range extending.

Considering that large amount of exhaust or residual gas withheld in the cylinders in advanced combustion mode, which will deteriorate the combustion quality in terms of high cyclic variation, as one good indicator to show the combustion smoothness, the trapped unburned fuel is estimated by using the information of in-cylinder oxygen concentration in paper 4. By taking the advantage of the strong relationship between the unburned fuel and the in-cylinder oxygen concentration, three filters, including the SVSF,

EKF and LPV are used to extract the unburned fuel from the oxygen concentration, respectively. Their robustness against modeling error is analyzed based on ISS theory. The analysis and simulation in GT-Power environment confirm that the SVSF has the best robustness amount the three filters.

6.2 Future Work

Several directions can be further investigated based on this thesis for the future research. Some of them are listed below:

1. Applying the advanced combustion mode on hybrid vehicles

The range limitations caused by the high battery cost and the low charging rate of the electric vehicles and the narrow load range of the advanced combustion mode in internal combustion engines (ICE) can be significantly attenuated by applying the advanced combustion mode on hybrid vehicles. The extreme low engine out emissions and high thermal efficiency of the advanced combustion mode can charge the battery in low and medium load situations. While on high load, the battery will compensate the torque shortage of the ICE. The motor can also be serviced as a starter for the ICE to simplify the whole power system. The obstacle of the cold start of the advanced combustion mode can also be attenuated to some extent by the battery-motor to achieved desired intake conditions. The control for advanced combustion mode of a hybrid vehicle, and optimize the torque portion of the ICE and motor will be a potential direction of the future work.

2. Control for advanced combustion mode and after-treatment system in an integrated fashion

The characteristic of the low engine-out emissions of the advanced combustion mode can significantly relax the requirement for the after-treatment system. The states estimation and control for the Diesel oxidation catalyst (DOC), Diesel particulate filter (DPF) and the selective catalyst reduction (SCR) of the after-treatment system can be combined with the advanced combustion mode control. To systematically utilize the advanced combustion mode control and the after-treatment control to optimize the overall fuel efficiency and the emissions is an extension of this thesis.